2011 Volume 2

The Journal on Advanced Studies in Theoretical and Experimental Physics, including Related Themes from Mathematics

PROGRESS IN PHYSICS

"All scientists shall have the right to present their scientific research results, in whole or in part, at relevant scientific conferences, and to publish the same in printed scientific journals, electronic archives, and any other media."
— Declaration of Academic Freedom, Article 8

ISSN 1555-5534

The Journal on Advanced Studies in Theoretical and Experimental Physics, including Related Themes from Mathematics

PROGRESS IN PHYSICS

A quarterly issue scientific journal, registered with the Library of Congress (DC, USA). This journal is peer reviewed and included in the abstracting and indexing coverage of: Mathematical Reviews and MathSciNet (AMS, USA), DOAJ of Lund University (Sweden), Zentralblatt MATH (Germany), Scientific Commons of the University of St. Gallen (Switzerland), Open-J-Gate (India), Referativnyi Zhurnal VINITI (Russia), etc.

Electronic version of this journal:
http://www.ptep-online.com

Postal Address

Department of Mathematics and Science,
University of New Mexico,
200 College Road, Gallup, NM 87301, USA

ISSN: 1555-5534 (print)
ISSN: 1555-5615 (online)

Standard Address Number: 297-5092
Printed in the United States of America

APRIL 2011 **VOLUME 2**

CONTENTS

Information for Authors and Subscribers

Progress in Physics has been created for publications on advanced studies in theoretical and experimental physics, including related themes from mathematics and astronomy. All submitted papers should be professional, in good English, containing a brief review of a problem and obtained results.

All submissions should be designed in LaTeX format using *Progress in Physics* template. This template can be downloaded from *Progress in Physics* home page http://www.ptep-online.com. Abstract and the necessary information about author(s) should be included into the papers. To submit a paper, mail the file(s) to the Editor-in-Chief.

All submitted papers should be as brief as possible. We accept brief papers, no larger than 8 typeset journal pages. Short articles are preferable. Large papers can be considered in exceptional cases to the section *Special Reports* intended for such publications in the journal. Letters related to the publications in the journal or to the events among the science community can be applied to the section *Letters to Progress in Physics*.

All that has been accepted for the online issue of *Progress in Physics* is printed in the paper version of the journal. To order printed issues, contact the Editors.

This journal is non-commercial, academic edition. It is printed from private donations. (Look for the current author fee in the online version of the journal.)

The Lorentz Transformation as a Planck Vacuum Phenomenon in a Galilean Coordinate System

William C. Daywitt
National Institute for Standards and Technology (retired), Boulder, Colorado, USA
E-mail: wcdaywitt@earthlink.net

In a seminal Masters' dissertation [1] Pemper derived the relativistic electric and magnetic fields of a uniformly moving charge from the response of some continuum to the perturbation from the charge's Coulomb field. The results seem to imply that the Maxwell equations and the Lorentz transformation are associated with some type of vacuum state. Unbeknownst at the time, Pemper had discovered the Planck vacuum (PV) quasi-continuum [2] and its interaction with the free charge. The importance of this derivation, its obscurity in the literature, and its connection to the PV justifies the following rework of that derivation.

1 Pemper Derivation

When a free, massless, bare charge e_* travels in a straight line at a uniform velocity v its bare Coulomb field e_*/r^2 perturbs (polarizes) the PV [2]. If there were no PV, the bare field would propagate as a frozen pattern with the same velocity and there would be no accompanying magnetic field. The corresponding force perturbing the PV is e_*^2/r^2, where one of the charges e_* in the product e_*^2 belongs to the free charge and the other to the individual Planck particles making up the degenerate negative-energy PV.

This charge-vacuum interaction is described by Pemper [1] as a series ($n = 1, 2, 3, \ldots$) of electric and magnetic fields (*generated by the vacuum*)

$$\nabla \times \mathbf{E}_n = -\frac{1}{c}\frac{\partial \mathbf{B}_n}{\partial t} \tag{1}$$

and

$$\mathbf{B}_{n+1} = \boldsymbol{\beta} \times \mathbf{E}_n \tag{2}$$

that respond in a iterative fashion to the bare charge's Coulomb field, leading to the well-known relativistic electric and magnetic fields that are traditionally ascribed to the charge as a single entity. The serial electric and magnetic fields are $\mathbf{E}_n$ and $\mathbf{B}_n$ and $\boldsymbol{\beta} = \mathbf{v}/c$. The curl equation in (1) is recognized as the Faraday equation and the magnetic field in (2) is due to the free-charge field rotating the induced dipoles within the PV. The series of partial fields is not envisioned as a series in time — the PV response is assumed to happen instantaneously at each field point.

The initial magnetic field in the series is $\mathbf{B}_1 = \boldsymbol{\beta} \times \mathbf{E}_0$, where the bare charge's laboratory-observed Coulomb field is

$$\mathbf{E}_0 = \frac{e\mathbf{r}}{r^3} = \frac{e}{e_*}\frac{e_*\mathbf{r}}{r^3} = \alpha^{1/2}\frac{e_*\mathbf{r}}{r^3}, \tag{3}$$

where α is Planck's constant. The serial electric fields are assumed to be radial; so the final electric field is radial with a magnitude equal to the sum

$$E = E_0 + E_1 + E_2 + E_3 + \ldots, \tag{4}$$

where the E_n are the magnitudes of the $\mathbf{E}_n$s and the final magnetic field is $\boldsymbol{\beta} \times \mathbf{E}$. Assuming that the $E_n = E_n(r, \theta)$, the charge-PV feedback equations (1) and (2) reduce to

$$\frac{\partial E_n}{\partial \theta} = \frac{r}{c}\frac{\partial B_n}{\partial t} \tag{5}$$

and

$$B_{n+1} = \beta E_n \sin\theta \tag{6}$$

in the azimuthal direction about the z-axis.

Calculating the first partial field E_1 in the series begins with (6)

$$B_1 = \beta E_0 \sin\theta \tag{7}$$

and leads to (Appendix A)

$$\dot{B}_1 = \frac{3c\beta^2 E_0 \sin\theta\cos\theta}{r}, \tag{8}$$

where the overhead dot represents a partial differentiation with respect to time. Then from (5)

$$dE_1 = \frac{r\dot{B}_1}{c}\,d\theta = 3\beta^2 E_0 \sin\theta\cos\theta\,d\theta, \tag{9}$$

which integrates over the limits $(0, \theta)$ to

$$E_1 = \frac{3\beta^2 E_0 \sin^2\theta}{2} - \lambda_1 E_0, \tag{10}$$

where the reference field $E_1(\theta = 0) = -\lambda_1 E_0$ with λ_1 a constant to be determined.

The second iteration for the electric field begins with

$$B_2 = \beta E_1 \sin\theta = \frac{3\beta^3 E_0 \sin^3\theta}{2} - \lambda_1 B_1 \tag{11}$$

and yields (Appendix A)

$$\dot{B}_2 = \frac{15c\beta^4 E_0 \sin^3\theta\cos\theta}{2r} - \lambda_1 \dot{B}_1\,. \tag{12}$$

Equation (5) then leads to

$$dE_2 = \frac{r\dot{B}_2}{c}\,d\theta = \left(\frac{15\beta^4 E_0 \sin^3\theta\cos\theta}{2} - \frac{\lambda_1 r\dot{B}_1}{c}\right)d\theta, \quad (13)$$

which integrates to

$$E_2 = \frac{15\beta^4 E_0 \sin^4\theta}{8} - \lambda_1\frac{3\beta^2 E_0 \sin^2\theta}{2} - \lambda_2 E_0, \quad (14)$$

where again $E_2(\theta = 0) = -\lambda_2 E_0$.

The third iteration proceeds as before and results in (Appendix A)

$$\dot{B}_3 = \frac{3\cdot 5\cdot 7c\beta^6 E_0 \sin^5\theta\cos\theta}{8r} - \lambda_1\frac{3\cdot 5c\beta^4 E_0 \sin^3\theta\cos\theta}{2r}$$
$$-\lambda_2\frac{3c\beta^2 E_0 \sin\theta\cos\theta}{r} \quad (15)$$

and

$$E_3 = \frac{3\cdot 5\cdot 7\beta^6 E_0 \sin^6\theta}{6\cdot 8} - \lambda_1\frac{3\cdot 5\beta^4 E_0 \sin^4\theta}{2\cdot 4}$$
$$-\lambda_2\frac{3\beta E_0 \sin^2\theta}{2} - \lambda_3 E_0 \quad (16)$$

for the third partial field.

Inserting (10), (14), and (16) (plus the remaining infinity of partial fields) into (4) gives

$$E = E_0 + \frac{3\beta^2 E_0 \sin^2\theta}{2} + \frac{3\cdot 5\beta^4 E_0 \sin^4\theta}{8}$$
$$+\frac{3\cdot 5\cdot 7\beta^6 E_0 \sin^6\theta}{48} + \ldots$$
$$-\lambda_1\left(E_0 + \frac{3\beta^2 E_0 \sin^2\theta}{2} + \frac{3\cdot 5\beta^4 E_0 \sin^4\theta}{8} + \ldots\right)$$
$$-\lambda_2\left(E_0 + \frac{3\beta E_0 \sin^2\theta}{2} + \ldots\right) - \lambda_3(E_0 + \ldots) + \ldots$$
$$= E_0\left(1 + \frac{3\beta^2 \sin^2\theta}{2} + \frac{3\cdot 5\beta^4 \sin^4\theta}{2\cdot 4}\right.$$
$$\left.+\frac{3\cdot 5\cdot 7\beta^6 \sin^6\theta}{2\cdot 4\cdot 6} + \ldots\right)(1-\lambda), \quad (17)$$

where

$$\lambda \equiv \sum_{n=1}^{\infty}\lambda_n \quad (18)$$

is a constant. The sum after the final equal sign in (17) is recognized as the function $(1-\beta^2\sin^2\theta)^{-3/2}$; so E can be expressed as

$$E = \frac{(1-\lambda)E_0}{(1-\beta^2\sin^2\theta)^{3/2}}\,. \quad (19)$$

Finally, the constant λ can be evaluated from Gauss' law and the conservation of bare charge e_*:

$$\int \mathbf{D}\cdot\mathbf{dS} = 4\pi e_* \longrightarrow \int \mathbf{E}\cdot\mathbf{dS} = 4\pi e, \quad (20)$$

where $\mathbf{D} = (e_*/e)\mathbf{E}$ is used to arrive at the second integral. Inserting (19) into (20) and integrating yields

$$\lambda = \beta^2, \quad (21)$$

which, inserted back into (19), gives the relativistic electric field of a uniformly moving charge. That this field is the same as that derived from the Lorentz transformed Coulomb field is shown in Appendix B.

2 Conclusions and Comments

The calculations of the previous section suggest that the Lorentz transformation owes its existence to interactions between free-space particles and the negative-energy PV. Free space is defined here as "the classical void + the zero-point electromagnetic vacuum" [3].

The fact that the bare charge is massless makes the Pemper derivation significantly less involved and more straightforward than the related case for the massive point charge (Dirac electron). Nevertheless, the uniform motion of the Dirac electron too exhibits electron-PV effects. When a bare charge is injected into free space (presumably from the PV) it very quickly ($\sim 10^{-30}$ sec) develops a mass from being driven by the random fields of the electromagnetic vacuum. The corresponding electron-PV connection is easily recognized in the Lorentz-covariant Dirac equation [4, p. 90], [5]:

$$\left(ic\hbar\gamma^\mu\partial_\mu - mc^2\right)\psi = 0 \longrightarrow \left(ie_*^2\gamma^\mu\partial_\mu - mc^2\right)\psi = 0, \quad (22)$$

where the PV relation $c\hbar = e_*^2$ is used to arrive at the equation on the right. A nonrelativistic expression for the electron mass is given by Puthoff [3, 6]

$$m = \frac{2}{3}\frac{\left\langle \dot{r}^2\right\rangle^{1/2}}{c}\,m_*, \quad (23)$$

where $\dot{\mathbf{r}}$ represents the random excursions of the zero-point-driven bare charge about its center of (random) motion at $\mathbf{r} = 0$ and m_* is the Planck mass.

The massive point charge perturbs the PV with the two-fold force [5]

$$\frac{e_*^2}{r^2} - \frac{mc^2}{r}, \quad (24)$$

where the first and second terms are the polarization and curvature* forces respectively. It is the interaction of this composite force with the PV that is responsible for the Dirac equation as evidenced by the e_*^2 and mc^2 in (22) and (24). Thus

*Using the PV relations $G = e_*^2/m_*^2$ and $e_*^2 = r_* m_* c^2$ in the curvature force leads to $mc^2/r = mm_*G/rr_*$ and shows the direct gravitational interaction between the electron mass and the Planck particle masses within the PV.

both the Pemper derivation and the Dirac equation argue compellingly for the existence of the Planck vacuum state and its place in the physical scheme of things. It is noted in passing that the force in (24) vanishes at the electron's Compton radius $r_c = e_*^2/mc^2$.

Appendix A: Galilean Coordinate System

The laboratory system in which the charge propagates is considered to be a Galilean reference system. In that system (x, y, z) represents the radius vector from the system origin to any field point (considered in the calculations to be fixed). The position of the charge traveling at a constant rate v along the positive z-axis is $(0, 0, vt)$; so at time $t = 0$ the charge crosses the origin. Since the field point is fixed, the vector in the x-y plane

$$\mathbf{b} = b\,\widehat{\mathbf{b}} \equiv \mathbf{x} + \mathbf{y} \tag{A1}$$

is constant. The radius vector from the position of the charge to the field point is then

$$\mathbf{r} = (x, y, z - vt)\,. \tag{A2}$$

Combining (A1) and (A2) gives

$$r = \left[b^2 + (z - vt)^2\right]^{1/2} \tag{A3}$$

for the magnitude of that vector.

If θ is the angle between the radius $\mathbf{r}$ and the positive z-axis, it is easy to show from (A1)—(A3) that

$$r \sin\theta = b \tag{A4}$$

and

$$r \cos\theta = z - vt \tag{A5}$$

and from (A3)—(A5) that

$$\dot{r} = -v \cos\theta \tag{A6}$$

and

$$r\dot{\theta} = v \sin\theta, \tag{A7}$$

where the overhead dot represents a partial derivative with respect to time.

From (7) the initial magnetic field in the charge-PV interaction is

$$B_1 = \beta E_0 \sin\theta = \beta \cdot \frac{e}{r^2} \cdot \frac{b}{r} = \frac{\beta e b}{\left[b^2 + (z - vt)^2\right]^{3/2}} \tag{A8}$$

whose time differential leads to

$$\dot{B}_1 = \frac{3c\beta^2 E_0 \sin\theta\cos\theta}{r} \tag{A9}$$

in a straightforward manner.
From (11) in the text

$$B_2 = \beta E_1 \sin\theta = \frac{3\beta^3 e b^3}{2\left[b^2 + (z - vt)^2\right]^{5/2}} - \lambda_1 B_1, \tag{A10}$$

which leads to

$$\dot{B}_2 = \frac{15c\beta^4 E_o \sin^3\theta\cos\theta}{2r} - \lambda_1 \dot{B}_1\,. \tag{A11}$$

From $B_3 = \beta E_2 \sin\theta$,

$$\begin{aligned} B_3 &= \frac{15\beta^5 E_0 \sin^5\theta}{8} - \lambda_1 \frac{3\beta^3 E_0 \sin^3\theta}{2} - \lambda_2 \beta E_0 \sin\theta \\ &= \frac{15\beta^5 e b^5}{8\left[b^2 + (z - vt)^2\right]^{7/2}} - \lambda_1 \frac{3\beta^3 e b^3}{2\left[b^2 + (z - vt)^2\right]^{5/2}} \\ &\quad -\lambda_2 \frac{\beta e b}{\left[b^2 + (z - vt)^2\right]^{3/2}} \end{aligned} \tag{A12}$$

and

$$\begin{aligned} \dot{B}_3 &= \frac{3 \cdot 5 \cdot 7c\beta^6 E_0 \sin^5\theta\cos\theta}{8r} - \lambda_1 \frac{3 \cdot 5c\beta^4 E_0 \sin^3\theta\cos\theta}{2r} \\ &\quad -\lambda_2 \frac{3c\beta^2 E_0 \sin\theta\cos\theta}{r}\,. \end{aligned} \tag{A13}$$

Appendix B: Lorentz Transformed Fields

The Lorentz transformation coefficients $a_{\mu\nu}$ in the coordinate transformation [7, pp. 380–381]

$$\begin{aligned} x'_\mu = a_{\mu\nu} x_\mu &= \begin{pmatrix} 1 & 0 & 0 & 0 \\ 0 & 1 & 0 & 0 \\ 0 & 0 & \gamma & i\beta\gamma \\ 0 & 0 & -i\beta\gamma & \gamma \end{pmatrix} \begin{pmatrix} x \\ y \\ z \\ ict \end{pmatrix} \\ &= \begin{pmatrix} x \\ y \\ \gamma(z - vt) \\ i\gamma(ct - \beta z) \end{pmatrix} \end{aligned} \tag{B1}$$

lead to the Lorentz transformed fields

$$F'_{\mu\nu} = a_{\mu\sigma} a_{\nu\tau} F_{\sigma\tau}, \tag{B2}$$

where the $F'_{\mu\nu}$, etc., are the electromagnetic field tensors. The primed and unprimed parameters refer respectively to the charge-at-rest and laboratory systems, where the charge system travels along the z-axis of the laboratory system with a constant velocity v.

Using the static Coulomb field in the charge system and transforming it to the laboratory system with the inverse of (B2) leads to the magnitude

$$E = \frac{\gamma e\left[b^2 + (z - vt)^2\right]^{1/2}}{\left[b^2 + \gamma(z - vt)^2\right]^{3/2}} \tag{B3}$$

for the electric field, where $\gamma = 1/(1 - \beta^2)^{1/2}$. (B3) reduces to (19) in the following way:

$$E = \frac{\gamma e\left[b^2 + (z - vt)^2\right]^{1/2}}{\gamma^3\left[b^2 + (z - vt)^2 - \beta^2 b^2\right]^{3/2}}$$

$$= \frac{e/\left[b^2 + (z - vt)^2\right]}{\gamma^2 \left[1 - \beta^2 b^2/[b^2 + (z - vt)^2]\right]^{3/2}}$$

$$= \frac{(1 - \beta^2)\, E_0}{\left(1 - \beta^2 \sin^2 \theta\right)^{3/2}} \,. \tag{B4}$$

Submitted on January 5, 2011 / Accepted on January 6, 2011

References

1. Pemper R.R. A classical foundation for electrodynamics. Master Dissertation, Univ. of Texas, El Paso, 1977. Barnes T.G. Physics of the Future – A Classical Unification of Physics, Institute for Creation Research, California, 1983.
2. Daywitt W.C. The Planck vacuum. *Progress in Physics*, 2009, v. 1, 20–26.
3. Daywitt W.C. The Source of the Quantum Vacuum. *Progress in Physics*, 2009, v. 1, 27–32.
4. Gingrich D.M. Practical Quantum Electrodynamics, CRC – The Taylor & Francis Group, Boca Raton, 2006.
5. Daywitt W.C. The Dirac Electron in the Planck Vacuum Theory. *Progress in Physics*, 2010, v. 4, 69–71.
6. Puthoff H.E. Gravity as a zero-point-fluctuation force. *Physical Review A*, 1989, v. 39, no. 5, 2333–2342.
7. Jackson J.D. Classical Electrodynamics. John Wiley & Sons, 1st ed., 2nd printing, New York, 1962.

Charged Polaritons with Spin 1

Vahan Minasyan and Valentin Samoilov
Scientific Center of Applied Research, JINR, Joliot-Curie 6, Dubna, 141980, Russia
E-mails: mvahan@scar.jinr.ru; scar@off-serv.jinr.ru

We present a new model for metal which is based on the stimulated vibration of independent charged Fermi-ions, representing as independent harmonic oscillators with natural frequencies, under action of longitudinal and transverse elastic waves. Due to application of the elastic wave-particle principle and ion-wave dualities, we predict the existence of two types of charged Polaritons with spin 1 which are induced by longitudinal and transverse elastic fields. As result of presented theory, at small wavenumbers, these charged polaritons represent charged phonons.

1 Introduction

In our recent paper [1], we proposed a new model for dielectric materials consisting of neutral Fermi atoms. By the stimulated vibration of independent charged Fermi-atoms, representing as independent harmonic oscillators with natural frequencies by actions of the longitudinal and transverse elastic waves, due to application of the principle of elastic wave-particle duality, we predicted the lattice of a solid consists of two types of Sound Boson-Particles with spin 1, with finite masses around 500 times smaller than the atom mass. Namely, we had shown that these lattice Sound-Particles excite the longitudinal and transverse phonons with spin 1. In this context, we proposed new model for solids representing as dielectric substance which is different from the well-known models of Einstein [2] and Debye [3] because: 1), we suggest that the atoms are the Fermi particles which are absent in the Einstein and Debye models; 2), we consider the stimulated oscillation of atoms by action of longitudinal and transverse lattice waves which in turn consist of the Sound Particles.

Thus, the elastic lattice waves stimulate the vibration of the fermion-atoms with one natural wavelength, we suggested that ions have two independent natural frequencies by under action of a longitudinal and a transverse wave. Introduction of the application of the principle of elastic wave-particle duality as well as the model of hard spheres we found an appearance of a cut off in the spectrum energy of phonons which have spin 1 [1].

In this letter, we treat the thermodynamic property of metal under action of the ultrasonic waves. We propose a new model for metal where the charged Fermi-ions vibrate with natural frequencies Ω_l and Ω_t, by under action of longitudinal and transverse elastic waves. Thus, we consider a model for metal as independent charged Fermi-ions of lattice and gas of free electrons or free Frölich-Schafroth charged bosons (singlet electron pairs) [4]. Each charged ion is coupled with a point of lattice knot by spring, creating an ion dipole [5,6]. The lattice knots define the equilibrium positions of all ions which vibrate with natural frequencies Ω_l and Ω_t, under action of longitudinal and transverse elastic fields which in turn leads to creation of the transverse electromagnetic fields moving with speeds c_l and c_t. These transverse electromagnetic waves describe the ions by the principle of ion-wave duality [7]. Using the representation of the electromagnetic field structure of one ion with ion-wave duality in analogous manner, as it was presented in a homogenous medium for an electromagnetic wave [8], we obtain that the neutral phonons cannot be excited in such substances as metals, they may be induced only in dielectric material [1]. In this respect, we find the charged polaritons with spin 1 which are always excited in a metal, and at small wavenumbers, they represent as charged phonons.

2 New model for metal

The Einstein model of a solid considers the solid as gas of N atoms in a box with volume V. Each atom is coupled with a point of the lattice knot. The lattice knots define the dynamical equilibrium position of each atom which vibrates with natural frequency Ω_0. The vibration of atom occurs near equilibrium position corresponding to the minimum of potential energy (harmonic approximation of close neighbors). We presented the model of ion-dipoles [5,6] which represents ions coupled with points of lattice knots. It differs from the Einstein model of solids where the neutral independent atoms are considered in lattice knots, these ions are vibrating with natural frequencies Ω_l and Ω_t forming ion-dipoles by under action longitudinal and transverse ultrasonic lattice fields.

Usually, matters are simplified assuming the transfer of heat from one part of the body to another occurs very slowly. This is a reason to suggest that the heat exchange during times of the order of the period of oscillatory motions in the body is negligible, therefore, we can regard any part of the body as thermally insulated, and there occur adiabatic deformations. Since all deformations are supposed to be small, the motions considered in the theory of elasticity are small elastic oscillations. In this respect, the equation of motion for elastic continuum medium [9] represents as

$$\varrho\ddot{\vec{u}} = c_t^2\nabla^2\vec{u} + (c_l^2 - c_t^2)\ grad\ div\ \vec{u}, \qquad (1)$$

where $\vec{u} = \vec{u}(\vec{r}, t)$ is the vectorial displacement of any particle in the solid; c_l and c_t are, respectively, the velocities of a longitudinal and a transverse ultrasonic wave.

We shall begin by discussing a plane longitudinal elastic wave with condition $curl\ \vec{u} = 0$ and a plane transverse elastic wave with condition $div\ \vec{u} = 0$ in an infinite isotropic medium. In this respect, the vector displacement $\vec{u}$ is the sum of the vector displacements of a longitudinal u_l and of a transverse ultrasonic wave u_t:

$$\vec{u} = \vec{u}_l + \vec{u}_t. \tag{2}$$

In turn, the equations of motion for a longitudinal and a transverse elastic wave take the form of the wave-equations:

$$\nabla^2 \vec{u}_l - \frac{1}{c_l^2} \frac{d^2 \vec{u}_l}{dt^2} = 0, \tag{3}$$

$$\nabla^2 \vec{u}_t - \frac{1}{c_t^2} \frac{d^2 \vec{u}_l}{dt^2} = 0. \tag{4}$$

It is well known, in quantum mechanics, a matter wave is determined by electromagnetic wave-particle duality or de Broglie wave of matter [7]. We argue that in analogous manner, we may apply the elastic wave-particle duality. This reasoning allows us to present a model of elastic field as the Bose-gas consisting of the Sound Bose-particles with spin 1 having non-zero rest masses which are interacting with each other. In this respect, we may express the vector displacements of a longitudinal u_l and of a transverse ultrasonic wave u_t via the second quantization vector wave functions of Sound Bosons as

$$\vec{u}_l = C_l \left(\vec{\phi}(\vec{r}, t) + \vec{\phi}^{+}(\vec{r}, t) \right) \tag{5}$$

and

$$\vec{u}_t = C_t \left(\vec{\psi}(\vec{r}, t) + \vec{\psi}^{+}(\vec{r}, t) \right), \tag{6}$$

where C_l and C_t are unknown constant normalization coefficients; $\vec{\phi}(\vec{r}, t)$ and $\vec{\phi}^{+}(\vec{r}, t)$ are, respectively, the second quantization wave vector functions for one Sound-Particle, corresponding to the longitudinal elastic wave, at coordinate $\vec{r}$ and time t; $\vec{\psi}(\vec{r}, t)$ and $\vec{\psi}^{+}(\vec{r}, t)$ are, respectively, the second quantization wave vector functions for one Sound-Particle, corresponding to the transverse elastic wave, at coordinate $\vec{r}$ and time t:

$$\vec{\phi}(\vec{r}, t) = \frac{1}{\sqrt{V}} \sum_{\vec{k},\sigma} \vec{a}_{\vec{k},\sigma} e^{i(\vec{k}\vec{r} + kc_l t)} \tag{7}$$

$$\vec{\phi}^{+}(\vec{r}, t) = \frac{1}{\sqrt{V}} \sum_{\vec{k},\sigma} \vec{a}^{+}_{\vec{k},\sigma} e^{-i(\vec{k}\vec{r} + kc_l t)} \tag{8}$$

and

$$\vec{\psi}(\vec{r}, t) = \frac{1}{\sqrt{V}} \sum_{\vec{k},\sigma} \vec{b}_{\vec{k},\sigma} e^{i(\vec{k}\vec{r} + kc_t t)} \tag{9}$$

$$\vec{\psi}^{+}(\vec{r}, t) = \frac{1}{\sqrt{V}} \sum_{\vec{k},\sigma} \vec{b}^{+}_{\vec{k},\sigma} e^{-i(\vec{k}\vec{r} + kc_t t)}, \tag{10}$$

where $\vec{a}^{+}_{\vec{k},\sigma}$ and $\vec{a}_{\vec{k},\sigma}$ are, respectively, the Bose vector-operators of creation and annihilation for one free longitudinal Sound Particle with spin 1, described by a vector $\vec{k}$ whose direction gives the direction of motion of the longitudinal wave; $\vec{b}^{+}_{\vec{k},\sigma}$ and $\vec{b}_{\vec{k},\sigma}$ are, respectively, the Bose vector-operators of creation and annihilation for one free transverse Sound Particle with spin 1, described by a vector $\vec{k}$ whose direction gives the direction of motion of the transverse wave.

In this respect, the vector-operators $\vec{a}^{+}_{\vec{k},\sigma}, \vec{a}_{\vec{k},\sigma}$ and $\vec{b}^{+}_{\vec{k},\sigma}, \vec{b}_{\vec{k},\sigma}$ satisfy the Bose commutation relations as:

$$\left[\hat{a}_{\vec{k},\sigma}, \hat{a}^{+}_{\vec{k}',\sigma'} \right] = \delta_{\vec{k},\vec{k}'} \cdot \delta_{\sigma,\sigma'}$$

$$[\hat{a}_{\vec{k},\sigma}, \hat{a}_{\vec{k}',\sigma'}] = 0$$

$$[\hat{a}^{+}_{\vec{k},\sigma}, \hat{a}^{+}_{\vec{k}',\sigma'}] = 0$$

and

$$\left[\hat{b}_{\vec{k},\sigma}, \hat{b}^{+}_{\vec{k}',\sigma'} \right] = \delta_{\vec{k},\vec{k}'} \cdot \delta_{\sigma,\sigma'}$$

$$[\hat{b}_{\vec{k},\sigma}, \hat{b}_{\vec{k}',\sigma'}] = 0$$

$$[\hat{b}^{+}_{\vec{k},\sigma}, \hat{b}^{+}_{\vec{k}',\sigma'}] = 0.$$

Thus, as we see the vector displacements of a longitudinal u_l and of a transverse ultrasonic wave u_t satisfy the wave-equations of (3) and (4) because they have the following forms due to application of (5) and (6):

$$\vec{u}_l = \frac{C_l}{\sqrt{V}} \sum_{\vec{k},\sigma} \left(\vec{a}_{\vec{k},\sigma} e^{i(\vec{k}\vec{r} + kc_l t)} + \vec{a}^{+}_{\vec{k},\sigma} e^{-i(\vec{k}\vec{r} + kc_l t)} \right) \tag{11}$$

and

$$\vec{u}_t = \frac{C_t}{\sqrt{V}} \sum_{\vec{k},\sigma} \left(\vec{b}_{\vec{k},\sigma} e^{i(\vec{k}\vec{r} + kc_t t)} + \vec{b}^{+}_{\vec{k},\sigma} e^{-i(\vec{k}\vec{r} + kc_t t)} \right). \tag{12}$$

In this context, we may emphasize that the Bose vector operators $\vec{a}^{+}_{\vec{k},\sigma}$, $\vec{a}_{\vec{k},\sigma}$ and $\vec{b}^{+}_{\vec{k}}, \sigma$ and $\vec{b}_{\vec{k}}, \sigma$ communicate with each other because the vector displacements of a longitudinal $\vec{u}_l$ and a transverse ultrasonic wave $\vec{u}_t$ are independent, and in turn, satisfy the condition of a scalar multiplication $\vec{u}_l \cdot \vec{u}_t = 0$.

Consequently, the Hamiltonian operator $\hat{H}$ of the system, consisting of the vibrating Fermi-ions with mass M, is represented in the following form:

$$\hat{H} = \hat{H}_l + \hat{H}_t, \tag{13}$$

where

$$\hat{H}_l = \frac{MN}{V}\int\left(\frac{d\vec{u}_l}{dt}\right)^2 dV + \frac{NM\Omega_l^2}{V}\int(\vec{u}_l)^2 dV \tag{14}$$

and

$$\hat{H}_t = \frac{MN}{V}\int\left(\frac{d\vec{u}_t}{dt}\right)^2 dV + \frac{NM\Omega_t^2}{V}\int(\vec{u}_t)^2 dV, \tag{15}$$

where Ω_l and Ω_t are, respectively, the natural frequencies of the atom through action of the longitudinal and transverse elastic waves.

To find the Hamiltonian operator $\hat{H}$ of the system, we use the formalism of Dirac [10]:

$$\frac{d\vec{u}_l}{dt} = \frac{ic_lC_l}{\sqrt{V}}\sum_{\vec{k},\sigma} k\left(\vec{a}_{\vec{k},\sigma}e^{ikc_lt} - \vec{a}^{+}_{-\vec{k},\sigma}e^{-ikc_lt}\right)e^{i\vec{k}\vec{r}} \tag{16}$$

and

$$\frac{d\vec{u}_t}{dt} = \frac{ic_tC_t}{\sqrt{V}}\sum_{\vec{k},\sigma} k\left(\vec{b}_{\vec{k},\sigma}e^{ikc_tt} - \vec{b}^{+}_{-\vec{k},\sigma}e^{-ikc_tt}\right)e^{i\vec{k}\vec{r}}, \tag{17}$$

which by substituting into (14) and (15), using (11) and (12), gives the reduced form of the Hamiltonian operators $\hat{H}_l$ and $\hat{H}_t$:

$$\hat{H}_l = \sum_{\vec{k},\sigma}\left(\frac{2MNC_l^2c_l^2k^2}{V} + \frac{2MNC_l^2\Omega_l^2}{V}\right)\vec{a}^{+}_{\vec{k},\sigma}\vec{a}_{\vec{k},\sigma} -$$

$$- \sum_{\vec{k},\sigma}\left(\frac{2MNC_l^2c_l^2k^2}{V} - \frac{2MNC_l^2\Omega_l^2}{V}\right)\left(a_{\vec{k},\sigma}\vec{a}_{-\vec{k},\sigma} + a^{+}_{-\vec{k}}\vec{a}^{+}_{\vec{k},\sigma}\right) \tag{18}$$

and

$$\hat{H}_t = \sum_{\vec{k},\sigma}\left(\frac{2MNC_t^2c_t^2k^2}{V} + \frac{2MNC_t^2\Omega_t^2}{V}\right)\vec{b}^{+}_{\vec{k},\sigma}\vec{b}_{\vec{k},\sigma} -$$

$$- \sum_{\vec{k},\sigma}\left(\frac{2MNC_t^2c_t^2k^2}{V} - \frac{2MNC_t^2\Omega_t^2}{V}\right)\left(b_{\vec{k},\sigma}\vec{b}_{-\vec{k},\sigma} + b^{+}_{-\vec{k}}\vec{b}^{+}_{\vec{k},\sigma}\right), \tag{19}$$

where the normalization coefficients C_l and C_t are defined by the first term of right side of (18) and (19) which represent the kinetic energies of longitudinal Sound Particles $\frac{\hbar^2k^2}{2m_l}$ and transverse Sound Particles $\frac{\hbar^2k^2}{2m_t}$ with masses m_l and m_t, respectively. Therefore we suggest to find C_l and C_t:

$$\frac{2MNC_l^2c_l^2k^2}{V} = \frac{\hbar^2k^2}{2m_l} \tag{20}$$

and

$$\frac{2MNC_t^2c_t^2k^2}{V} = \frac{\hbar^2k^2}{2m_t}, \tag{21}$$

which in turn determine

$$C_l = \frac{\hbar}{2c_l\sqrt{m_l\rho}} \tag{22}$$

and

$$C_t = \frac{\hbar}{2c_t\sqrt{m_t\rho}}, \tag{23}$$

where $\rho = \frac{MN}{V}$ is the density of solid.

As we had shown in [1], at absolute zero $T = 0$, the Fermi ions fill the Fermi sphere in momentum space. Thus, there are two type Fermi atoms by the value of its spin z-component $\mu = \pm\frac{1}{2}$ with the boundary wave number k_f of the Fermi, which, in turn, is determined by a condition:

$$\frac{V}{2\pi^2}\int_0^{k_f} k^2dk = \frac{N}{2},$$

where N is the total number of Fermi-ions in the solid. This reasoning together with the model of hard spheres claims the important condition to introduce the boundary wave number $k_f = \left(\frac{3\pi^2N}{V}\right)^{\frac{1}{3}}$ coinciding with k_l and k_t. Then, there is an important condition $k_f = k_l = k_t$ which determines a relationship between natural oscillator frequencies

$$k_f = \frac{\Omega_l}{c_l} = \frac{\Omega_t}{c_t}. \tag{24}$$

3 Charged Polaritons

In papers [5, 6], we demostrated the so-called transformation of longitudinal and transverse elastic waves into transverse electromagnetic fields with vectors of the electric waves $\vec{E}_l$ and $\vec{E}_t$, corresponding to the ion displacements $\vec{u}_l$ and $\vec{u}_t$, respectively. In turn, the equations of motion are presented in the following forms [5, 6]:

$$M\frac{d^2\vec{u}_l}{dt^2} + M\Omega_l^2\vec{u}_l = -e\vec{E}_l \tag{25}$$

and

$$M\frac{d^2\vec{u}_t}{dt^2} + M\Omega_t^2\vec{u}_t = -e\vec{E}_t. \tag{26}$$

The vector of the electric waves $\vec{E}_l$ and $\vec{E}_t$ are defined by substitution of the meaning of $\vec{u}_l$ and $\vec{u}_t$ from (11) and (12), respectively, into (25) and (26):

$$\vec{E}_l(\vec{r},t)=\frac{C_l}{e\sqrt{V}}\sum_{\vec{k},\sigma}\gamma_{\vec{k},l}\left(\vec{a}_{\vec{k},\sigma}e^{i(\vec{k}\vec{r}+kc_lt)}+\vec{a}^{+}_{\vec{k},\sigma}e^{-i(\vec{k}\vec{r}+kc_lt)}\right) \quad (27)$$

and

$$\vec{E}_t(\vec{r},t)=\frac{C_t}{e\sqrt{V}}\sum_{\vec{k},\sigma}\gamma_{\vec{k},t}\left(\vec{b}_{\vec{k},\sigma}e^{i(\vec{k}\vec{r}+kc_tt)}+\vec{b}^{+}_{\vec{k},\sigma}e^{-i(\vec{k}\vec{r}+kc_tt)}\right), \quad (28)$$

where

$$\gamma_{\vec{k},l}=M\left(k^2c_l^2-\Omega_l^2\right) \quad (29)$$

and

$$\gamma_{\vec{k},t}=M\left(k^2c_t^2-\Omega_t^2\right). \quad (30)$$

On the other hand, by action of the longitudinal and transverse ultrasonic waves on the charged ion [5, 6], these ultrasonic waves are transformed into transverse electromagnetic fields with electric wave vectors $\vec{E}_l$ and $\vec{E}_t$ which in turn describe the de Broglie wave of charged ions expressed via electric $\vec{E}_l(\vec{r},t)$ and $\vec{E}_t(\vec{r},t)$ fields of one ion-wave particle in homogeneous medium. In fact, these electric $\vec{E}_l(\vec{r},t)$ and $\vec{E}_t(\vec{r},t)$ fields satisfy the Maxwell's equations in dielectric medium:

$$curl\,\vec{H}_l-\frac{\varepsilon_l}{c}\frac{d\vec{E}_l}{dt}=0 \quad (31)$$

$$curl\,\vec{E}_l+\frac{1}{c}\frac{d\vec{H}_l}{dt}=0 \quad (32)$$

$$div\,\vec{E}_l=0 \quad (33)$$

$$div\,\vec{H}_l=0 \quad (34)$$

and

$$curl\,\vec{H}_t-\frac{\varepsilon_t}{c}\frac{d\vec{E}_t}{dt}=0 \quad (35)$$

$$curl\,\vec{E}_t+\frac{1}{c}\frac{d\vec{H}_t}{dt}=0 \quad (36)$$

$$div\,\vec{E}_t=0 \quad (37)$$

$$div\,\vec{H}_t=0 \quad (38)$$

with

$$\sqrt{\varepsilon_l}=\frac{c}{c_l} \quad (39)$$

and

$$\sqrt{\varepsilon_l}=\frac{c}{c_l}, \quad (40)$$

where $\vec{H}_l=\vec{H}_l(\vec{r},t)$ and $\vec{H}_t=\vec{H}_t(\vec{r},t)$ are, respectively, the local magnetic fields, corresponding to longitudinal and transverse ultrasonic waves, depending on space coordinate $\vec{r}$ and time t; ε_l and ε_t are, respectively, the dielectric constants for transverse electric fields $\vec{E}_l(\vec{r},t)$ and $\vec{E}_t(\vec{r},t)$ corresponding to longitudinal and transverse ultrasonic waves; c is the velocity of electromagnetic wave in vacuum; $\mu=1$ is the magnetic susceptibility.

When using Eqs. (31–40) and results of letter [8], we may present the transverse electric fields $\vec{E}_l(\vec{r},t)$ and $\vec{E}_t(\vec{r},t)$ by the quantization forms:

$$\vec{E}_l(\vec{r},t)=\frac{A_l}{\sqrt{V}}\sum_{\vec{k}}\left(\vec{c}_{\vec{k}}e^{i(\vec{k}\vec{r}+kc_lt)}+\vec{c}^{+}_{\vec{k}}e^{-i(\vec{k}\vec{r}+kc_lt)}\right) \quad (41)$$

and

$$\vec{E}_t(\vec{r},t)=\frac{A_t}{\sqrt{V}}\sum_{\vec{k}\neq0}\left(\vec{d}_{\vec{k}}e^{i(\vec{k}\vec{r}+kc_tt)}+\vec{d}^{+}_{\vec{k}}e^{-i(\vec{k}\vec{r}+kc_tt)}\right), \quad (42)$$

where A_l and A_t are the unknown constants which are found as below; $\vec{c}^{+}_{\vec{k}}$, $\vec{d}^{+}_{\vec{k}}$ and $\vec{c}_{\vec{k}}$, $\vec{d}_{\vec{k}}$ are, respectively, the Bose vector-operators of creation and annihilation of electric fields of one ion-wave particle with wave vector $\vec{k}$ which are directed along of the wave normal $\vec{s}$ or $\vec{k}=k\vec{s}$. These Bose vector-operators $\vec{E}_l(\vec{r},t)$ and $\vec{E}_t(\vec{r},t)$ are directed to the direction of the unit vectors $\vec{l}$ and $\vec{t}$ which are perpendicular to the wave normal $\vec{s}$; $\hat{N}$ is the operator total number of charged ions.

In this context, we indicate that the vector-operators $\vec{c}^{+}_{\vec{k},\sigma}$, $\vec{c}_{\vec{k},\sigma}$ and $\vec{d}^{+}_{\vec{k},\sigma}$, $\vec{d}_{\vec{k},\sigma}$ satisfy the Bose commutation relations as:

$$\left[\hat{c}_{\vec{k},\sigma},\hat{c}^{+}_{\vec{k}',\sigma'}\right]=\delta_{\vec{k},\vec{k}'}\cdot\delta_{\sigma,\sigma'}$$

$$[\hat{c}_{\vec{k},\sigma},\hat{c}_{\vec{k}',\sigma'}]=0$$

$$[\hat{c}^{+}_{\vec{k},\sigma},\hat{c}^{+}_{\vec{k}',\sigma'}]=0$$

and

$$\left[\hat{d}_{\vec{k},\sigma},\hat{d}^{+}_{\vec{k}',\sigma'}\right]=\delta_{\vec{k},\vec{k}'}\cdot\delta_{\sigma,\sigma'}$$

$$[\hat{d}_{\vec{k},\sigma},\hat{d}_{\vec{k}',\sigma'}]=0$$

$$[\hat{d}^{+}_{\vec{k},\sigma},\hat{d}^{+}_{\vec{k}',\sigma'}]=0.$$

Comparing (41) with (27) and (42) with (28), we get

$$\vec{d}_{\vec{k},\sigma}=\frac{eA_l}{C_l\gamma_{\vec{k},l}}\vec{c}_{\vec{k},\sigma} \quad (43)$$

and

$$\vec{b}_{\vec{k},\sigma} = \frac{eA_t}{C_t\gamma_{\vec{k},t}}\vec{d}_{\vec{k},\sigma}. \tag{44}$$

Now, substituting $\vec{a}_{\vec{k},\sigma}$ and $\vec{b}_{\vec{k},\sigma}$ into (18) and (19), we obtain the reduced form of the Hamiltonian operators $\hat{H}_l$ and $\hat{H}_l$ which are expressed via terms of the electric fields of the ion-wave particle:

$$\begin{aligned}\hat{H}_l = \sum_{\vec{k},\sigma}\frac{e^2A_l^2}{\gamma^2_{\vec{k},l}}\left[\left(\frac{2MNc_l^2k^2}{V}+\frac{2MN\Omega_l^2}{V}\right)\vec{c}^{+}_{\vec{k},\sigma}c_{\vec{k},\sigma}-\right.\\ \left.-\left(\frac{MNc_l^2k^2}{V}-\frac{MN\Omega_l^2}{V}\right)\left(\vec{c}_{-\vec{k},\sigma}\vec{c}_{\vec{k},\sigma}+\vec{c}^{+}_{\vec{k},\sigma}\vec{c}^{+}_{-\vec{k},\sigma}\right)\right]\end{aligned} \tag{45}$$

and

$$\begin{aligned}\hat{H}_t = \sum_{\vec{k},\sigma}\frac{e^2A_t^2}{\gamma^2_{\vec{k},l}}\left[\left(\frac{2MNc_t^2k^2}{V}+\frac{2MN\Omega_t^2}{V}\right)\vec{d}^{+}_{\vec{k},\sigma}d_{\vec{k},\sigma}-\right.\\ \left.-\left(\frac{MNc_t^2k^2}{V}-\frac{MN\Omega_t^2}{V}\right)\left(\vec{d}_{-\vec{k},\sigma}\vec{d}_{\vec{k},\sigma}+\vec{d}^{+}_{\vec{k},\sigma}\vec{d}^{+}_{-\vec{k},\sigma}\right)\right].\end{aligned} \tag{46}$$

To evaluate the energy levels of the operators $\hat{H}_l$ (45) and $\hat{H}_t$ (46) within the diagonal form, we use a transformation of the vector-Bose-operators:

$$\vec{c}_{\vec{k},\sigma} = \frac{\vec{l}_{\vec{k},\sigma}+L_{\vec{k}}\vec{l}^{+}_{-\vec{k},\sigma}}{\sqrt{1-L^2_{\vec{k}}}} \tag{47}$$

and

$$\vec{d}_{\vec{k},\sigma} = \frac{\vec{t}_{\vec{k},\sigma}+M_{\vec{k}}\vec{t}^{+}_{-\vec{k},\sigma}}{\sqrt{1-M^2_{\vec{k}}}}, \tag{48}$$

where $L_{\vec{k}}$ and $M_{\vec{k}}$ are, respectively, the real symmetrical functions of a wave vector $\vec{k}$.

Consequently,

$$\hat{H}_l = \sum_{k<k_f,\sigma}\varepsilon_{\vec{k},l}\vec{l}^{+}_{\vec{k},\sigma}\vec{l}_{\vec{k},\sigma} \tag{49}$$

and

$$\hat{H}_t = \sum_{k<k_f,\sigma}\varepsilon_{\vec{k},t}\vec{t}^{+}_{\vec{k},\sigma}\vec{t}_{\vec{k},\sigma} \tag{50}$$

at

$$L^2_{\vec{k}} = \frac{\frac{2MNc_l^2k^2}{V}+\frac{2MN\Omega_l^2}{V}-\varepsilon_{\vec{k},l}}{\frac{2MNc_l^2k^2}{V}+\frac{2MN\Omega_l^2}{V}+\varepsilon_{\vec{k},l}}$$

$$M^2_{\vec{k}} = \frac{\frac{2MNc_t^2k^2}{V}+\frac{2MN\Omega_l^2}{V}-\varepsilon_{\vec{k},t}}{\frac{2MNc_t^2k^2}{V}+\frac{2MN\Omega_l^2}{V}+\varepsilon_{\vec{k},t}}.$$

Hence, we infer that the Bose-operators $\vec{l}^{+}_{\vec{k},\sigma}$, $\vec{l}_{\vec{k},\sigma}$ and $\vec{t}^{+}_{\vec{k},\sigma}$, $\vec{t}_{\vec{k},\sigma}$ are, respectively, the vector of "creation" and the vector of "annihilation" operators of charged polaritons with spin 1 with the energies:

$$\varepsilon_{\vec{k},l} = \frac{4e^2\rho c_lA_l^2\Omega_lk}{\gamma^2_{\vec{k},l}} \tag{51}$$

and

$$\varepsilon_{\vec{k},t} = \frac{4e^2\rho c_tA_t^2\Omega_tk}{\gamma^2_{\vec{k},t}}. \tag{52}$$

Hence, we note that these polaritons are charged because the Hamiltonian contains the square of charge, e^2. This picture is similar to the Coulomb interaction between two charges.

Obviously, at small wave numbers $k \ll \frac{\Omega_l}{c_l}$ and $k \ll \frac{\Omega_t}{c_t}$, these charged polaritons are presented as charged phonons with energies:

$$\varepsilon_{\vec{k},l} \approx \hbar kv_l \tag{53}$$

and

$$\varepsilon_{\vec{k},t} \approx \hbar kv_t, \tag{54}$$

where $v_l = \frac{4\rho c_le^2A_l^2}{\hbar M^2\Omega_l^3}$ and $v_t = \frac{4\rho c_te^2A_t^2}{\hbar M^2\Omega_t^3}$ are, respectively, the velocities of charged phonons with spin 1 corresponding to the longitudinal and transverse acoustic fields. To find the unknown constants A_l^2 and A_t^2, we suggest that $v_l = c_l$ and $v_t = c_t$ as it was presented in [1]. This suggestion leads to the results obtained in [1] and in turn presented in Debye's theory. Thus, when choosing $A_l^2 = \frac{\hbar M^2\Omega_l^3}{4\rho e^2}$ and $A_t^2 = \frac{\hbar M^2\Omega_t^3}{4\rho e^2}$, the energies of charged polaritons represent as

$$\varepsilon_{\vec{k},l} = \frac{\hbar\Omega_l^4c_lk}{\left(k^2c_l^2-\Omega_l^2\right)^2} \tag{55}$$

and

$$\varepsilon_{\vec{k},t} = \frac{\hbar\Omega_t^4c_tk}{\left(k^2c_t^2-\Omega_t^2\right)^2}, \tag{56}$$

which at large wave numbers $k \gg \frac{\Omega_l}{c_l}$ and $k \gg \frac{\Omega_t}{c_t}$, and taking into account (24), leads to the following form for the energies of charged polaritons:

$$\varepsilon_{\vec{k},l} = \frac{\hbar k_f^4c_l}{k^3}. \tag{57}$$

In fact, the stimulated vibration of ions by elastic waves lead to the formation of the charged polaritons with spin 1.

Thus, we predicted the existence of a new type of charged quasiparticles in nature. On the other hand, we note that the quantization of elastic fields is fulfilled for the new model of metals. In analogous manner, as it was presented in [1], we may show that the acoustic field operator does not commute with its momentum density.

Submitted on January 6, 2011 / Accepted on January 10, 2011

References

1. Minasyan V. N., Samoilov V. N. Sound-Particles and Phonons with Spin 1. *Progress in Physics*, 2011, v. 1, 81–86.
2. Einstein A. Die Plancksche Theorie der Strahlung und die Theorie der spezifischen Warme. *Annalen der Physik*, 1907, v. 22, 180–190.
3. Debye P. Zur Theorie der spezifischen Waerme. *Annalen der Physik*, 1912, v. 39, 789–839.
4. Minasyan V. N., Samoilov V. N. Formation of Singlet Fermion Pairs in the Dilute Gas of Boson-Fermion Mixture. *Progress in Physics*, 2010, v. 4, 3–9.
5. Minasyan V. N., Samoilov V. N. The Intensity of the Light Diffraction by Supersonic Longitudinal Waves in Solid, *Progress in Physics*, 2010, v. 2, 60–63.
6. Minasyan V. N., Samoilov V. N. Dispersion of Own Frequency of Ion-dipole by Supersonic Transverse Wave in Solid, *Progress in Physics*, 2010, v. 4, 10–12.
7. de Broglie L. Researches on the quantum theory. *Annalen der Physik*, 1925, v. 3, 22–32.
8. Minasyan V. N., Samoilov V. N. New resonance-polariton Bose-quasiparticles enhances optical transmission into nanoholes in metal films. *Physics Letters A*, 2011, v. 375, 698–711.
9. Landau L. D., Lifshiz E. M. Theory of Elasticity. *Theoretical Physics*, 1987, v. 11, 124–127.
10. Dirac P. A. M. The Principles of Quantum Mechanics. Clarendon press, Oxford, (1958).

New Fundamental *Light Particle* and Breakdown of Stefan-Boltzmann's Law

Vahan Minasyan and Valentin Samoilov
Scientific Center of Applied Research, JINR, Dubna, 141980, Russia
E-mails: mvahan@scar.jinr.ru; scar@off-serv.jinr.ru

Recently, we predicted the existence of fundamental particles in Nature, neutral *Light Particles* with spin 1 and rest mass $m = 1.8{\times}10^{-4}m_e$, in addition to electrons, neutrons and protons. We call these particles Light Bosons because they create electromagnetic field which represents Planck's gas of massless photons together with a gas of *Light Particles* in the condensate. Such reasoning leads to a breakdown of Stefan–Boltzmann's law at low temperature. On the other hand, the existence of new fundamental neutral *Light Particles* leads to correction of such physical concepts as Bose-Einstein condensation of photons, polaritons and exciton polaritons.

1 Introduction

First, the quantization scheme for the local electromagnetic field in vacuum was presented by Planck in his black body radiation studies [1]. In this context, the classical Maxwell equations lead to appearance of the so-called ultraviolet catastrophe; to remove this problem, Planck proposed the model of the electromagnetic field as an ideal Bose gas of massless photons with spin one. However, Dirac [2] showed the Planck photon-gas could be obtained through a quantization scheme for the local electromagnetic field, presenting a theoretical description of the quantization of the local electromagnetic field in vacuum by use of a model Bose-gas of local plane electromagnetic waves propagating by speed c in vacuum.

In a different way, in regard to Plank and Dirac's models, we consider the structure of the electromagnetic field [3] as a non-ideal gas consisting of N neutral *Light Bose Particles* with spin 1 and finite mass m, confined in a box of volume V. The form of potential interaction between *Light Particles* is defined by introduction of the principle of wave-particle duality of de Broglie [4] and principle of gauge invariance. In this respect, a non-ideal Bose-gas consisting of *Light Particles* with spin 1 and non-zero rest mass is described by Planck's gas of massless photons together with a gas consisting of *Light Particles* in the condensate. In this context, we defined the *Light Particle* by the model of hard sphere particles [5]. Such definition of *Light Particles* leads to cutting off the spectrum of the electromagnetic wave by the boundary wave number $k_0 = \frac{mc}{\hbar}$ or boundary frequency $\omega_\gamma = 10^{18}$ Hz of gamma radiation at the value of the rest mass of the *Light Particle* $m = 1.8 \times 10^{-4}m_e$. On the other hand, the existence of the boundary wave number $k_0 = \frac{mc}{\hbar}$ for the electromagnetic field in vacuum is connected with the characteristic length of the interaction between two neighboring *Light Bosons* in the coordinate space with the minimal distance $d = \frac{1}{k_0} = \frac{\hbar}{mc} = 2{\times}10^{-9}m$. This reasoning determines the density of *Light Bosons* $\frac{N}{V}$ as $\frac{N}{V} = \frac{3}{4\pi d^3} = 0.3{\times}10^{26}m^{-3}$.

It is well known that Stefan-Boltzmann's law [6] for thermal radiation, presented by Planck's formula [1], determines the average energy density $\frac{U}{V}$ as

$$\frac{U}{V} = \frac{2}{V}\sum_{0\le k<\infty} \hbar kc\overline{i^{+}_{\vec{k}} i_{\vec{k}}} = \sigma T^4, \qquad (1)$$

where $\hbar$ is the Planck constant; σ is the Stefan-Boltzmann constant; $\overline{i^{+}_{\vec{k}} i_{\vec{k}}}$ is the average number of photons with the wave vector $\vec{k}$ at the temperature T:

$$\overline{i^{+}_{\vec{k}} i_{\vec{k}}} = \frac{1}{e^{\frac{\hbar kc}{kT}} - 1}. \qquad (2)$$

Obviously, at $T = 0$, the average energy density vanishes in Eq.(1), i.e. $\frac{U}{V} = 0$, which follows from Stefan-Boltzmann's law.

However, as we show, the existence of the predicted *Light Particles* breaks Stefan-Boltzmann's law for black body radiation at low temperature.

2 Breakdown of Stefan-Boltzmann's law

Now, we consider the results of letter [3], where the average energy density of black radiation $\frac{U}{V}$ is represented as:

$$\frac{U}{V} = \frac{mc^2 N_{0,T}}{V} + \frac{2}{V}\sum_{0\le k<k_0} \hbar kc\overline{i^{+}_{\vec{k}} i_{\vec{k}}}, \qquad (3)$$

where $\frac{mc^2 N_{0,T}}{V}$ is a new term, in regard to Plank's formula (1), which determines the energy density of *Light Particles* in the condensate; $\frac{N_{0,T}}{V}$ is the density of *Light Particles* in the condensate.

In this respect, the equation for the density of *Light Particles* in the condensate $\frac{N_{0,T}}{V}$ represents as

$$\frac{N_{0,T}}{V} = \frac{N}{V} - \frac{1}{V}\sum_{0<k<k_0} \frac{L^2_{\vec{k}}}{1 - L^2_{\vec{k}}} - \frac{1}{V}\sum_{0<k<k_0} \frac{1 + L^2_{\vec{k}}}{1 - L^2_{\vec{k}}}\overline{i^{+}_{\vec{k}} i_{\vec{k}}} \qquad (4)$$

with the real symmetrical function $L_{\vec{k}}$ from the wave vector $\vec{k}$:

$$L^2_{\vec{k}} = \frac{\frac{\hbar^2 k^2}{2m} + \frac{mc^2}{2} - \hbar kc}{\frac{\hbar^2 k^2}{2m} + \frac{mc^2}{2} + \hbar kc}. \quad (5)$$

Our calculation shows that at absolute zero the value of $\overline{\vec{i}^+_{\vec{k}} \vec{i}_{\vec{k}}} = 0$, and therefore the average energy density of black radiation $\frac{U}{V}$ reduces to

$$\frac{U}{V} = \frac{mc^2 N_{0,T=0}}{V} = \frac{mc^2 N}{V} - \frac{m^4 c^5 B(2,3)}{4\pi^2 \hbar^3} \approx \frac{mc^2 N}{V}, \quad (6)$$

where $B(2,3) = \int_0^1 x(1-x)^2 dx = 0.1$ is the beta function.

Thus, the average energy density of black radiation $\frac{U}{V}$ is a constant at absolute zero. In fact, there is a breakdown of Stefan-Boltzmann's law for thermal radiation.

In conclusion, it should be also noted that *Light Bosons* in vacuum create photons, while *Light Bosons* in a homogeneous medium generate the so-called polaritons. This fact implies that photons and polaritons are quasiparticles, therefore, Bose-Einstein condensation of photons [7], polaritons [8] and exciton polaritons [9] has no physical sense.

Acknowledgements

This work is dedicated to the memory of the Great British Physicist Prof. Marshall Stoneham, F.R.S., (London Centre for Nanotechnology, and Department of Physics and Astronomy University College London, UK), who helped us with English. We are very grateful to him.

Submitted on January 6, 2011 / Accepted on January 25, 2011

References

1. Planck M. On the Law of Distribution of Energy in the Normal Spectrum. *Annalen der Physik*, 1901, v. 4, 553–563.
2. Dirac P. A. M. The Principles of Quantum Mechanics. Clarendon Press, Oxford, 1958.
3. Minasyan V. N., Samoilov V. N. New resonance-polariton Bose-quasiparticles enhances optical transmission into nanoholes in metal films. *Physics Letters A*, 2011, v. 375, 698–711.
4. de Broglie L. Researches on the quantum theory. *Annalen der Physik*, 1925, v. 3, 22–32.
5. Huang K. Statistical Mechanics. John Wiley, New York, 1963.
6. Stefan J. Uber die Beziehung zwischen der Warmestrahlung und der Temperatur. In: Sitzungsberichte der mathematisch-naturwissenschaftlichen Classe der kaiserlichen Akademie der Wissenschaften, Bd. 79 (Wien 1879), 391–428.
7. Klaers J., Schmitt J., Vewinger F., Weitz M. Bose-Einstein condensation of photons in an optical microcavity. *Nature*, 2010, v. 468, 545–548.
8. Balili R., Hartwell V., Snoke D., Pfeiffer L., West K. Bose-Einstein condensation of microcavity polaritons in a trap. *Science*, 2007, v. 316, 1007–1010.
9. Kasprzak J. et al. Bose-Einstein condensation of exciton polaritons. *Nature*, 2006, v. 443, 409–414.

The Point Mass Concept

Bo Lehnert

Alfvén Laboratory, Royal Institute of Technology, SE–10044 Stockholm, Sweden. E-mail: Bo.Lehnert@ee.kth.se

A point-mass concept has been elaborated from the equations of the gravitational field. One application of these deductions results in a black hole configuration of the Schwarzschild type, having no electric charge and no angular momentum. The critical mass of a gravitational collapse with respect to the nuclear binding energy is found to be in the range of 0.4 to 90 solar masses. A second application is connected with the speculation about an extended symmetric law of gravitation, based on the options of positive and negative mass for a particle at given positive energy. This would make masses of equal polarity attract each other, while masses of opposite polarity repel each other. Matter and antimatter are further proposed to be associated with the states of positive and negative mass. Under fully symmetric conditions this could provide a mechanism for the separation of antimatter from matter at an early stage of the universe.

1 Introduction

In connection with an earlier elaborated revised quantum-electrodynamic theory, a revised renormalisation procedure has been developed to solve the problem of infinite self-energy of the point-charge-like electron [1, 2]. In the present investigation an analogous procedure is applied to the basic equations of gravitation, to formulate a corresponding point mass concept. Two applications result from such a treatment. The first concerns the special Schwarzschild case of a black hole with its critical limit of gravitational collapse. The second application is represented by the speculation about an extended form of the gravitation law, in which full symmetry is obtained by including both positive and negative mass concepts. This further leads to the question whether such concepts could have their correspondence in matter and antimatter, and in their mutual separation.

2 The conventional law of gravitation

In this investigation the analysis is limited to the steady case of spherical symmetry, in a corresponding frame where r is the only independent variable.

2.1 Basic equations

Following Bergmann [3], a steady gravitational field strength

$$\mathbf{g} = -\nabla\phi \tag{1}$$

is considered which originates from the potential $\phi(r)$. The source of the field strength is a mass density ρ related to $\mathbf{g}$ by

$$-\mathrm{div}\,\mathbf{g} = 4\pi G\rho = \nabla^2\phi = \frac{1}{r^2}\frac{d}{dr}\left(r^2\frac{d\phi}{dr}\right), \tag{2}$$

where $G = 6.6726\times10^{-11}\ \mathrm{m^3kg^{-1}s^{-2}}$ is the constant of gravitation in SI units. The associated force density becomes

$$\mathbf{f} = \rho\,\mathbf{g}\,. \tag{3}$$

In the conventional interpretation there only exists a positive mass density $\rho \geqslant 0$. This makes in a way the gravitational field asymmetric, as compared to the electrostatic field which includes both polarities of electric charge density.

A complete form of the potential ϕ would consist of a series of both positive and negative powers of r, but the present analysis will be restricted and simplified by studying each power separately, in the form

$$\phi(r) = \phi_0\left(\frac{r}{r_0}\right)^{\alpha}. \tag{4}$$

Here ϕ_0 is a constant, r_0 represents a characteristic dimension and α is a positive or negative integer. Equation (2) yields

$$4\pi G\rho = \frac{\phi_0}{r_0^{\alpha}}\,\alpha(\alpha+1)\,r^{\alpha-2} > 0\,. \tag{5}$$

When limiting the investigations by the condition $\rho > 0$, the cases $\alpha = 0$ and $\alpha = -1$ have to be excluded, leaving the regimes of positive $\alpha = (1, 2, \ldots)$ and negative $\alpha = (-2, -3, \ldots)$ to be considered for *positive* values of ϕ_0.

2.2 Point mass formation

For reasons to become clear from the deductions which follow, we now study a spherical configuration in which the mass density ρ is zero within an inner hollow region $0 \leqslant r \leqslant r_i$, and where $\rho > 0$ in the outer region $r > r_i$. From relation (5) the total integrated mass $P(r)$ inside the radius r then becomes

$$P(r) = \int_0^r \rho\,4\pi r^2 dr = \frac{1}{G}\frac{\phi_0}{r_0^{\alpha}}\,\alpha\left(r^{\alpha+1} - r_i^{\alpha+1}\right) > 0 \tag{6}$$

with a resulting local field strength $\mathbf{g} = (g, 0, 0)$ given by

$$g(r) = -G\frac{P(r)}{r^2} = -\frac{\phi_0}{r_0^{\alpha}}\,\frac{\alpha}{r^2}\left(r^{\alpha+1} - r_i^{\alpha+1}\right) < 0 \tag{7}$$

and a local force density $\mathbf{f} = (f, 0, 0)$ where

$$f(r) = -\frac{1}{4\pi G}\frac{\phi_0}{r_0^{\alpha}}^2 \alpha^2(\alpha+1) r^{\alpha-4}\left(r^{\alpha+1} - r_i^{\alpha+1}\right) < 0\,. \quad (8)$$

Here all (P, g, f) refer to the range $r \geqslant r_i$, and $\phi_0 > 0$.

A distinction is further made between the two regimes of positive and negative α:

- When $\alpha = (1, 2, \ldots)$ of a convergent potential (4), this hollow configuration has an integrated mass (6) which increases monotonically with r, from zero at $r = r_i$ to large values. This behaviour is the same for a vanishing r_i and does not lead to a point-like mass at small r_i.
- When $\alpha = (-2, -3, \ldots)$ of a divergent potential (4), the hollow configuration leads to a point-mass-like geometry at small r_i. This is similar to a point-charge-like geometry earlier treated in a model of the electron [1, 2], and will be considered in the following analysis.

2.3 The renormalised point mass

In the range $\alpha \leqslant -2$ expressions (6)–(8) are preferably cast into a form with $\gamma = -\alpha \geqslant 2$ where

$$P(r) = \frac{1}{G}\left(\phi_0 r_0^{\gamma}\right)\gamma\left(r_i^{-\gamma+1} - r^{-\gamma+1}\right) > 0\,, \quad (9)$$

$$g(r) = -\left(\phi_0 r_0^{\gamma}\right)\frac{\gamma}{r^2}\left(r_i^{-\gamma+1} - r^{-\gamma+1}\right) < 0\,, \quad (10)$$

$$f(r) = -\frac{1}{4\pi G}\left(\phi_0 r_0^{\gamma}\right)^2 \gamma^2(\gamma-1) r^{-\gamma-4}\left(r_i^{-\gamma+1} - r^{-\gamma+1}\right) < 0. \quad (11)$$

Here an erroneous result would be obtained if the terms including r_i are dropped and the hollow configuration is abandoned. Due to eqs. (9)–(11) this would namely result in a negative mass P, a positive field strength g, and a repulsive local gravitational force density f.

The radius r_i of the hollow inner region is now made to approach zero. The total integrated mass of eq. (9) is then concentrated to an infinitesimally small layer. Applying a revised renormalisation procedure in analogy with an earlier scheme [1, 2], we "shrink" the combined parameters $\phi_0 r_0^{\gamma}$ and $r_i^{\gamma-1}$ in such a way that

$$\phi_0 r_0^{\gamma} = c_{\phi r}\cdot\varepsilon \qquad r_i^{\gamma-1} = c_i\cdot\varepsilon \qquad 0 < \varepsilon \ll 1\,, \quad (12)$$

where ε is a smallness parameter and $c_{\phi r}$ and c_i are positive constants. A further introduction of

$$P_0 \equiv \frac{1}{G}\frac{\gamma\, c_{\phi r}}{c_i} \quad (13)$$

results in $P(r) = 0$ for $r \leqslant r_i$ and

$$P(r) = P_0\left[1 - \left(\frac{r_i}{r}\right)^{\gamma-1}\right] \qquad r > r_i\,. \quad (14)$$

In the limit $\varepsilon \to 0$ and $r_i \to 0$ there is then a point mass P_0 at the origin. This mass generates a field strength

$$g(r) = -G\frac{P_0}{r^2} \quad (15)$$

at the distance r according to equations (10), (12) and (13). With another point mass P_1 at the distance r, there is a mutual attraction force

$$F_{01} = P_1 g(r) = -G\frac{P_0 P_1}{r^2}\,, \quad (16)$$

which is identical with the gravitation law for two point masses.

To further elucidate the result of eqs. (12)-(16) it is first observed that, in the conventional renormalisation procedure, the divergent behaviour of an infinite self-energy is outbalanced by adding extra infinite ad-hoc *counter-terms* to the Lagrangian, to obtain a finite difference between two "infinities". Even if such a procedure has been successful, however, it does not appear to be quite acceptable from the logical and physical points of view. The present revised procedure represented by expressions (12) implies on the other hand that the "infinity" of the divergent potential ϕ_0 at a shrinking radius r_i is instead outbalanced by the "zeros" of the inherent shrinking *counter-factors* $c_{\phi r}\cdot\varepsilon$ and $c_i\cdot\varepsilon$.

3 A black hole of Schwarzschild type

A star which collapses into a black hole under the compressive action of its own gravitational field is a subject of ever increasing interest. In its most generalized form the physics of the black hole includes both gravitational and electromagnetic fields as well as problems of General Relativity, to account for its mass, net electric charge, and its intrinsic angular momentum. The associated theoretical analysis and related astronomical observations have been extensively described in a review by Misner, Thorne and Wheeler [4] among others. Here the analysis of the previous section will be applied to the far more simplified special case by Schwarzschild, in which there is no electric charge and no angular momentum. Thereby it has also to be noticed that no black hole in the universe has a substantial electric charge [4].

3.1 The inward directed gravitational pressure

From eq. (11) is seen that the inward directed local force density is zero for $r \leqslant r_i$, increases with r to a maximum within a thin shell, and finally drops to zero at large r. The integrated inward directed gravitational pressure on this shell thus becomes

$$p = \int_0^{\infty} f\,dr = -\frac{G}{8\pi}\frac{(\gamma-1)^2}{(\gamma+1)(\gamma+3)}\frac{P_0^2}{r_i^4} \quad (17)$$

in the limit of small ε and r_i.

When this pressure becomes comparable to the relevant energy density of the compressed matter, a corresponding gravitational collapse is expected to occur.

3.2 Gravitational collapse of the nuclear binding forces

Here we consider the limit at which matter is compressed into a body of densely packed nucleons, and when the pressure of eq. (17) tends to exceed the energy density of the nucleon binding energy. The radius of a nucleus is [5]

$$r_N = 1.5 \times 10^{-15} A^{1/2} \quad [\mathrm{m}], \tag{18}$$

where A is the mass number. A densely packed sphere of N nuclei has the volume

$$V_N = \frac{4}{3}\pi N r_N^3 = \frac{4}{3}\pi r_{eq}^3 , \tag{19}$$

where r_{eq} is the equivalent radius of the sphere. The total binding energy of a nucleus is further conceived as the work required to completely dissociate it into its component nucleons. This energy is about 8 MeV per nucleon [5, 6]. With A nucleons per nucleus, the total binding energy of a body of N nuclei thus becomes

$$W_N = NA\, w_N , \tag{20}$$

where $w_N = 8$ MeV $= 1.28 \times 10^{-12}$ J. The equivalent binding energy density of the body is then

$$p_N = \frac{W_N}{V_N} = \frac{3}{4}\frac{A w_N}{\pi r_N^3} = 0.907 \times 10^{32} A^{-1/2} \quad [\mathrm{J \times m^{-3}}]. \tag{21}$$

The shell-like region of gravitational pressure has a force density (11) which reaches its maximum at the radius

$$r_m = r_i \left(\frac{2\gamma + 3}{\gamma + 4}\right)^{1/(\gamma-1)} \tag{22}$$

being only a little larger than r_i. This implies that the radius r_{eq} of eq. (19) is roughly equal to r_i and

$$r_i \cong r_N N^{1/3}. \tag{23}$$

With N nuclei of the mass Am_p and m_p as the proton mass, the total mass becomes

$$P_0 = NAm_p , \tag{24}$$

which yields

$$r_i \cong r_N \left(\frac{P_0}{Am_p}\right)^{1/3} = 1.26 \times 10^{-6} A^{1/6} P_0^{1/3} \quad [\mathrm{m}]. \tag{25}$$

This result finally combines with eq. (17) to an equivalent gravitational pressure

$$p = -1.1 \times 10^{12} \frac{(\gamma-1)^2}{(\gamma+1)(\gamma+3)} A^{-2/3} P_0^{2/3} \quad [\mathrm{J \times m^{-3}}]. \tag{26}$$

For a gravitational collapse defined by $-p > p_N$ the point mass P_0 then has to exceed the critical limit

$$P_{0c} \cong 7.5 \times 10^{29} \left[\frac{(\gamma+1)(\gamma+3)}{(\gamma-1)^2}\right]^{3/2} A^{1/4} \quad [\mathrm{kg}]. \tag{27}$$

For $\gamma \geqslant 2$ and $1 \leqslant A \leqslant 250$, the critical mass would then be found in the range of about $0.4 \leqslant P_{0c} \leqslant 90$ solar masses of about 1.98×10^{30} kg.

4 Speculations about a generalized law of gravitation

The Coulomb law of interaction between electrically charged bodies is symmetric in the sense that it includes both polarities of charge and attractive as well as repulsive forces. The classical Newtonian law of gravitation includes on the other hand only one polarity of mass and only attractive forces. In fact, this asymmetry does not come out as a necessity from the basic equations (1)–(3) of a curl-free gravitational field strength. The question could therefore be raised whether a more general and symmetric law of gravitation could be deduced from the same equations, and whether this could have a relevant physical interpretation.

4.1 Mass polarity

In relativistic mechanics the momentum $\mathbf{p}$ of a particle with the velocity $\mathbf{u}$ and rest mass m_0 becomes [7]

$$\mathbf{p} = m_0 \mathbf{u} \left[1 - \left(\frac{u}{c}\right)^2\right]^{-1/2} . \tag{28}$$

With the energy E of the particle, the Lorentz invariance further leads to the relation

$$p^2 - \frac{E^2}{c^2} = -m_0^2 c^2, \tag{29}$$

where $p^2 = \mathbf{p}^2$ and $u^2 = \mathbf{u}^2$. Equations (28) and (29) yield

$$E^2 = m_0^2 c^4 \left[1 - \left(\frac{u}{c}\right)^2\right]^{-1} \equiv m^2 c^4, \tag{30}$$

leading in principle to two roots

$$E = \pm mc^2. \tag{31}$$

In this investigation the discussion is limited to a positive energy E, resulting in positive and negative gravitational masses

$$m = \pm \frac{E}{c^2} \qquad E > 0 . \tag{32}$$

This interpretation differs from that of the negative energy states of positrons proposed in the "hole" theory by Dirac [8] corresponding to the plus sign in eq. (31) and where both E and m are negative.

4.2 An extended law of gravitation

With the possibility of negative gravitational masses in mind, we now return to the potential ϕ of equations (1) and (4) where the amplitude factor ϕ_0 can now adopt both positive and negative values, as defined by the notation $\phi_{0+} > 0$ and $\phi_{0-} < 0$, and where corresponding subscripts are introduced for (P, g, f, P_0) of eqs. (9)–(11) and (13). Then $P_+ > 0$, $P_- < 0$, $P_{0+} > 0$, $P_{0-} < 0$, $g_+ < 0$, $g_- > 0$, but $f_+ < 0$ and $f_- < 0$ always represent an attraction force due to the quadratic dependence on ϕ_0 in eq. (11). With P_{1+} or P_{1-} as an additional point mass

at the distance r from P_{0+} or P_{0-}, there is then an extended form of the law (16), as represented by the forces

$$P_{1+}g_{+} = -G\frac{P_{0+}P_{1+}}{r^2} = P_{1-}g_{-} = -G\frac{P_{0-}P_{1-}}{r^2}\,, \qquad (33)$$

$$P_{1+}g_{-} = G\frac{P_{0-}P_{1+}}{r^2} = P_{1-}g_{+} = G\frac{P_{0-}P_{1+}}{r^2}\,. \qquad (34)$$

These relations are symmetric in the gravitational force interactions, where masses of equal polarity attract each other, and masses of opposite polarity repel each other. It would imply that the interactions in a universe consisting entirely of negative masses would become the same as those in a universe consisting entirely of positive masses. In this way specific mass polarity could, in fact, become a matter of definition.

4.3 A possible rôle of antimatter

At this point the further question may be raised whether the states of positive and negative mass could be associated with those of matter and antimatter, respectively. A number of points become related to such a proposal.

The first point concerns an experimental test of the repulsive behaviour due to eq. (34). If an electrically neutral beam of anti-matter, such as of antihydrogen atoms, could be formed in a horizontal direction, such a beam would be deflected upwards if consisting of negative mass. However, the deflection is expected to be small and difficult to measure.

A model has earlier been elaborated for a particle with elementary charge, being symmetric in its applications to the electron and the positron [1, 2]. The model includes an electric charge q_0, a rest mass m_0, and an angular momentum s_0 of the particle. The corresponding relations between included parameters are easily seen to be consistent with electron-positron pair formation in which $q_0 = -e$, $m_0 = +E/c^2$ and $s_0 = +h/4\pi$ for the electron and $q_0 = +e$, $m_0 = -E/c^2$ and $s_0 = +h/4\pi$ for the positron when the formation is due to a photon of spin $+h/2\pi$. The energy of the photon is then at least equal to $2E$ where the electron and the photon both have positive energies E.

The energy of photons and their electromagnetic radiation field also have to be regarded as an equivalent mass due to Einstein's mass-energy relation. This raises the additional question whether full symmetry also requires the photon to have a positive or negative gravitational mass, as given by

$$m_\nu = \pm\frac{h\nu}{c^2}\,. \qquad (35)$$

If equal proportions of matter and antimatter would have been formed at an early stage of the universe, the repulsive gravitational force between their positive and negative masses could provide a mechanism which expels antimatter from matter and vice versa, also under fully symmetric conditions. Such a mechanism can become important even if the gravitational forces are much weaker than the electrostatic ones, because matter and antimatter are expected to appear as electrically quasi-neutral cosmical plasmas. The final result would come out to be separate universes of matter and antimatter.

In a theory on the metagalaxy, Alfvén and Klein [9] have earlier suggested that there should exist limited regions in our universe which contain matter or antimatter, and being separated by thin boundary layers within which annihilation reactions take place. A simplified model of such layers has been established in which the matter-antimatter "ambiplasma" is immersed in a unidirectional magnetic field [10]. The separation of the cells of matter from those of antimatter by a confining magnetic field geometry in three spatial directions is, however, a problem of at least the same complication as that of a magnetically confined fusion reactor.

5 Conclusions

From the conventional equations of the gravitational field, the point-mass concept has in this investigation been elaborated in terms of a revised renormalisation procedure. In a first application a black hole configuration of the Schwarzschild type has been studied, in which there is no electric charge and no angular momentum. A gravitational collapse in respect to the nuclear binding energy is then found to occur at a critical point mass in the range of about 0.4 to 90 solar masses. This result becomes modified if the collapse is related to other restrictions such as to the formation of "primordial black holes" growing by the accretion of radiation and matter [4], or to phenomena such as a strong centrifugal force.

A second application is represented by the speculation about an extended law of gravitation, based on the options of positive and negative mass of a particle at a given positive energy, and on the basic equations for a curl-free gravitational fieldstrength. This would lead to a fully symmetric law due to which masses of equal polarity attract each other, and masses of opposite polarity repel each other. A further proposal is made to associate matter and antimatter with the states of positive and negative mass. Even under fully symmetric conditions, this provides a mechanism for separating antimatter from matter at an early stage of development of the universe.

After the completion of this work, the author has been informed of a hypothesis with negative mass by Choi [11], having some points in common with the present paper.

Submitted on January 15, 2011 / Accepted on January 17, 2011

References

1. Lehnert B. A revised electromagnetic theory with fundamental applications. Swedish Physics Archive. Edited by D. Rabounski, The National Library of Sweden, Stockholm, 2008; and Bogolyubov Institute for Theoretical Physics. Edited by Z. I. Vakhnenko and A. Zagorodny, Kiev, 2008.
2. Lehnert B. Steady particle states of revised electromagnetics. *Progress in Physics*, 2006, v. 3, 43–50.
3. Bergmann P. G. Introduction to the theory of relativity. Prentice Hall, Inc., New York, 1942, Ch. X.

4. Misner C. W., Thorne K. S., Wheeler J. A. Gravitation. W. H. Freeman and Co., San Francisco and Reading, 1973, Ch. 33.
5. Bethe H. A. Elementary nuclear theory. John Wiley & Sons, Inc., New York, Chapman and Hall, Ltd., London, 1947, pp. 8 and 17.
6. Fermi E. Nuclear physics. Revised edition. The University of Chicago Press, 1950, p. 3.
7. Møller C. The theory of relativity. Oxford, Claredon Press, 1952, Ch. III.
8. Schiff L. I. Quantum mechanics. McGrawHill Book Comp., Inc., New York, Toronto, London, 1949, Ch. XII, Sec. 44.
9. Alfvén H., Klein O. Matter-antimatter annihilation and cosmology. *Arkiv för Fysik*, 1962, v. 23, 187–195.
10. Lehnert B. Problems of matter-antimatter boundary layers. *Astrophysics and Space Science*, 1977, v. 46, 61–71.
11. Choi Hyoyoung. Hypothesis of dark matter and dark energy with negative mass. viXra.org/abs/0907.0015, 2010.

Quark Annihilation and Lepton Formation versus Pair Production and Neutrino Oscillation: The Fourth Generation of Leptons

T. X. Zhang

Department of Physics, Alabama A & M University, Normal, Alabama
E-mail: tianxi.zhang@aamu.edu

The emergence or formation of leptons from particles composed of quarks is still remained very poorly understood. In this paper, we propose that leptons are formed by quark-antiquark annihilations. There are two types of quark-antiquark annihilations. Type-I quark-antiquark annihilation annihilates only color charges, which is an incomplete annihilation and forms structureless and colorless but electrically charged leptons such as electron, muon, and tau particles. Type-II quark-antiquark annihilation annihilates both electric and color charges, which is a complete annihilation and forms structureless, colorless, and electrically neutral leptons such as electron, muon, and tau neutrinos. Analyzing these two types of annihilations between up and down quarks and antiquarks with an excited quantum state for each of them, we predict the fourth generation of leptons named lambda particle and neutrino. On the contrary quark-antiquark annihilation, a lepton particle or neutrino, when it collides, can be disintegrated into a quark-antiquark pair. The disintegrated quark-antiquark pair, if it is excited and/or changed in flavor during the collision, will annihilate into another type of lepton particle or neutrino. This quark-antiquark annihilation and pair production scenario provides unique understanding for the formation of leptons, predicts the fourth generation of leptons, and explains the oscillation of neutrinos without hurting the standard model of particle physics. With this scenario, we can understand the recent OPERA measurement of a tau particle in a muon neutrino beam as well as the early measurements of muon particles in electron neutrino beams.

1 Introduction

Elementary particles can be categorized into hadrons and leptons in accord with whether they participate in the strong interaction or not. Hadrons participate in the strong interaction, while leptons do not. All hadrons are composites of quarks [1-3]. There are six types of quarks denoted as six different flavors: up, down, charm, strange, top, and bottom, which are usually grouped into three generations: $\{u, d\}$, $\{c, s\}$, $\{t, b\}$. Color charge is a fundamental property of quarks, which has analogies with the notion of electric charge of particles. There are three varieties of color charges: red, green, and blue. An antiquark's color is antired, antigreen, or antiblue. Quarks and antiquarks also hold electric charges but they are fractional, $\pm e/3$ or $\pm 2e/3$, where $e = 1.6 \times 10^{-19}$ C is the charge of proton.

There are also six types of leptons discovered so far, which are electron, muon, and tau particles and their corresponding neutrinos. These six types of leptons are also grouped into three generations: $\{e^-, \nu_e\}$, $\{\mu^-, \nu_\mu\}$, $\{\tau^-, \nu_\tau\}$. The antiparticles of the charged leptons have positive charges. It is inappropriate to correspond the three generations of leptons to the three generations of quarks because all these three generations of leptons are formed or produced directly in association with only the first generation of quarks. We are still unsure that how leptons form and whether the fourth generation of leptons exists or not [4-8].

In this paper, we propose that leptons, including the fourth generation, are formed by quark-antiquark annihilations. Electrically charged leptons are formed when the color charges of quarks and antiquarks with different flavors are annihilated, while neutrinos are formed when both the electric and color charges of quarks and antiquarks with the same flavor are annihilated. We also suggest that quarks and antiquarks can be produced in pairs from disintegrations of leptons. This quark-antiquark annihilation and pair production model predicts the fourth generation of leptons and explains the measurements of neutrino oscillations.

2 Quark Annihilation and Lepton Formation

Quark-antiquark annihilation is widely interested in particle physics [9-13]. A quark and an antiquark may annihilate to form a lepton. There are two possible types of quark-antiquark annihilations. Type-I quark-antiquark annihilation only annihilates their color charges. It is an incomplete annihilation usually occurred between different flavor quark and antiquark and forms structureless and colorless but electrically charged leptons such as e^-, e^+ , μ^-, μ^+, τ^-, and τ^+. Type-II quark-antiquark annihilation annihilates both electric and color charges. It is a complete annihilation usually occurred between same flavor quark and antiquark and forms

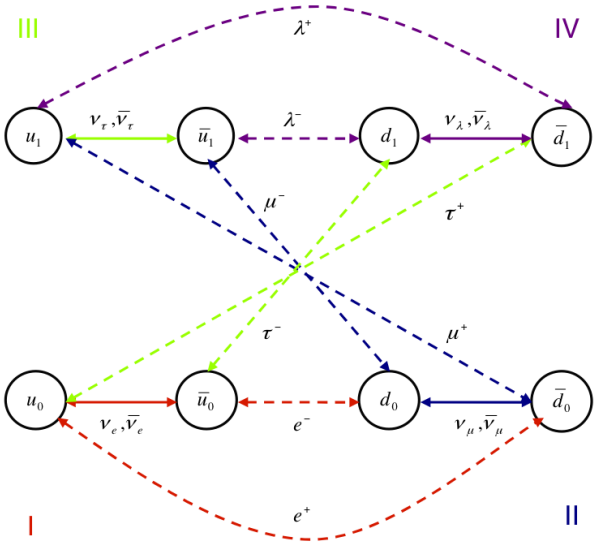

Fig. 1: Formation of the four generations of leptons by annihilations of up and down quarks and antiquarks with an excited quantum state.

Quarks	u_0	d_0	u_1	d_1
$\bar{u}_0$	$\nu_e, \bar{\nu}_e$	e^-	-	τ^-
$\bar{d}_0$	e^+	$\nu_\mu, \bar{\nu}_\mu$	μ^+	-
$\bar{u}_1$	-	μ^-	$\nu_\tau, \bar{\nu}_\tau$	λ^-
$\bar{d}_1$	τ^+	-	λ^+	$\nu_\lambda, \bar{\nu}_\lambda$

Table 1: The up and down quarks and antiquarks in ground and excited quantum states and four generations of leptons

structureless, colorless, and electrically neutral leptons such as ν_e, $\bar{\nu}_e$, ν_μ, $\bar{\nu}_\mu$, ν_τ, and $\bar{\nu}_\tau$.

Mesons are quark-antiquark mixtures without annihilating their charges. For instance, the meson pion π^+ is a mixture of one up quark and one down antiquark. Meson's color charges are not annihilated and thus participate in the strong interaction. Leptons do not participate in the strong interaction because their color charges are annihilated. Particles formed from annihilations do not have structure such as γ-rays formed from particle-antiparticle annihilation. A baryon is a mixture of three quarks such as that a proton is composed of two up quarks and one down quark and that a neutron is composed of one up quark and two down quarks.

Recently, Zhang [14-15] considered the electric and color charges of quarks and antiquarks as two forms of imaginary energy in analogy with mass as a form of real energy and developed a classical unification theory that unifies all natural fundamental interactions with four natural fundamental elements, which are radiation, mass, electric charge, and color charge. According to this consideration, the type-I quark-antiquark annihilation cancels only the color imaginary energies of a quark and a different flavor antiquark, while the type-II quark-antiquark annihilation cancels both the electric and color imaginary energies of a quark and a same flavor antiquark.

Figure 1 is a schematic diagram that shows formations of four generations of leptons from annihilations of up and down quarks and antiquarks with one excited quantum state for each of them. The existence of quark excited states, though not yet directly discovered, has been investigated over three decades [16-18]. That ρ^+ is also a mixture of one up quark and one down antiquark but has more mass than π^+ and many similar examples strongly support that quarks and antiquarks have excited states. In Figure 1, the subscript '0' denotes the ground state and '1' denotes the excited state. The higher excited states are not considered in this study. The dashed arrow lines refer to type-I annihilations of quarks and antiquarks that form electrically charged leptons, while the solid arrow lines refer to type-II annihilations of quarks and antiquarks that form colorless and electrically neutral leptons. These annihilations of quarks and antiquarks and formations of leptons can also be represented in Table 1.

The first generation of leptons is formed by annihilations between the ground state up, ground state antiup, ground state down, and ground state antidown quarks (see the red arrow lines of Figure 1). The up quark u_0 and the antiup quark $\bar{u}_0$ completely annihilate into an electron neutrino ν_e or an electron antineutrino $\bar{\nu}_e$. The antiup quark $\bar{u}_0$ and the down quark d_0 incompletely annihilate into an electron e^-. The up quark u_0 and the antidown quark $\bar{d}_0$ incompletely annihilate into a positron e^+.

The second generation of leptons are formed by annihilations between the ground state down, ground state antidown, excited up, and excited antiup quarks (see the blue arrow lines of Figure 1). The down quark d_0 and the antidown quark $\bar{d}_0$ completely annihilate into a muon neutrino ν_μ or an antimuon neutrino $\bar{\nu}_\mu$. The antiup quark $\bar{u}_1$ and the down quark d_0 incompletely annihilate into a negative muon μ^-. The up quark u_1 and the antidown quark $\bar{d}_0$ incompletely annihilate into a positive muon μ^+.

The third generation of leptons are formed by annihilations between the ground state up, excited up, ground state antiup, excited antiup, excited down, and excited antidown quarks (see the green lines of Figure 1). The up quark u_1 and the antiup quark $\bar{u}_1$ completely annihilate into a tau neutrino ν_τ or a tau antineutrino $\bar{\nu}_\tau$. The antiup quark $\bar{u}_0$ and the down quark d_1 incompletely annihilate into a negative tau τ^-. The up quark u_0 and the antidown quark $\bar{d}_1$ incompletely annihilate into a positive tau τ^+.

The fourth generation of leptons are formed by annihilations between excited up, excited antiup, excited down, and excited antidown quarks (see the purple lines of Figure 1). The down quark d_1 and the antidown quark $\bar{d}_1$ completely annihilate into a lambda neutrino ν_λ or a lambda antineutrino

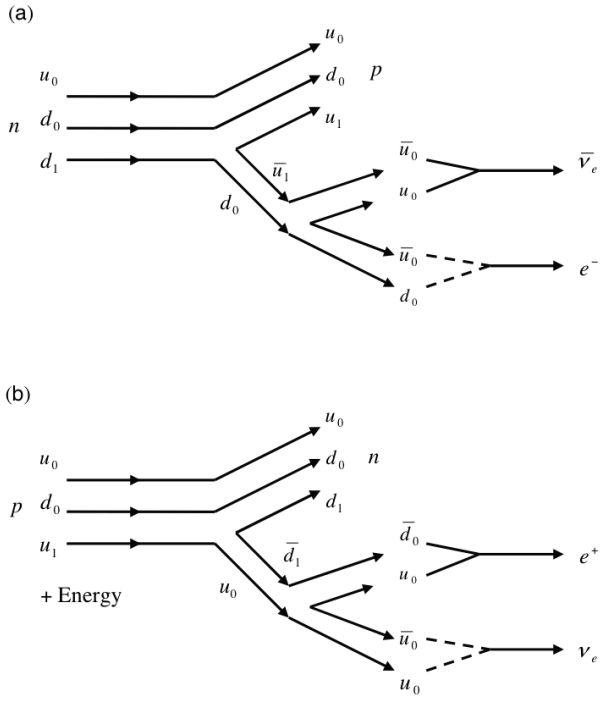

Fig. 2: Formation of the first generation of leptons: (a) e^- and $\bar{\nu}_e$ through beta decay and (b) e^+ and ν_e through positron emission.

$\bar{\nu}_\lambda$. The antiup quark $\bar{u}_1$ and the down quark d_1 incompletely annihilate into a negative lambda λ^-. The up quark u_1 and the antidown quark $\bar{d}_1$ incompletely annihilate into a positive lambda λ^+.

3 Quark Pair Production and Lepton Disintegration

The first generation of leptons can be produced through the beta decay of a neutron, $n \longrightarrow p + e^- + \bar{\nu}_e$ (Figure 2a), and the positron emission of a proton, energy $+ p \longrightarrow n + e^+ + \nu_e$ (Figure 2b).

In the beta decay, an excited down quark in the neutron degenerates into a ground state down quark and an excited up and antiup quark pair, $d_1 \longrightarrow d_0 + (u_1\bar{u}_1)$. The excited antiup quark further degenerates into a ground state up quark and a ground state up and antiup quark pair, $\bar{u}_1 \longrightarrow \bar{u}_0 + (u_0\bar{u}_0)$. The ground state antiup quark incompletely annihilates with the ground state down quark into an electron, $\bar{u}_0 + d_0 \longrightarrow e^-$. The ground state up and antiup quark pair completely annihilates into an electron antineutrino, $u_0 + \bar{u}_0 \longrightarrow \bar{\nu}_e$.

In the positron emission, an excited up quark in the positron after absorbing a certain amount of energy degenerates into a ground state up quark and produces an excited state down and antidown quark pair, energy $+ u_1 \longrightarrow u_0 + (d_1\bar{d}_1)$. The excited antidown quark further degenerates into a ground state antidown quark and produces a ground state up and antiup quark pair, $\bar{d}_1 \longrightarrow \bar{d}_0 + (u_0\bar{u}_0)$. The ground state up quark incompletely annihilates with the ground state antidown quark to form a positron, $u_0 + \bar{d}_0 \longrightarrow e^+$. The ground state up and antiup quark pair completely annihilates into an electron neutrino, $u_0 + \bar{u}_0 \longrightarrow \nu_e$.

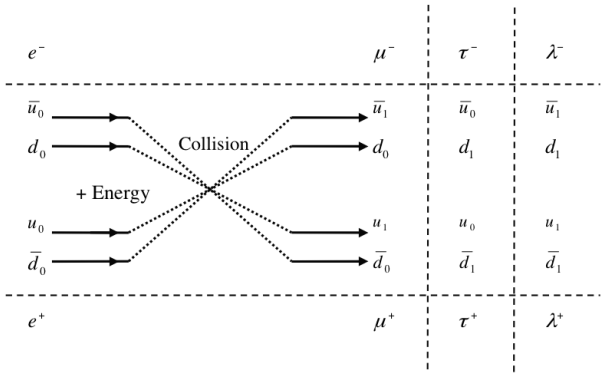

Fig. 3: Production of other three electrically charged leptons from an energetic electron-positron collision. In the collision, electron and positron are first disintegrated into quark-antiquark pairs, which are then excited and annihilated into other generations of electrically charge leptons.

The other three generations of electrically charged leptons can be produced by an energetic electron-positron collision,

$$\text{energy} + e^- + e^+ \longrightarrow \begin{cases} \mu^- + \mu^+ \\ \tau^- + \tau^+ \\ \lambda^- + \lambda^+ \end{cases}, \qquad (1)$$

as also shown in Figure 3. In the particle physics, it has been experimentally shown that the energetic electron-positron collision can produce (μ^-, μ^+) and (τ^-, τ^+). But how the electron-positron collisions produce μ and τ leptons is still remained very poorly understood.

With the quark annihilation and pair production model proposed in this paper, we can understand why an electron-positron can produce μ and τ particles. In addition, we predict the existence of the fourth generation of leptons, λ particle and neutrino. The energetic electron-positron collision disintegrates the electron into a ground state antiup-down quark pair $e^- \longrightarrow (\bar{u}_0 d_0)$ and the positron into a ground state up-antidown quark pair $e^+ \longrightarrow (u_0\bar{d}_0)$. During the collision, the quarks and antiquarks in the disintegrated electron and positron quark-antiquark pairs absorb energy and become excited. The excited quark-antiquark pairs incompletely annihilate into another generation of electrically charged leptons.

There are three possible excitation patterns, which lead to three generations of leptons from the electron-positron collision. If the antiup quark in the disintegrated electron quark-antiquark pair and the up quark in the disintegrated positron quark-antiquark pair are excited, then the annihilations produce leptons μ^- and μ^+. If the down quark in the disintegrated electron quark-antiquark pair and the antidown quark in the disintegrated positron quark-antiquark pair are excited,

then the annihilations produce leptons τ^- and τ^+. If both the antiup and down quarks in the disintegrated electron quark-antiquark pair and both the up and antidown quarks in the disintegrated positron quark-antiquark pair are excited, the annihilations produce the leptons λ^- and λ^+. An electron-positron collision in a different energy level produces a different generation of electrically charged leptons. To produce the λ particles, a more energetic electron-positron collision is required than μ and τ lepton productions. On the other hand, the electron and positron, if they are not disintegrated into quark-antiquark pairs during the collision, can directly annihilate into photons. The disintegrated electron and positron quark-antiquark pairs, if they are excited but not annihilated, can form the weak particles W^- and W^+.

A quark or antiquark can be excited when it absorbs energy or captures a photon. An excited quark or antiquark can degenerate into its corresponding ground state quark or antiquark after it releases a photon and/or one or more quark-antiquark pairs. The decays of these three generations of electrically charged leptons (μ, τ, and λ particles) can produce their corresponding neutrinos through degenerations and annihilations of quarks and antiquarks.

The currently discovered three generations of leptons including the fourth generation predicted in this paper are formed through the annihilations of the up and down quarks and antiquarks with an excited state. All these leptons are corresponding to or associated with the first generation of quarks and antiquarks. Considering the annihilations of other four flavor quarks and antiquarks, we can have many other types of leptons that are corresponding to the second and third generations of quarks and antiquarks. These leptons must be hardly generated and observed because a higher energy is required [4].

4 Quark Annihilation and Pair Production: Neutrino Oscillation

The complete (or type-II) annihilation between a quark and its corresponding antiquark forms a colorless and electrically neutral neutrino. On the contrary quark-antiquark annihilation, a neutrino, when it collides with a nucleon, may be disintegrated into a quark-antiquark pair. The disintegrated quark-antiquark pairs can be excited if it absorbs energy (e.g., $\gamma + u_0 \longrightarrow u_1$) and changed in flavor if it exchanges a weak particle (e.g., $u_0 + W^- \longrightarrow d_0$) during the disintegration. The excited and/or flavor changed quark-antiquark pair then either annihilates into another type of neutrino or interacts with the nucleon to form hadrons and electrically charged leptons. This provides a possible explanation for neutrino oscillations [19-20]. This scenario of neutrino oscillations does not need neutrinos to have mass and thus does not conflict with the standard model of particle physics.

Figure 4 and 5 show all possible oscillations among the four types of neutrinos. An electron neutrino can oscillate into a tau neutrino if the disintegrated quark-antiquark pair ($u_0\bar{u}_0$) is excited into ($u_1\bar{u}_1$) (Figure 4a), a muon neutrino if the disintegrated quark-antiquark pair ($u_0\bar{u}_0$) is changed in flavor into ($d_0\bar{d}_0$) (Figure 4b), and a lambda neutrino if the disintegrated quark-antiquark pair ($u_0\bar{u}_0$) is excited into ($u_1\bar{u}_1$) and then changed in flavor into ($d_1\bar{d}_1$) (Figure 4c). Similarly, A muon neutrino can oscillate into a tau neutrino if the disintegrated quark-antiquark pair ($d_0\bar{d}_0$) is excited and changed in flavor into ($u_1\bar{u}_1$) (Figure 5a) and a lambda neutrino if the disintegrated quark-antiquark pair ($d_0\bar{d}_0$) is excited and changed into ($d_1\bar{d}_1$) (Figure 5b). A tau neutrino can oscillate into a lambda neutrino if the disintegrated quark-antiquark pair ($u_1\bar{u}_1$) is changed in flavor into ($d_1\bar{d}_1$) (Figure 5c). All these oscillations described above are reversible processes. The right arrows in Figures 4 and 5 denote the neutrino oscillations when the disintegrated quark-antiquark pair absorbs energy to be excited or capture weak particles to be changed in flavor. Neutrinos can also oscillate when the disintegrated quark-antiquark pair emits energy and/or releases weak particles. In this cases, the right arrows in Figure 4 and 5 are replaced by left arrows and neutrinos oscillate from heavier ones to lighter ones.

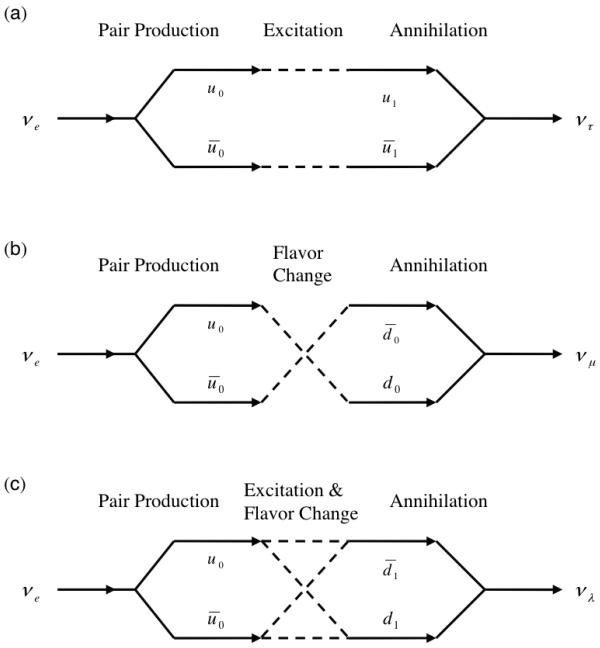

Fig. 4: Neutrino oscillations. (a) Oscillation between electron and tau neutrinos. (b) Oscillation between electron and muon neutrinos. (c) Oscillation between electron and lambda neutrinos.

The recent OPERA experiment at the INFN's Gran Sasso laboratory in Italy first observed directly a tau particle in a muon neutrino beam generated by pion and kaon decays and sent through the Earth from CERN that is 732 km away [21-23]. This significant result can be explained with a muon neutrino disintegration, excitation, and interaction with a nu-

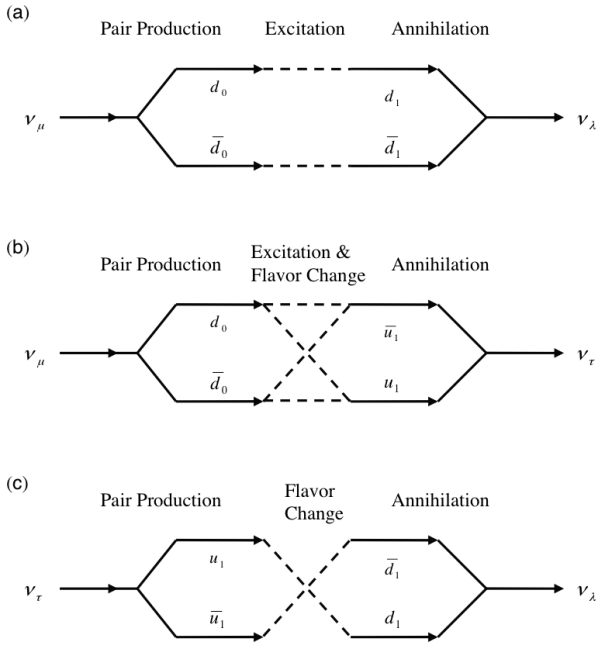

Fig. 5: Neutrino oscillations. (a) Oscillation between muon and lambda neutrinos. (b) Oscillation between muon and tau neutrinos. (c) Oscillation between tau and lambda neutrinos.

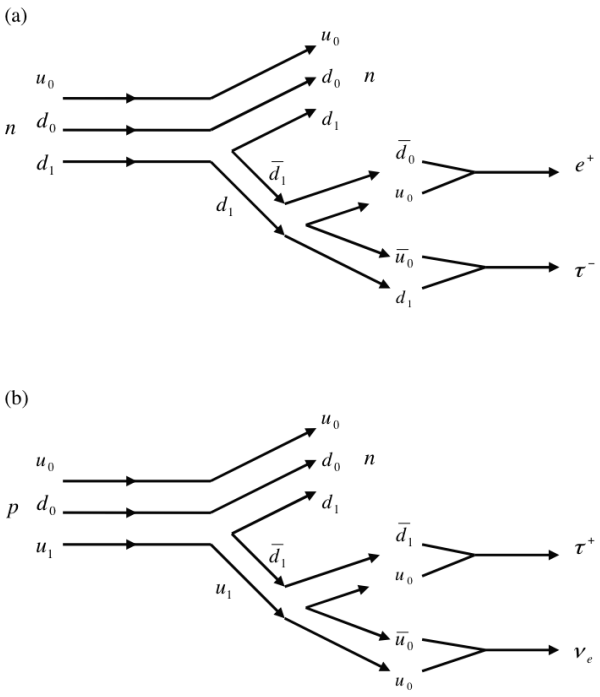

Fig. 6: Production of tau particles by a muon neutrino beam. (a) A negative tau particle is produced when an excited quark-antiquark pair, which is disintegrated from a muon neutrino and excited, interacts with a neutron. (b) A positive tau particle is produced when an excited quark-antiquark pair, which is disintegrated from a muon neutrino and excited, interacts with a proton.

cleon. Colliding with a neutron, a muon neutrino ν_μ is disintegrated into a ground state down-antidown quark pair ($d_0\bar{d}_0$), which can be excited into ($d_1\bar{d}_1$) and ($u_1\bar{u}_1$) when the flavor is also changed. The excited down-antidown quark pair ($d_1\bar{d}_1$) can either completely annihilate into a lambda neutrino ν_λ (Figure 5a) or interact with the neutron to generate a negative tau particle τ^- when the excited antidown quark degenerates into a ground state antidown and a ground state up-antiup quark pair, $\bar{d}_1 \longrightarrow \bar{d}_0 + (u_0\bar{u}_0)$ (Figure 6a). As shown in Figure 6a, the excited down quark in the neutron can incompletely annihilate with the ground state antiup quark into a negative tau particle τ^- and the ground state antidown quark can incompletely annihilate the ground state up quark into a positron e^+. Interacting with a proton (Figure 6b), the excited down-antidown quark pair ($d_1\bar{d}_1$) can generate a positive tau particle τ^+ when the excited up quark in the proton degenerates into a ground state up quark and a ground state up-antiup quark pair, $u_1 \longrightarrow u_0 + (u_0\bar{u}_0)$. The excited antidown quark can incompletely annihilate with the ground state up quark into a positive tau particle τ^+ and the ground state antiup quark can completely annihilate with the ground state up quark into an electron neutrino ν_e. If the excited up quark is not degenerated but directly annihilate with the excited antidown quark, a lambda particle λ^+ is produced (as shown in Figure 3).

On the other hand, for an electron neutrino beam, colliding with a nucleon, an electron neutrino ν_e is disintegrated into a ground state up-antiup quark pair ($u_0\bar{u}_0$) and excited into ($u_1\bar{u}_1$), which may be also from the disintegration of a muon neutrino with the favor change. This excited up-antiup quark-antiquark pair can either completely annihilate into a tau neutrino as shown in Figure 1 or interact with the nucleon to generate a muon particle (Figure 7). If the flavor is also changed, the annihilation and interaction with nucleons will produce the tau particles and neutrinos as shown in Figure 6 or lambda particles and neutrinos as shown in Figure 3.

Therefore, with the lepton formation and quark-antiquark pair production model developed in this paper, we can understand the recent measurement of a tau particle in a muon neutrino beam as well as the early measurements of muon particles in electron neutrino beams. More future experiments of the Large Electron-Positron Collider at CERN and measurements of neutrino oscillations are expected to validate this lepton formation and quark-antiquark pair production model and detect the fourth generation of leptons.

5 Conclusions

This paper develops a quark-antiquark annihilation and pair production model to explain the formation of leptons and the oscillation of neutrinos and further predict the fourth generation of leptons named as lambda particle and neutrino. It

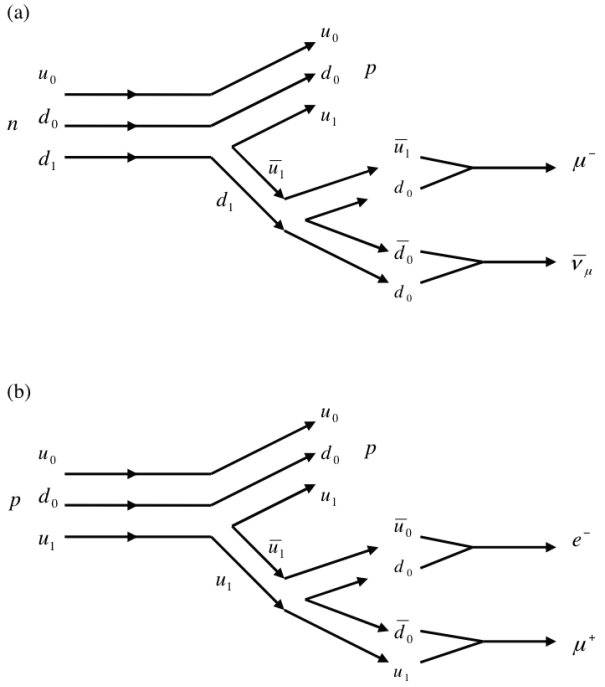

Fig. 7: Production of muon particles by an electron neutrino beam. (a) A negative muon particle is produced when an excited up-antiup quark pair, which is disintegrated from an electron neutrino and excited, interacts with a neutron. (b) A positive tau particle is produced when an excited quark-antiquark pair, which is disintegrated from a muon neutrino and excited, interacts with a proton.

is well known that all known or discovered leptons can be formed or emerged from particles or hadrons that are composed of only up and down quarks. This fact indicates that leptons must be consequences of activities of the up and down quarks and antiquarks. As quarks contain color charges, they participate in the strong interaction. Leptons do not contain color charges so that they do not participate in the strong interaction. In this paper, we suggested that all leptons are formed from quark-antiquark annihilations. There are two types of quark-antiquark annihilations. Type-I quark-antiquark annihilation annihilates only color charges, which forms structueless and colorless but electrically charged leptons such as electron, muon, tau, and lambda particles. Type-II quark-antiquark annihilation annihilates both electric and color charges, which forms structureless, colorless, and electrically neutral leptons such as electron, muon, tau, and lambda neutrinos. For the two types (up and down) of quarks and antiquarks to generate all four generation leptons from annihilations, they must have at least one excited state. Analyzing these two types of annihilations between up and down quarks and antiquarks with one excited quantum state for each of them, we predict the formation of the fourth generation of leptons named lambda particle and lambda neutrino. On the other hand, a lepton, when it collides with a nucleon, can be disintegrated into a quark-antiquark pair, which can be exited and/or changed in flavor. The quark-antiquark pair disintegrated from a neutrino can be excited and/or changed in flavor during the collision and then annihilate into another type of neutrino or interact with a nucleon to form electrically charged leptons. This quark-antiquark annihilation and pair production model provides a possible explanation for neutrino oscillations without hurting the standard model of particle physics. With it, we can understand the recent OPERA measurement of a tau particle in a muon neutrino beam as well as the early measurements of muon particles in electron neutrino beams.

Acknowledgement

This work was supported by the Title III program of Alabama A & M University, the NASA Alabama EPSCoR Seed grant (NNX07AL52A), and the National Natural Science Foundation of China (G40890161).

Submitted on January 20, 2011 / Accepted on January 26, 2011

References

1. Gell-Mann M. A schematic model of baryons and mesons. *Physics Letters*, 1964, v. 8, 214–215.
2. Zweig G. *CERN Report* No. 8182/TH.401, 1964.
3. Fritzsch H. Quarks. Basic Books, Inc., 1983.
4. Sher M., Yuan Y. Cosmological bounds on the lifetime of a fourth generation charged lepton. *Physics Letters B*, 1992, v. 285, 336–342.
5. Frampton P. H., Ng D., Sher M., Yuan Y. Search for heavy charged leptons at hadron colliders. *Physical Review D*, 1993, v. 48, 3128–3135.
6. Bhattacharyya G., Choudhury D. Fourth-generation leptons at LEP2. *Nuclear Physics B*, 1996, v. 468, 59-71.
7. Frandsen M. T., Masina I., Sannino F. Fourth lepton family is natural in technicolor. *Physical Review D*, 2010, v. 81, 35010.
8. Aguilar-Saavedra J. A. Heavy lepton pair production at LHC: Model discrimination with multi-lepton signals. *Nuclear Physics B*, 2010, v. 828, 289–316.
9. Nandi S., Rittenberg V., Schneider H. R. Quark-antiquark annihilation and small-pT inclusive spectra. *Physical Review D*, 1978, v. 17, 1336–1343.
10. Frenkel J., Gatheral J. G. M., Taylor J. C. Quark-antiquark annihilation is infrared safe at high energy to all orders. *Nuclear Physics B*, 1984, v. 233, 307–335.
11. Boros C., Liang Z. T., Meng T. C. Quark spin distribution and quark-antiquark annihilation in single-spin hadron-hadron collisions. *Physical Review Letters*, 1993, v. 70, 1751–1754.
12. Berrneuther W., Fucker M. and Si Z. G. Mixed QCD and Weak Corrections to tbar t Production by Quark-Antiquark Annihilation. *International Journal of Modern Physics A*, 2006, v. 21, 914–817.
13. Bredenstein A., Denner A., Dittmaier S., Pozzorini S. NLO QCD corrections to $t\bar{t}b\bar{b}$ production at the LHC: 1. quark-antiquark annihilation. *Journal of High Energy Physics*, 2008, v. 8, 108–108.
14. Zhang T. X. Electric charge as a form of imaginary energy. *Progress in Physics*, 2008, v. 2, 79–83.
15. Zhang T. X. Fundamental elements and interaction of the Nature: a classical unification theory. *Progress in Physics*, 2010, v. 2, 36–42.
16. DeGrand T. A., Jaffe R. L. Excited states of confined quarks. *Annals of Physics*, 1976, v. 100, 425–456.

17. de Rujula A., Maiani L., Petronzio R. Search for excited quarks. *Physics Letters B*, 1984, v. 140, 253–258.

18. Baur U., Spira M., Zerwas P. M. Excited-quark and -lepton production at hadron colliders. *Physical Review D*, 1990, v. 42, 815–824.

19. Wolfenstein L. Neutrino oscillations in matter. *Physical Review D*, 1978, v. 17, 2369–2374.

20. Aguilar A. et al. Evidence for neutrino oscillations from the observation of $\bar{\nu}_e$ appearance in a $\bar{\nu}_\mu$ beam. *Physical Review D*, 2001, v. 64, 112007.

21. Acquafredda R. et al. The OPERA experiment in the CERN to Gran Sasso neutrino beam. *Journal of Instrumentation*, 2009, v. 4, 4018.

22. Agafonova N. et al. Observation of a first ν candidate event in the OPERA experiment in the CNGS beam. *Physics Letters B*, 2010, v. 691, 139–145.

23. Dusini S. The OPERA experiment: A direct search of the $\nu_\mu \longrightarrow \nu_\tau$ oscillations. *Progress in Particle and Nuclear Physics*, 2010, v. 64, 187–189.

On the Independent Determination of the Ultimate Density of Physical Vacuum

Anatoly V. Belyakov

E-mail: belyakov.lih@gmail.com

In this paper, we attempt to present physical vacuum as a topologically non-unitary coherent surface. This representation follows with J. A. Wheeler's idea about fluctuating topology, and provides a possibility to express some parameters of the unit space element through the fundamental constants. As a result, we determined the ultimate density of physical vacuum without use of Hubble's constant.

The ultimate density of physical vacuum is regularly calculated through the experimentally obtained quantity — Hubble's constant. This constant follows from astronomical observations, and therefore its numerical value is under permanent update. On the other hand, the ultimate density of physical vacuum can also be determined in an independent way, through only the fundamental constants. Moreover, in the framework of this mechanistic model, it does not matter what we mean saying "physical vacuum": a material substance, or space itself.

As an initial model of the space micro-element of matter, it is reasonable to use J. A. Wheeler's idea about fluctuating topology. In particular, electric charges are considered therein as singular points located in a three-dimensional surface, and connected to each other through "wormholes" or current tubes of the input-output (source-drain) kind in an additional dimension, thus forming a closed contour. Is this additional dimension really required? It is probably that the three-dimensional space, if considered at a microscopic scale, has really lesser number of dimensions, but is topologically non-unitary coherent and consists of linkages [1].

The most close analogy to this model, in the scale of our world, could be the surface of an ideal liquid, vortical structures in it and their interactions which form both relief of the surface and sub-surface structures (vortical grids, etc.).

From the purely mechanistic point of view, this model should not contain the *electric charge* as a special kind of matter: the electric charge only manifests the degree of the non-equilibrium state of physical vacuum; it is proportional to the momentum of physical vacuum in its motion along the contour of the vortical current tube. Respectively, the *spin* is proportional to the angular momentum of the physical vacuum with respect to the longitudinal axis of the contour, while the *magnetic interaction* of the conductors is analogous to the forces acting among the current tubes.

Of course, in the framework of this model, both point and line are means physical objects, which have specific sizes. We assume the classical radius of the electron r_e as the minimal size. This approach was already justified in determination of the numerical value of the electron's charge, and the constants of radiation [2].

Thus matter itself can finally be organized with step-by-step complication of the initial contours, and be a "woven cloth", which, in its turn, is deformed into the objects we observe. The objects therefore are very fractalized (upto the micro-world scales) *surfaces*, which have a fractional dimension of the number almost approaching three and presupposingly equal to the number e.

The latter conclusion verifies that fact that the function $n^{1/n}$, which can be interpreted as the length of a ridge of the unit cube (its volume is equivalent to the summary volume of n cubes of the nth dimension), reach its maximum at exact $n = e$. We can understand this result so that the world of this dimension $n = e$ is most convex to the other worlds.

As a result, the surface being non-deformed can logically be interpreted as empty space, while the deformed and fractalized surface, i.e. the surface bearing an information about local deformations — as substance, masses. What is about an absolutely continuous three-dimensional body, it has not any internal structure thus does not bear any information about its interior (except, as probably, its own mass): such bodies do not really exist, even in the real micro world. In other words, the surface is material. However, being non-deformed, it does not manifest its material properties.

It should be noted that it is impossible to discuss the real geometry of topology of the world in the framework of this concept. Moreover, it is quite complicate to differ the surface from space, and space from matter, because such a step means at least a conceivable leaving our surface, which consists ourselves and the Universe itself. On the other hand, our model does not require such a step.

To calculate the density of physical vacuum in the framework of our suggested model, it is sufficient to determine the square, thickness, and mass of the "smoothed" surface (non-perturbed physical vacuum), then reduce the mass to the ultimate volume. To do it, we need to determine parameters of the initial micro-element and elementary contour.

According to the assumed model, we write down the electric forces F_e and the magnetic forces F_m in the "coulombless" form, where we replace the electric charge with the ultimate momentum of the electron $m_e c$. We obtain, for the electric forces,

$$F_e = \frac{z_1 z_2 (m_e c)^2}{\varepsilon_0 r^2}, \qquad (1)$$

where z_1 and z_2 are the numbers of the electric charges, c is the velocity of light, m_e is the electron's mass, while $\varepsilon = \frac{m_e}{r_e}$ is a new electric constant, which is 3.23×10^{-16} kg/m and is the linear density of the vortical tube. Respectively, for the magnetic forces, we obtain

$$F_m = \frac{z_1 z_2 \mu_0 (m_e c)^2 L}{2\pi r \times [\sec^2]}, \qquad (2)$$

where $\mu_0 = \frac{1}{\varepsilon_0 c^2}$ is a new magnetic constant, whose numerical value is 0.034 H^{-1}, L is the length of the conductors of the current (vortical tubes), while r is the distance between them. Numerically, the electric forces (1) and the magnetic forces (2) coincide with those calculated according to the standard equations of electrodynamics.

Thus, the quantity inverse to the magnetic constant, is the centrifugal force which appears due to the rotation of the vortical tube's element whose mass is m_e, with the velocity of light c around the radius r_e. The centrifugal force is also equivalent to the force acting among two elementary electric charges at this radius. We note, that the latter conclusion is the same as that W. C. Daywitt arrived at in the paper [3].

In the non-perturbed physical vacuum the electric, magnetic, and other forces should be compensated. In particular, proceeding from the equality of the electric and magnetic forces, one can deduce the *geometric mean value*, which is a linear parameter independent from the direction of the vortical tubes and the number of the electric charges

$$R_c = \sqrt{Lr} = \sqrt{2\pi}\, c \times [\sec] = 7.51 \times 10^8 \text{ [m]}. \qquad (3)$$

This fundamental length is close to the radius of the Sun and also the sizes of many typical stars.

Thus equation (3) represents the ratio between the contour's length and the distance between the vortical tubes. Now, assuming that the figures of the contours satisfy the formula (3), we are going to calculate the total mass of physical vacuum, which fills the Universe, and also its density.

Let the "smoothed" surface of physical vacuum has a size of $L \times L$, and is densely woven on the basis of parallel vortical tubes (they have parameters L and r) which, in their turn, are filled with the unit threads (each of the threads has a radius equal to the radius of the electron r_e). Also, assume that, even if there exist structures whose size is lesser than r_e, they do not change the longitudinal density ε_0. Thus, the total mass of the surface of the thickness r, which is the mass of physical vacuum M_v (including all hidden masses), is obviously determined by the formula

$$M_v = \frac{\pi}{4} \varepsilon_0 L \frac{L}{r} \left(\frac{r}{r_e}\right)^2. \qquad (4)$$

The average density of the substance of physical vacuum ρ_v is expressed through the ratio of the mass M_v to the spherical volume $\frac{4}{3}\pi L^3$. As a result, extending the formula of ε_0 then expressing L from (3), we obtain

$$M_v = \frac{\pi}{4} \frac{\rho_e R_c^4}{r}, \qquad (5)$$

$$\rho_v = \frac{3}{16} \rho_e \left(\frac{r}{R_c}\right)^2, \qquad (6)$$

where ρ_e is the density of the electron derived from its classical parameters, and is $\rho_e = \frac{m_e}{r_e^3} = 4.07 \times 10^{13}$ kg/m^3.

The main substance of the Universe is hydrogen. Therefore, it is naturally to assume r equal to the size of the standard proton-electron contour, which is the Bohr 1st radius 0.53×10^{-10} m.

Thus we obtain: the ultimate large length of the contour $L = 1.06 \times 10^{28}$ m, the total mass of substance in the Universe $M_v = 1.92 \times 10^{59}$ kg, and the ultimate density of physical vacuum $\rho_v = 3.77 \times 10^{-26}$ kg/m^3 (or $\rho_v = 3.77 \times 10^{-29}$ g/cm^3 in the CGS units).

The calculated numerical value of the average density of matter (physical vacuum) in the Universe is close to the modern esteems of the crucial density (the density of the *Einsteinian vacuum*).

With breaking the homogeneity of physical vacuum the anisotropy appears in the Universe. This is subjectively perceived in our world as manifestations of the pace of time, and the preferred directions in space. It is possible to suppose that the Universe as a whole evolutionary oscillates near its state of equilibrium, thus deforming the vacuum medium and creating the known forms of matter as a result. The stronger deformation, the larger contours (the heavier elements of substance) appear. Proceeding from the fact that elements with more than seven electron shells are unknown, we can conclude that the scale of the evolutionary oscillations of the Universe in the part of deformations of its own "tissue" is very limited. This is despite, as is probably, the Universe goes through the zero-state of equilibrium of physical vacuum during its evolution, where all real masses approach to zero, and the forces of gravitation — to their minimum. Here we see a relative connexion to *Mach's principle*, i.e. a dependency of the masses of objects on the mass of the entire Universe (of course, if meaning the mass of the entire Universe as the mass of physical vacuum, which is much greater than the summary mass of regular substance).

In conclusion, we suggest a supposition. Because masses or physical objects are merely forms of the relief of the surface of the vacuum medium, *which can only exist if the forming medium moves permanently along ordered trajectories*, in the framework of this interpretation *time* manifests evolution, change of objects and structures along the direction of motion of matter they consist of. Therefore, all paradoxes of time vanish here: the hypothetical displacement of an observer toward or backward with the current of matter leads only to his arrival at his alternative past or future; his actions

therein cannot change his own present — his own evolving section of the Universe.

Submitted on January 07, 2011 / Accepted on January 10, 2011

References

1. Dewitt B. S. Quantum gravity. *Scientific American*, v. 249, December 1983, 112–129.
2. Belyakov A. V. Charge of the electron, and the constants of radiation according to J. A. Wheeler's geometrodynamic model. *Progress in Physics*, 2010, v. 4, 90–94.
3. Daywitt W. C. The Relativity Principle: space and time and the Plank vacuum. *Progress in Physics*, 2010, v. 4, 34–35.

An Elegant Argument that $P \neq NP$

Craig Alan Feinstein

2712 Willow Glen Drive, Baltimore, Maryland 21209. E-mail: cafeinst@msn.com

In this note, we present an elegant argument that $P \neq NP$ by demonstrating that the Meet-in-the-Middle algorithm must have the fastest running-time of all deterministic and exact algorithms which solve the SUBSET-SUM problem on a classical computer.

Consider the following problem: Let $A = \{a_1, \ldots, a_n\}$ be a set of n integers and b be another integer. We want to find a subset of A for which the sum of its elements (we shall call this quantity a *subset-sum*) is equal to b (we shall call this quantity the *target integer*). We shall consider the sum of the elements of the empty set to be zero. This problem is called the *SUBSET-SUM problem* [1,2]. Now consider the following algorithm for solving the SUBSET-SUM problem:

Meet-in-the-Middle Algorithm - First, partition the set A into two subsets, $A^+ = \{a_1, \ldots, a_{\lceil \frac{n}{2} \rceil}\}$ and $A^- = \{a_{\lceil \frac{n}{2} \rceil + 1}, \ldots, a_n\}$. Let us define S^+ and S^- as the sets of subset-sums of A^+ and A^-, respectively. Sort sets S^+ and $b - S^-$ in ascending order. Compare the first elements in both of the lists. If they match, then output the corresponding solution and stop. If not, then compare the greater element with the next element in the other list. Continue this process until there is a match, in which case there is a solution, or until one of the lists runs out of elements, in which case there is no solution.

This algorithm takes $\Theta(\sqrt{2^n})$ time, since it takes $\Theta(\sqrt{2^n})$ steps to sort sets S^+ and $b - S^-$ and $O(\sqrt{2^n})$ steps to compare elements from the sorted lists S^+ and $b - S^-$. It turns out that no deterministic and exact algorithm with a better worst-case running-time has ever been found since Horowitz and Sahni discovered this algorithm in 1974 [3, 4]. In this paper, we shall prove that it is impossible for such an algorithm to exist.

First of all, we shall assume, without loss of generality, that the code of any algorithm considered in our proof does not contain full or partial solutions to any instances of SUBSET-SUM. This is because only finitely many such solutions could be written in the code, so such a strategy would not be helpful in speeding up the running-time of an algorithm solving SUBSET-SUM when n is large. We now give a definition:

Definition 1: *We define a γ-comparison (a generalized comparison) between two integers, x and y, as any finite procedure that directly or indirectly determines whether or not $x = y$.*

For example, a finite procedure that directly compares $f(x)$ and $f(y)$, where x and y are integers and f is a one-to-one function, γ-compares the two integers x and y, since $x = y$ if and only if $f(x) = f(y)$. Using this expanded definition of compare, it is not difficult to see that the Meet-in-the-Middle algorithm γ-compares subset-sums with the target integer until it finds a subset-sum that matches the target integer. We shall now prove two lemmas:

Lemma 2: *Let x and y be integers. If $x = y$, then the only type of finite procedure that is guaranteed to determine that $x = y$ is a γ-comparison between x and y. And if $x \neq y$, then the only type of finite procedure that is guaranteed to determine that $x \neq y$ is a γ-comparison between x and y.*

Proof: Suppose there is a finite procedure that is guaranteed to determine that $x = y$, if $x = y$. Then if the procedure does not determine that $x = y$, this implies that $x \neq y$. Hence, the procedure always directly or indirectly determines whether or not $x = y$, so the procedure is a γ-comparison between x and y.

And suppose there is a finite procedure that is guaranteed to determine that $x \neq y$, if $x \neq y$. Then if the procedure does not determine that $x \neq y$, this implies that $x = y$. Hence, the procedure always directly or indirectly determines whether or not $x = y$, so the procedure is a γ-comparison between x and y. ■

Lemma 3: *Any deterministic and exact algorithm that finds a solution to SUBSET-SUM whenever a solution exists must (whenever a solution exists) γ-compare the subset-sum of the solution that it outputs with the target integer.*

Proof: Let Q be a deterministic and exact algorithm that finds a solution, $\{a_{k_1}, \ldots, a_{k_m}\}$, to SUBSET-SUM whenever a solution exists. Before Q outputs this solution, it must verify that $a_{k_1} + \ldots + a_{k_m} = b$, since we are assuming that the code of Q does not contain full or partial solutions to any instances of SUBSET-SUM. (See above for an explanation.) In order for Q to verify that $a_{k_1} + \ldots + a_{k_m} = b$, Q must γ-compare the subset-sum, $a_{k_1} + \ldots + a_{k_m}$, with the target integer, b, since a γ-comparison between $a_{k_1} + \ldots + a_{k_m}$ and b is the only type of finite procedure that is guaranteed to determine that $a_{k_1} + \ldots + a_{k_m} = b$, by Lemma 2. ■

As we see above, the Meet-in-the-Middle algorithm makes use of sorted lists of subset-sums in order to obtain a faster

worst-case running-time, $\Theta(\sqrt{2^n})$, than that of a naïve brute-force search of the set of all subset-sums, $\Theta(2^n)$. The following lemma shows that sorted lists of subset-sums are necessary to achieve such an improved worst-case running-time.

Lemma 4: *If a deterministic and exact algorithm that finds a solution to SUBSET-SUM whenever a solution exists does not make use of sorted lists of subset-sums, it must run in* $\Omega(2^n)$ *time in the worst-case scenario.*

Proof: Let Q be a deterministic and exact algorithm that finds a solution to SUBSET-SUM whenever a solution exists without making use of sorted lists of subset-sums. By Lemma 3, Q must (whenever a solution exists) γ-compare the subset-sum of the solution that it outputs with the target integer. In order for Q to avoid wasting time γ-comparing the target integer with subset-sums that do not match the target integer, Q must be able to rule out possible matches between subset-sums and the target integer without γ-comparing these subset-sums with the target integer.

But by Lemma 2, the only type of finite procedure that is guaranteed to rule out a possible match between a subset-sum and the target integer, if they do not match, is a γ-comparison. So in the worst-case scenario, there is no way for Q to avoid wasting time γ-comparing the target integer with subset-sums that do not match the target integer. And since Q does not make use of sorted lists of subset-sums like the Meet-in-the-Middle algorithm does, its γ-comparisons between these subset-sums and the target integer will not rule out possible matches between any other subset-sums and the target integer. Hence, in the worst-case scenario Q must γ-compare each of the 2^n subset-sums with the target integer, which takes $\Omega(2^n)$ time. ■

It is now possible, using Lemma 4, to solve the problem of finding a nontrivial lower-bound for the worst-case running-time of a deterministic and exact algorithm that solves the SUBSET-SUM problem:

Theorem 5: *It is impossible for a deterministic and exact algorithm that solves the SUBSET-SUM problem to have a worst-case running-time of* $o(\sqrt{2^n})$.

Proof: Let T be the worst-case running-time of an algorithm Q that solves SUBSET-SUM, and let M be the size of the largest list of subset-sums that Q sorts. Since it is necessary for Q to make use of sorted lists of subset-sums in order to have a faster worst-case running-time than $\Theta(2^n)$ by Lemma 4 and since it is possible for Q to make use of sorted lists of size M of subset-sums to rule out at most M possible matches of subset-sums with the target integer at a time (just as the Meet-in-the-Middle algorithm does, with $M = \Theta(\sqrt{2^n})$), we have $MT \geq \Theta(2^n)$. And since creating a sorted list of size M must take at least M units of time, we have $T \geq M \geq 1$.

Then in order to find a nontrivial lower-bound for the worst-case running-time of an algorithm solving SUBSET-SUM, let us minimize T subject to $MT \geq \Theta(2^n)$ and $T \geq M \geq 1$. Because the running-time of $T = \Theta(\sqrt{2^n})$ is the solution to this optimization problem and because the Meet-in-the-Middle algorithm achieves this running-time, we can conclude that $\Theta(\sqrt{2^n})$ is a tight lower-bound for the worst-case running-time of any deterministic and exact algorithm which solves SUBSET-SUM. And this conclusion implies that $P \neq NP$ [1, 5]. ■

Acknowledgments

I thank God, my parents, my wife, and my children for their support.

Submitted on January 11, 2011 / Accepted on January 15, 2011

References

1. Cormen T. H., Leiserson C. E., Rivest R. L. Introduction to Algorithms, McGraw-Hill, 1990.
2. Menezes A., van Oorschot P., Vanstone S. Handbook of Applied Cryptography, CRC Press, 1996.
3. Horowitz E., Sahni S. Computing Partitions with Applications to the Knapsack Problem. *Journal of the ACM*, v. 2l, no. 2, April 1974, pp. 277–292.
4. Woeginger G. J. Exact Algorithms for NP-Hard Problems, *Lecture Notes in Computer Science*, 2003, v. 2570, pp. 185–207.
5. Bovet P. B., Crescenzi P. Introduction to the Theory of Complexity, Prentice Hall, 1994.

The Compton Radius, the de Broglie Radius, the Planck Constant, and the Bohr Orbits

William C. Daywitt

National Institute for Standards and Technology (retired), Boulder, Colorado, USA
E-mail: wcdaywitt@earthlink.net

The Bohr orbits of the hydrogen atom and the Planck constant can be derived classically from the Maxwell equations and the assumption that there is a variation in the electron's velocity about its average value [1]. The resonant nature of the circulating electron and its induced magnetic and Faraday fields prevents a radiative collapse of the electron into the nuclear proton. The derived Planck constant is $h = 2\pi e^2/\alpha c$, where e, α, and c are the electronic charge, the fine structure constant, and the speed of light. The fact that the Planck vacuum (PV) theory [2] derives the same Planck constant independently of the above implies that the two derivations are related. The following highlights that connection.

In the Beckmann derivation [1], the electromagnetic-field mass and the Newtonian mass are assumed to have the same magnitude in which case the electron's average kinetic energy can be expressed as

$$\left(\frac{mv^2}{2}\right)_{\text{em}} + \left(\frac{mv^2}{2}\right)_{\text{n}} = mv^2 = mv\cdot v = mv\cdot\lambda\nu = mv\lambda\cdot\nu = h\nu \quad (1)$$

where v is the average electron velocity and $v = \lambda\nu$ is a simple kinematic relation expressing the fact that the electron's instantaneous velocity varies periodically at a frequency ν over a path length equal to the wavelength λ. The constant $h\,(= mv\lambda)$ turns out to be the Planck constant.

The Beckmann derivation assumes with Maxwell and those following thereafter that the magnetic and Faraday fields are part of the electron makeup. On the other hand the PV theory assumes that these fields constitute a reaction of the negative-energy PV quasi-continuum to the movement of the massive point charge (the Dirac electron). In its rest frame the electron exerts the two-fold force [3]

$$\frac{e_*^2}{r^2} - \frac{mc^2}{r} \quad (2)$$

on each point r of the PV, where e_* $(= e/\sqrt{\alpha})$ is the electron's bare charge, e is the laboratory-observed charge, and m is the electron mass. The vanishing of this composite force at the radius $r = r_c$ leads to

$$r_c mc^2 = e_*^2 = c\hbar = e^2/\alpha, \quad (3)$$

where r_c is the electron's Compton radius and $\hbar$ is the (reduced) Planck constant. From the introductory paragraph and (3), the Beckmann and PV results clearly lead to the same Planck constant $\hbar = e^2/\alpha c = e_*^2/c$.

The Planck constant then is associated only with the bare charge $|e_*|$ and not the electron mass—thus the quantum theory reflects the fact that, although the various elementary particles have different masses, they are associated with only one electric charge.

The expression $mv\lambda = h$ used in (1) to arrive at the total electron kinetic energy is the de Broglie relation expressed in simple, physically intuitive terms: the de Broglie relation yields the product of the electron mass m, its average velocity v, and the path length λ over which its instantaneous velocity varies. The relativistic version of the relationship (which is arrived at in the Appendix by assuming the vanishing of (2) at $r = r_c$ to be a Lorentz invariant constant) is

$$m\gamma v = \frac{\hbar}{r_d} = \frac{\gamma\hbar}{r_c/\beta} = \frac{\gamma h}{\lambda_c/\beta} = \frac{\gamma h}{\lambda} \quad (4)$$

where $m\gamma v$ is the relativistic momentum; and $\lambda = \lambda_c/\beta$, where λ_c is the Compton wavelength $2\pi r_c$. Thus Beckmann's de Broglie relation is in relativistic agreement with the PV result.

The preceding demonstrates that Bohr's introduction of the quantum concept in terms of an ad-hoc Planck constant [4] can be derived from classical electromagnetism and the assumption that the electron interacts with some type of negative-energy vacuum state (the PV in the present case). That the Lorentz transformation can also be derived from the same assumptions is shown in a previous paper [5].

Acknowledgment

The present author's first contact with the late Professor Petr Beckmann was in a course he taught at the University of Colorado (USA) around 1960 on 'Statistical Communication Theory' and later (~circa 1989) in a number of phone conversations concerning his book *Einstein Plus Two* [1]. Much of the work on the PV theory was inspired by Prof. Beckmann's relentless search for the physical truth of things. In addition to authoring a number of interesting books, he founded the scientific journal *Galilean Electrodynamics* and the news letter *Access to Energy* both of which are still active today.

Appendix: de Broglie Radius

The Dirac electron exerts two distortion forces on the collection of Planck particles constituting the degenerate PV, the

polarization force e_*^2/r^2 and the curvature force mc^2/r. The equality of the two forces at the electron Compton radius r_c is assumed to be a fundamental property of the electron-PV interaction. The vanishing of the force difference $e_*^2/r_c^2 - mc^2/r_c = 0$ (a Lorentz invariant constant) at the Compton radius can be expressed as a vanishing 4-force difference tensor [6]. In the primed rest frame of the electron, where these static forces apply, this force difference $\Delta F'_\mu$ is

$$\Delta F'_\mu = \left[\mathbf{0}, i\left(\frac{e_*^2}{r_c^2} - \frac{mc^2}{r_c}\right)\right] = [0, 0, 0, i\,0] \qquad \text{(A1)}$$

where $i = \sqrt{-1}$. Thus the vanishing of the 4-force component $\Delta F'_4 = 0$ in (A1) is the Compton-radius result from (2) and can be expressed in the form $mc^2 = e_*^2/r_c = (e_*^2/c)(c/r_c) = \hbar\omega_c$, where $\omega_c \equiv c/r_c = mc^2/\hbar$ is the corresponding Compton frequency.

The 4-force difference in the laboratory frame, $\Delta F_\mu = a_{\mu\nu}\Delta F'_\nu = 0_\mu$, follows from its tensor nature and the Lorentz transformation $x_\mu = a_{\mu\nu}\, x'_\nu$ [6], where $x_\mu = (x, y, z, ict)$,

$$a_{\mu\nu} = \begin{pmatrix} 1 & 0 & 0 & 0 \\ 0 & 1 & 0 & 0 \\ 0 & 0 & \gamma & -i\beta\gamma \\ 0 & 0 & i\beta\gamma & \gamma \end{pmatrix} \qquad \text{(A2)}$$

$\gamma = 1/\sqrt{1-\beta^2}$, and $\mu, \nu = 1, 2, 3, 4$. Thus (A1) becomes

$$\Delta F_\mu = \left[0, 0, \beta\gamma\left(\frac{e_*^2}{r_c^2} - \frac{mc^2}{r_c}\right), i\,\gamma\left(\frac{e_*^2}{r_c^2} - \frac{mc^2}{r_c}\right)\right]$$

$$= \left[0, 0, \left(\frac{e_*^2}{\beta\gamma r_d^2} - \frac{mc^2}{r_d}\right), i\left(\frac{e_*^2}{\gamma r_L^2} - \frac{mc^2}{r_L}\right)\right] = [0, 0, 0, i\,0] \qquad \text{(A3)}$$

in the laboratory frame. The equation $\Delta F_3 = 0$ from the final two brackets yields the de Broglie relation

$$p = \frac{e_*^2/c}{r_d} = \frac{\hbar}{r_d} \qquad \text{(A4)}$$

where $p = m\gamma v$ is the relativistic electron momentum and $r_d \equiv r_c/\beta\gamma$ is the de Broglie radius.

The equation $\Delta F_4 = 0$ from (A3) leads to the relation $p = \hbar/r_L$, where $r_L \equiv r_c/\gamma$ is the length-contracted r_c in the *ict* direction. The Synge primitive quantization of flat spacetime [7] is equivalent to the force-difference transformation in (A3): the ray trajectory of the particle in spacetime is divided (quantized) into equal lengths of magnitude $\lambda_c = 2\pi r_c$ (this projects back on the '*ict*' axis as $\lambda_L = 2\pi r_L$); and the de Broglie wavelength calculated from the corresponding spacetime geometry. Thus the development in the previous paragraphs provides a physical explanation for Synge's spacetime quantization in terms of the two perturbations e_*^2/r^2 and mc^2/r the Dirac electron exerts on the PV.

Submitted on February 01, 2011 / Accepted on February 05, 2011

References

1. Beckmann P. Einstein Plus Two, The Golem Press, Boulder, Colorado, 1987, (see Chapter 2).
2. Daywitt W.C. The Planck vacuum, *Progress in Physics*, 2009, v. 1, 20–26.
3. Daywitt W.C. The Dirac Electron in the Planck Vacuum Theory, *Progress in Physics*, 2010, v. 4, 69–71.
4. Leighton R. B. Principles of Modern Physics, McGraw-Hill Book Co., New York, 1959.
5. Daywitt W. C. The Lorentz Transformation as a Planck Vacuum Phenomenon in a Galilean Coordinate System, *Progress in Physics*, 2011, v. 1, 3–6.
6. Jackson J.D. Classical Electrodynamics, John Wiley & Sons, 1st ed., 2nd printing, New York, 1962.
7. Synge J.L. Geometrical Mechanics and de Broglie Waves, Cambridge University Press, 1954, (see pages 106–107).

Histograms Constructed from the Data of ^{239}Pu Alpha-Activity Manifest a Tendency for Change in the Similar Way as at the Moments when the Sun, the Moon, Venus, Mars and Mercury Intersect the Celestial Equator

Simon E. Shnoll[*†§], Ilya A. Rubinstein[‡], Sergey N. Shapovalov[♯], Valery A. Kolombet[†], Dmitri P. Kharakoz[†]

[*]Department of Physics, Moscow State University, Moscow, Russia
[†]Institute of Theor. and Experim. Biophysics, Russ. Acad. Sci., Pushchino, Russia
[‡]Skobeltsin Inst. of Nuclear Physics at Moscow State Univ., Moscow, Russia
[§]Pushchino State University, Pushchino, Russia
[♯]Arctic and Antarctic Research Institute, St. Petersburg, Russia

E-mail: shnoll@mail.ru (Simon E. Shnoll, the corresponding author)

Earlier, the shape of histograms of the results of measurements obtained in processes of different physical nature had been shown to be determined by cosmophysical factors [1]. Appearance of histograms of a similar shape is repeated periodically: these are the near-a-day, near-27-days and annual periods of increased probability of the similar shapes. There are two distinctly distinguished near-a-day periods: the sidereal-day (1,436 minutes) and solar-day (1,440 minutes) ones. The annual periods are represented by three sub-periods: the "calendar" (365 average solar days), "tropical" (365 days 5 hours and 48 minutes) and "sidereal" (365 days 6 hours and 9 minutes) ones. The tropical year period indicates that fact that histogram shape depends on the time elapsed since the spring equinox [2]. The latter dependence is studied in more details in this work. We demonstrate that the appearance of similar histograms is highly probable at the same time count off from the moments of equinoxes, independent from the geographic location where the measurements had been performed: in Pushchino, Moscow Region (54° NL, 37° EL), and in Novolazarevskaya, Antarctic (70° SL, 11° EL). The sequence of the changed histogram shapes observed at the spring equinoxes was found to be opposite to that observed at the autumnal equinoxes. As the moments of equinoxes are defined by the cross of the celestial equator by Sun, we also studied that weather is not the same as observed at the moments when the celestial equator was crossed by other celestial bodies — the Moon, Venus, Mars and Mercury. Let us, for simplicity, refer to these moments as a similar term "planetary equinoxes". The regularities observed at these "planetary equinoxes" had been found to be the same as in the case of true solar equinoxes. In this article, we confine ourselves to considering the phenomenological observations only; their theoretical interpretation is supposed to be subject of further studies.

1 Materials and methods

A many-year monitoring of the alpha-activity of ^{239}Pu samples (performed with devices constructed by one of the authors, I. A. Rubinstein [3]) was used as a basis for this study. Round-the-clock once-a-second measurements were made in Pushchino, at the Institute of Theoretical and Experimental Biophysics, Russian Academy of Sciences, and at Novolazarevskaya Antarctic Polar Station of the Arctic and Antarctic Institute.

Semi-conductor detectors used were either collimator-free or equipped with collimators limiting the beam of registered alpha-particles by a spatial angle (about 0.1 radian) within which the particles travelled along a certain direction: towards the Sun, Polar Star, West or East. The number of registered alpha-particles during one-second interval was the measured parameter. Results of the continuous once-a-second measurements of the decay activity were stored in a computer databank.

One-minute histograms constructed from 60 results of the once-a-second measurements of activity were the main objects of analysis in our study. The histograms were visually compared with each other in order to estimate the resemblance of their shape. The estimation was made by the method of expert judgment. This analysis was performed with the assistance of Edwin Pozharsky's computer program (described in [1]) which allowed to construct histograms for each one-minute interval in a series of measurements and, further, to smooth and scale them, and to mirror (if needed) in order to superimpose the histograms and visually compare their shape. At the final step of analysis, we constructed the distribution of the number of pairs of similar histograms versus the interval separating the histograms in each pair. Fig. 1 presents a diagram explaining three kinds of comparison of the series of histograms.

Method A; direct alignment (parallel). These two compared histogram series are aligned with each other as parallel

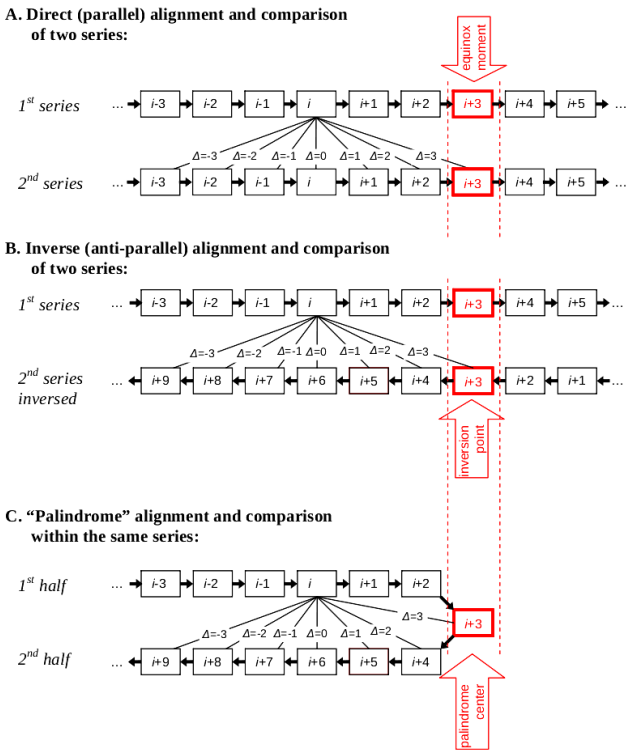

Fig. 1: Boxes indicate histograms constructed for the measured radioactivity within each minute of time. Arrows connecting the boxes indicate the direction of time separating the one-minute histograms. The interval between the histograms, Δ, is measured in minutes or in position numbers in the aligned series.

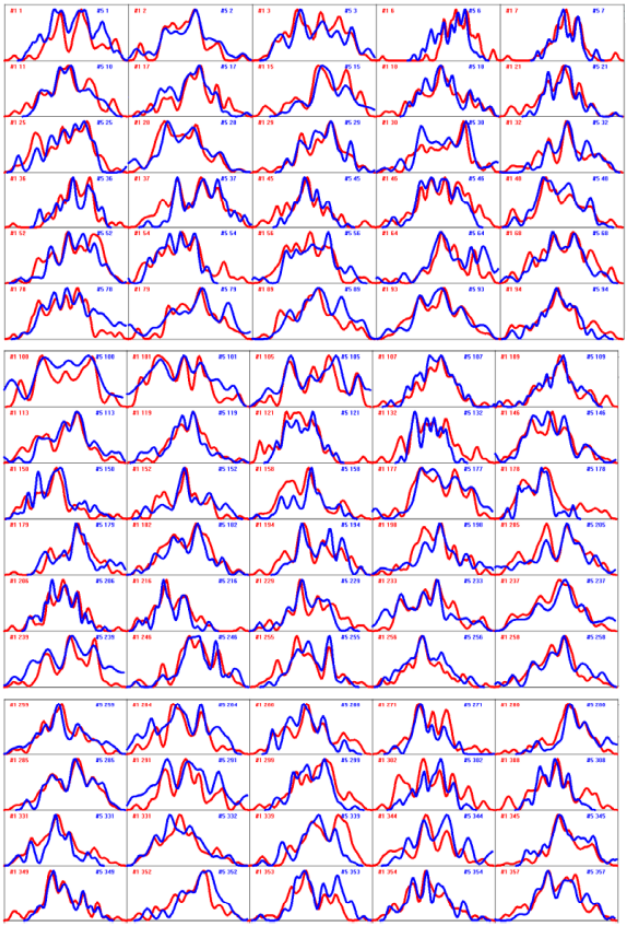

Fig. 2: Extract from a laboratory log: pairs of similar histograms of ^{239}Pu alpha-activity taken at the same time count off from the moments of Moon-2005-March-11 and Venus-2001-October-18 equinoxes. Each histogram is constructed by 60 one-second measurements (total time being equal to 1 minute). The doubled figures in upper corners of each picture specify the series number (No.1 or No.5) and the position number of a histogram in the series. Histograms of Moon-2005-March-11 equinox are drawn in red and those of Venus-2001-October-18 in blue. The data presented here correspond to the extreme in the blue curve in Fig. 4.

sequences in which the equinox moments occur at the same place. Then each i-th histogram of one series is compared with the number of neighboring histograms of the other series, as shown in Fig. 1, case A.

Method B; inverse alignment (anti-parallel). These two series are aligned in the same way but the second one is reversed at the point of equinox. This is illustrated in Fig. 1B.

Method C; "palindrome" alignment. Two parts of the same sequence are compared with each other. To do that, we assume the equinox moment to be the inversion center of a palindrome. Therefore, the second half of the sequence (following the center) is reversed and aligned with the first half as shown in Fig. 1C. Then the two halves of the sequence are compared with each other.

Fig. 2 presents an extract from the laboratory log-file to illustrate what shapes are considered similar from the expert's viewpoint. Final results are presented as the plots of the frequency of similar pairs of histograms versus the interval (measured in minutes) separating the position of items in the pairs (Fig. 3, e.g.).

The true equinox moments and the equivalent moments when the Moon, Mars, Venus or Mercury intersect the celestial equator (called here, by analogy, "planetary equinoxes") were determined by nonlinear interpolation of the data tabulated in the annual astronomy tables [4]; the residual error of this interpolation was much within the time resolution of our observations.

2 Results

2.1 Comparison of the histogram series obtained at the successive (in turn) "equinoxes"

It had been found earlier [2, 5, 6], in studying the variation of shape of the successive sequences of histograms obtained at vernal and autumnal equinoxes, the sequences related to "homonymous" equinoxes (vernal-and-vernal or autumnal-and-autumnal ones) display the similarity higher than that of "heteronymous" equinoxes. This fact gave a hint for a hypothesis that the histogram shape may depend not only on the

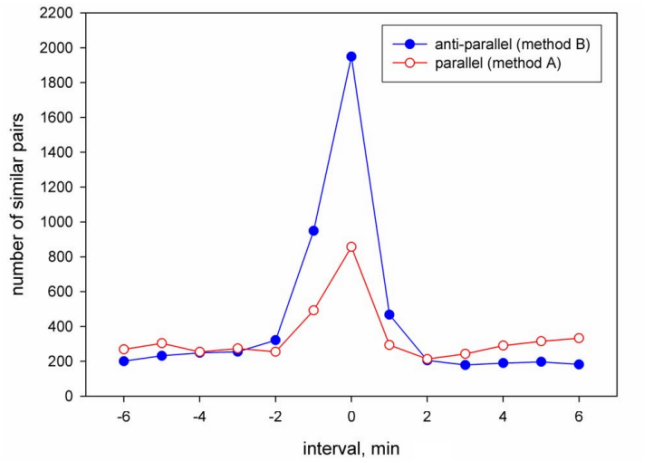

Fig. 3: Total number of similar pairs of histogram as function of time interval separating the histograms in the pair. The compared histogram sequences were related to the successive (neighboring) equinoxes. The sequences compared were aligned parallel or anti-parallel around the very "equinox" moment. First what is seen in the figure is that the probability to find a similar pair of histograms sharply decreases with the distance between the items in the pair. Second important moment is that the maximum probability (which is a measure of similarity of the sequences) is three times higher in the case the sequences compared are oriented anti-parallel. That means the histogram shape depends not only on the proximity of a planet or Sun to the celestial equator but also on the direction a celestial body moves to it. The diagram represents a summary of data for 24 pairs of compared series of alpha-activity aligned around the Sun, the Moon, Mars, Venus and Mercury "equinoxes". The series were 720 minutes long each. The data used have been obtained either in Pushchino and Novolazarevskaya.

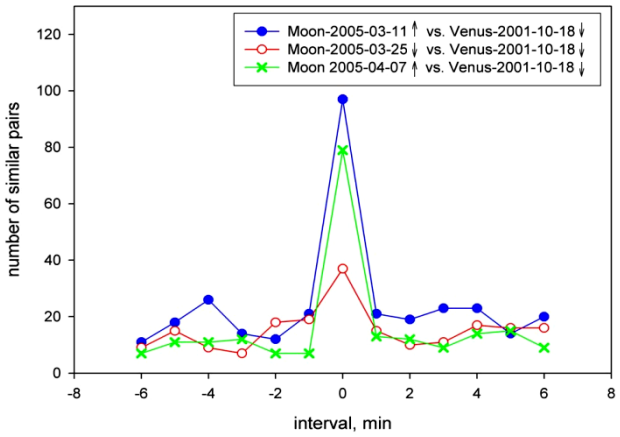

Fig. 4: Histogram series at the Venus setting "equinox" 2001-October-18(↓) is highly similar to those at the Moon rising "equinoxes" 2005-March-11(↑), 2005-April-7(↑) and considerably less similar to the series at the Moon setting "equinox" 2005-March-25(↓). (The extreme of this distribution is formed with the pairs of histograms presented in Fig. 2, to illustrate the extent of their similarity.)

proximity to the equinox moment, but also on the direction the Sun is moving to the celestial equator: from the northern or from the southern hemisphere. The hypothesis has been confirmed by comparison of the *direct* series of the autumn histograms with the inverse series of the spring histograms [2, 5, 6] (cf. in Fig. 1, method B).

In this work, the same analysis is applied to the data including "planetary equinoxes". Namely, not only solar but also lunar, venusian, martian and mercurian "equinoxes" have been considered. Fig. 3 summarizes the results of 24 pairs of such "equinox" events. Only the pairs of *successive* "equinoxes" were here compared; i.e., a series of histograms obtained at one "equinox" was compared with that of just next "equinox" for the same celestial body. The series were compared with use of either procedure A (parallel) and B (anti-parallel) (cf. in Fig. 1).

Fig. 3 shows that:

1. The phenomenon of similarity of the temporal change of the histogram shape near the moments of intersection of the celestial equator by a celestial body appears to be independent of the nature of the body (whatever the Sun, the Moon, Venus, Mars or Mercury). Hence, the sequential changes of histograms do not show any gravitational influence of the bodies;
2. Neither does it depend on the geographic point where the measurements have been performed: the data obtained in Pushchino and Novolazarevskaya (Antarctic) display similarity of histograms at the same absolute time, to within one-minute accuracy;
3. Neither does it depend on the velocity a celestial body moves across the equator. Despite a great difference in both angular and linear velocities of the bodies, the changes of histogram shape are correlated in the sequences aligned along the same time scale. This is a surprising result that has not a simple kinematic explanation. This fact, again, is an indication of that the phenomenon observed is not a matter of any "influence" exerted by a celestial bodies on the observable value;
4. What we can learn from the fact that the similarity of histogram sequences is higher in the case of anti-parallel orientation of compared sequences is as follows. The variation of histogram shape shows not only the extent of proximity of the Sun or a planet to the celestial equator but also their location in one or another celestial hemisphere. In other words, the "northern" histograms of a vernal equinox display higher similarity to the "southern" histograms of the next autumnal equinox despite the movement of the body on the sky sphere are reciprocal at these two cases.

The fact that the histogram shape variations do not depend on the nature of celestial body is confirmed also by pairwise comparison of the "equinoxes" of different planets. For example, Fig. 4 presents the results of comparison of a Venus "equinox" (2001-October-18 (↓)) with three Moon "equi-

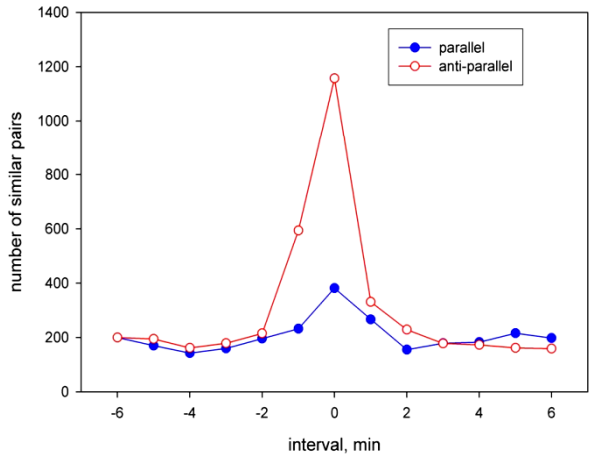

Fig. 5: The palindrome effect. The number of similar pairs of histograms in two compared halves of a sequence separated by the equinox moment as function of time shift between the halves. Total numbers obtained in the analysis of 17 equinox and "planetary equinox" events are presented here. Comparison of half-sequences was performed with the procedure C in Fig. 1. Palindrome effect is indicated by the fact that the similarity of anti-parallel half-sequences is 3-fold higher then that of parallel half-sequences.

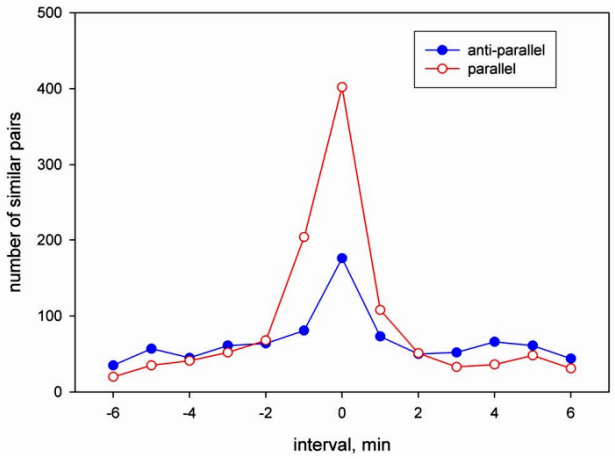

Fig. 6: Summarized data on 8 different Moon, Sun and Mars "equinoxes" when the ^{239}Pu alpha-activity was measured with the collimators directed towards Polar Star. Parallel oriented sequences of histograms display 3-fold higher similarity than those oriented anti-parallel.

noxes" (2005-March-11(↑); 2005-March-25(↓), and 2005-April-7(↑)). The figure shows that:

1. The histogram series adjusted to "equinox" moments are similar even if the events considered are separated by years (four years in this particular case);
2. The similarity of histograms depends on the direction of movement towards the celestial equator. However, in this particular case, symbate "equinoxes" (Venus-2001-October-18(↓) and Moon-2005-March-25(↓)) happened to be less similar then the counter-directed ones (Venus-2001-October-18(↓) and the other two Moon "equinoxes", both rising).

2.2 Comparison of direct and inverse halves of the same series of histograms (the "palindrome" effect)

The "palindrome effect" has been described in a number of earlier works; this is the presence of specific inversion points in the time series of histograms after which the same histograms occur in the reverse order [2, 5, 6]. Over a daily period, 6 am and 6 pm of local time have been found to be such inversion points. Any point on the Earth's surface participates in two movements, one due to the rotation of the Earth about its axis and another due to the movement of the center of the Earth along its circumsolar orbit. One finds that, the projections of the two movements onto the circumsolar orbit are counter-directional during the daytime (6 am to 6 pm) and co-directional during the nighttime (6 pm to 6 am). This is a probable "kinematic" reason for these two time moments are featured.

A question arose if there are a number of such "palindrome" centers existing at the equinoxes and "planetary equinoxes", separating the celestial body movement towards and away from the celestial equator. This supposition has proved to be true. Indeed, the histogram sequences preceding the equinox moments were similar to the inverse sequences following this moments. The palindrome effect (detected with the procedure C; cf. Fig. 1), is illustrated in Fig. 5. As revealed from the picture, the probability to find similar histograms is 3-fold higher if one of the compared half-sequences is inverted — this is exact the essence of the palindrome effect.

Phenomenological meaning of this observation is that the "equinox" moments are just the points at which the order of changing the histogram shapes is reverted. Sharpness of the peak is an indication of a high accuracy (one minute) of detection of the "equinox" moment. Mirror symmetry of the histogram sequences around an equinox means that histogram shape depends on how far distant is the celestial body from the equator plane, whatever on the northern or southern side of the celestial sphere. This result might seem to conflict with the data presented in Fig. 3 indicating that the direction of the movement also does matter. However, the seeming conflict is resolved by the fact (revealed from our special investigation) that these two phenomena are determined by different, not overlapping sets of similar histograms.

2.3 Equinox effects in the data obtained with collimators

The phenomena presented in Figs. 3-5 have been observed in the data on the alpha-activity measured with either collimator-free detectors and those supplied with the collimator permanently directed towards West or East or towards the Sun. No dependence of the observed phenomenology on the orientation of the collimator was found in these cases. The only

dramatic difference has been found for the case where the collimator was directed towards the Polar Star.

In this series of data, the sequences of histograms obtained at the sequential (neighboring) "equinoxes" displayed higher similarity when they were compared as parallel sequences (procedure A in Fig. 1) and lesser similarity when they were anti-parallel. This observation is illustrated in Fig. 6, summarizing the results of eight equinox events with the Moon, the Sun and Mars. Therefore, the difference between the northern and southern hemispheres is not reflected in the measurements with the collimator directed to Northern Pole.

3 Discussion

A number of phenomenological conclusions follow from the results presented herein:

1. The shape of histograms obtained from the measurements performed in different geographic locations near the time of "equinoxes" is changing synchronously, within one minute accuracy. For instance, they occur simultaneously in Pushchino and Novolazarevskaya despite 104 minutes of local time difference between these two places. This means this is a global phenomenon independent of the Earth axial rotation;
2. The changes of histograms obtained near the solar or planetary "equinoxes" do not depend on the nature of the "acting" celestial body, whatever the Sun, Mercury, Mars, Venus or Mercury. Individual features of the bodies — different masses and different rates of their orbital movement — are not essential;
3. At very equinox moments, the inversion of the sequence of the histogram shapes occurs: the sequence preceding this moment is reciprocal to that observed after it. A moment when the celestial equator is intersected by a celestial body is a particular point in the histogram series. Its position on the time scale can be determined, with a high accuracy, from the palindrome effect;
4. Changes of histograms near the "equinoxes" depend on the direction in which the celestial body intersects the equator plane (from the northern or from southern hemisphere);
5. Seeming contradiction between these two phenomena — the similarity of the anti-parallel sequences obtained at successive equinoxes, and the mirror similarity of two halves of each histogram sequence (the "palindrome effect") — is, probably, resolved by the fact that these two kinds of symmetry are determined by different, not overlapping sets of similar histograms;
6. Phenomena observed with collimators can be considered as an indication of the anisotropy of space. Vanishing of the "palindrome" phenomena when the collimator is oriented towards the Polar Star is, perhaps, the most indicative fact favoring the conclusion on the anisotropy. Analysis of this phenomenon should be subjected to further studies.

B. V. Komberg attracted our attention to the fact that the direction of the equinox line (the line of intersection of the equatorial and ecliptic planes) may coincide with direction of the line of the minimum temperature of the Cosmic Microwave Backgroud (relict) Radiation, called the "axis of evil" in the scientific literature [7].

Acknowledgements

We sincerely appreciate A. E. Shnoll and A. E. Rodin's participation in the calculation of the moments the celestial equator is intersected by the Moon, Venus and Mars and valuable advice in the data analysis. We sincerely appreciate valuable discussion with S. A. Vasiliev and his interpretation of our results [8]. We sincerely appreciate A. A. Andreyeva's work as a "second expert" in the analysis of similarity of histograms. We are much obliged to our colleagues from the Laboratory for Physical Biochemistry of the Institute for Theoretical and Experimental Biophysics of RAS and from Chair of Biophysics at Physics Department of MSU, for useful discussions at our seminars, and especially to O. Yu. Seraya for discussion and English translation of the article. We appreciate T. A. Zenchenko's systematic job on the development and support of a computer databank for radioactivity monitoring. We are grateful to D. D. Rabounski for his valuable discussion. The work would be impossible without M. N. Kondrashova and her continuous attention, support and discussion of results. Financial support from D. B. Zimin is greatly appreciated.

Submitted on January 01, 2011 / Accepted on January 05, 2011

References

1. Shnoll S. E. Cosmo-Physical Factors in Stochastic Processes. Svenska Fisikarkivet, Stockholm, 2009.
2. Shnoll S. E., Panchelyuga V. A., and Shnoll A. E. The Palindrome Effect. *Progress in Physics*, 2008, v. 2, 151–153.
3. Shnoll S. E. and Rubinstein I. A. Regular changes in the fine structure of histograms revealed in the experiments with collimators which isolate beams of alpha-particles flying at certain directions. *Progress in Physics*, 2009, v. 2, 83–95.
4. Astronomical Yearbook. St. Petersburg, Nauka, 2000–2008.
5. Shnoll S. E. The "scattering of the results of measurements" of processes of diverse nature is determined by the Earth's motion in the inhomogeneous space-time continuum. The effect of "half-year palindromes. *Progress in Physics*, 2009, v. 1, 3–7.
6. Shnoll S. E., Rubinstein I. A., Vedenkin N. N. The "arrow of time" in the experiments in which alpha-activity was measured using collimators directed East and West. *Progress in Physics*, 2010, v. 1, 26–29.
7. Schild R. E., Gibson C. H. Goodness in the Axis of Evil. arXiv: astro-ph/0802.3229.
8. Vasiliev S. A. On the physical model of the phenomena registered in the experiments by Shnoll's group and Smirnov's group. *Progress in Physics*, 2009, v. 2, 29–43.

Electron Configuration, and Element No.155 of the Periodic Table of Elements

Albert Khazan

E-mail: albkhazan@gmail.com

Blocks of the Electron Configuration in the atom are considered with taking into account that the electron configuration should cover also element No.155. It is shown that the electron configuration formula of element No.155, in its graphical representation, completely satisfies Gaussian curve.

1 Introduction

As is known, even the simpliests atoms are very complicate systems. In the centre of such a system, a massive nucleus is located. It consists of protons, the positively charged particles, and neutrons, which are charge-free. Masses of protons and neutrons are almost the same. Such a particle is almost two thousand times heavier than the electron. Charges of the proton and the electron are opposite, but the same in the absolute value. The proton and the neutron differ from the viewpoint on electromagnetic interactions. However in the scale of atomic nuclei they does not differ. The electron, the proton, and the neutron are subatomic articles. The theoretical physicists still cannot solve Schrödinger's equation for the atoms containing two and more electrons. Therefore, they process the calculations for only the single-electron atom of hydrogen, with use of the dualistic property of the electron, according to which it can be respresented, equally, as a particle and a wave. At the same time, the conclusions provided after the quantum theory cannot be considered as the finally true result.

To make the further text simpler, we assume the following brief notations: the Periodic Table of Elements containing 118, 168, and 218 elements will be referred to as T.118, T.168, and T.218 respectively.

2 Calculation of the electron shell for element No.155

Electron shells of the atoms (known also as the *levels*) are regularly denoted as K, L, M, N, O, or as plain numbers from 1 to 5. Each level consists of numerous sub-levels, which are split into atomic orbitales. For instance, the 1st level K consists of a single sub-level 1s. The second level L consists of two sub-levels 2s and 2p. The third level M consists of the 3s, 3p, and 3d sub-levels. The fourth level N consists of the 4s, 4p, 4d, and 4f sub-levels. At the same distance from the atomic nucleus, only the following orbitales can exist: one -s-, three -p-, five -d-, seven -f-, while no more than two electrons can be located in each single orbital (according to Pauli's principle). Hence, the number of electrons in each level can be calculated according to the formula $2N^2$. Results of the calculation are given in Table 1.

As is seen from this Table, the complete external electron level is the configuration s2+p6, known as octet.

	K	L	M	N	O	Sum	Content in the shells
s	2					2	in each shell
p	2	6				8	in each, commencing in the 2nd shell
d	2	6	10			18	in each, commencing in the 3rd shell
f	2	6	10	14		32	in each, commencing in the 4th shell
g	2	6	10	14	18	50	in each, commencing in the 5th shell

Table 1: Number of electrons in each level.

The elements, whose electrons occupy the respective sublevels, have one of the denotations: s-, p-, d-, f-, or g-elements (in analogy to electrons).

2.1 Electron Configuration in the other elements

In the regular form of the Periodic Table of Elements, each cell of the Table bears a large information about the element, including the electron constitution of the atom. The cells containing the same sub-levels are often the same-coloured in the Table, and are joined into the following blocks (T.118):

s-elements, the 1st and the 2nd groups, 7 periods;

p-elements, 6 groups × 6 periods (periods 5–10, 13–18, 31–36, 49–54, 81–86, 113–118);

d-elements, 10 groups × 4 periods, between s- and p-elements;

f-elements, 2 lines of 14 elements each (lantanides and actinides).

Fig. 1 shows distribution of the blocks of T.118, with the assumption of that all last elements are known (the lower arc) [1]. The tabular data of the blocks are easy-to-convert into a graph, if using the known number of the elements. It should be noted that the abscissa axis means number of the blocks (not number of the periods). The form of this arc is close to parabola, and is easy-to-describe by the cubic equation with the value of true approximation $R^2 = 1$.

One can find, in the scientific press, suggestions about the possibility of introducing, into the version T.118 of the Periodic Table, two additional periods of 50 elements in each thus

making it T.218. Therefore, we checked this variant as well (the upper arc), for clarity of the experiments [2, 3]. According to the reference data [4], we assumed five blocks which join all elements of the Periodic Table as follows:

s-elements = 18,
p-elements = 48,
d-elements = 60,
f-elements = 56,
g-elements = 36.

As is seen, the upper arc in Fig. 1 is absolutely similar to that of T.118 (the lower arc). The larger size of the upper arc (T.218) are due to the larger number of elements.

Having these two examples considered, we clearly understand that the aforeapplied method we suggested can as well be applied to the version of the Periodic Table which ends at element No.155.

In order to check this supposition, we created Table 2 wherein we present the respective data for Fig. 1 and Fig. 2.

The upper arc of Fig. 2 shows distribution of the blocks of the electron configuration, calculated according to the reference data of T.168. Lower, another arc is presented. It is created according to our calculation for T.155 (i.e. for the Table of Elements, whose upper limit if element No.155). As is seen, the left branches of the arcs differ from each other for a little, while the right branches actually met each other. The absence of any bends or breaks, and also smooth form of both arcs, and their complete satisfying the approximation equation $R^2 = \sim 1$, manifests the presence of the same law in the basis of these data.

Therefore, we now can claim that element No.155 is included into the blocks of the electron configuration as the last element of the Periodic Table of Elements.

2.2 Electron shells of the atoms

Because our method of comparing the electron configuration of the elements was successful for element No.155, we are going to apply it to theoretical constructing the electron shells. Here we should take into account that: the electrons of the external shells bear more powerful energy, they are more distantly located from the nucleus, and determine the chemical properties of reactions due to the fact that their connexion with the nucleus is weaker thus easier to break. All data, we collected in order to check the aforementioned suggestion, are presented in Table 3. Line 4 of the Table contains the data for the version of element No.155 as that continuing the Table of Elements, while Line 5 contains the respective data suggested by me according to [5].

As is seen, from Fig. 3, all the arcs have the form which is very close to parabola, with a clearly observed maximum and the joined left branches. The difference in their ordinates is due to the difference in the number of the electrons (column 5 of Table 3). The right branches are parallel to each other, and are shifted with respect to each other for the shell number. The main result means here the presence of a qualitative connexion between the electron shells and their graphical representation. For only this reason, we had the possibility to compare the data of the last lines of Table 3.

Fig. 4 manifests that the upper arc is similar to the previous of Fig. 3, while the lower arc (T.155 Author) very differs from all them. According to its form, this is a differential function of normal distribution (the Gauss arc). The difference between the ends of the left and right branches is 0.645%. The branches are very symmetric to each other with respect to the vertical axis coming through the top with coordinates (5, 36). Hence, here is also a strong dependency between the regular method of description of the electron shells and its graphical representation.

This fact is most illustrative manifested in Fig. 5. The left straight covers four electron shells (2, 8, 18, 32), which are the same for all versions of Table 3 (as follows from the equation of the straight line $Y = 2X + 0.6931$. As is seen, once the arcs reach their maximum, they come down very fast (this is because the number of electrons decreases very fast in the shells).

3 Conclusion

Thus, element No.155 has really lawful to be positioned in the Periodic Table of Elements. This element points out not only the upper limit of the Table, found in my earlier study on the basis of the hyperbolic law [6, 7], but also can be presented as a graphical sequel of the calculations produced according to Quantum Mechanics (they have a high precision).

Submitted on February 01, 2011 / Accepted on March 08, 2011

References

1. http://webelements.com; See also: http://en.wikipedia.org/wiki/File:Electron_Configuration_Table.jpg
2. Seaborg G. T. and Bloom J. L. The synthetic elements. *Scientific American*, 1969, v. 220, no. 4, 56.
3. Goldanskii V. I. About connections nuclear and chemical physics. *Progress in Physical Sciences*, 1976, v. 118, issue 2.
4. Nebegrall W. H., Schmidt F. C., Holtzclaw H. F., Jr. General Chemistry. Fourth edition, D. C. Heath and Company, Massachusetts, 1972, pp. 668–670; Also: Extended Periodic Table (suggested by Jeries A. Rihani in 1984), http://jeries.rihani.com
5. FLW, Inc. provides ISO certified calibration for physical measurement, test and control, http://www.flw.com/datatools/periodic/
6. Khazan A. Upper limit in the Periodic System of Elements. *Progress in Physics*, 2007, v. 1, 38–41.
7. Khazan A. Upper Limit in Mendeleev's Periodic Table — Element No.155. Svenska fysikarkivet, Stockholm, 2010.

Number of the elements	Number of the blocks				
	s	p	d	f	g
T.218	18	48	60	56	36
T.168	16	42	50	42	18
T.118	14	36	40	28	—
T.155	16	36	46	42	15

Table 2: Blocks of the electron configuration.

Number of the elements	Number of the electrons in the shells								
T.218	2	8	18	32	50	50	32	18	8
T.168	2	8	18	32	50	32	18	8	—
T.118	2	8	18	32	32	18	8	—	—
T.155 Table	2	8	18	32	50	32	11	2	—
T.155 Author	2	8	18	32	36	32	18	8	1

Table 3: Electron shells of the atoms.

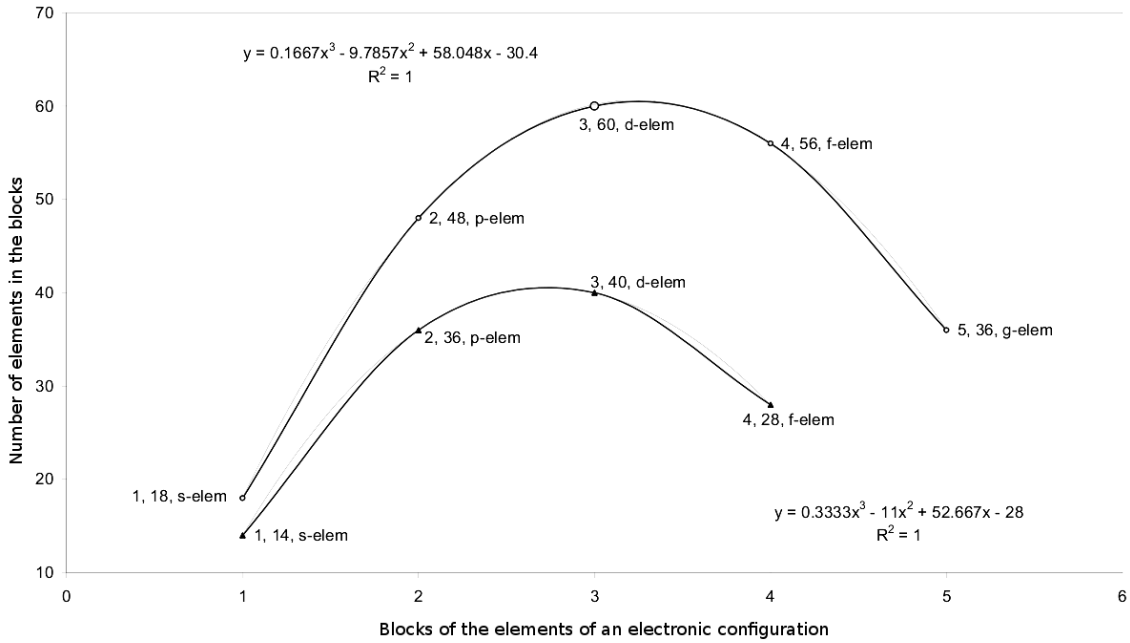

Fig. 1: Location of the blocks of the electron configuration in the Periodic Table of Elements, containing different number of the elements. The upper arc — the Table of 218 elements. The lower arc — the Table of 118 elements.

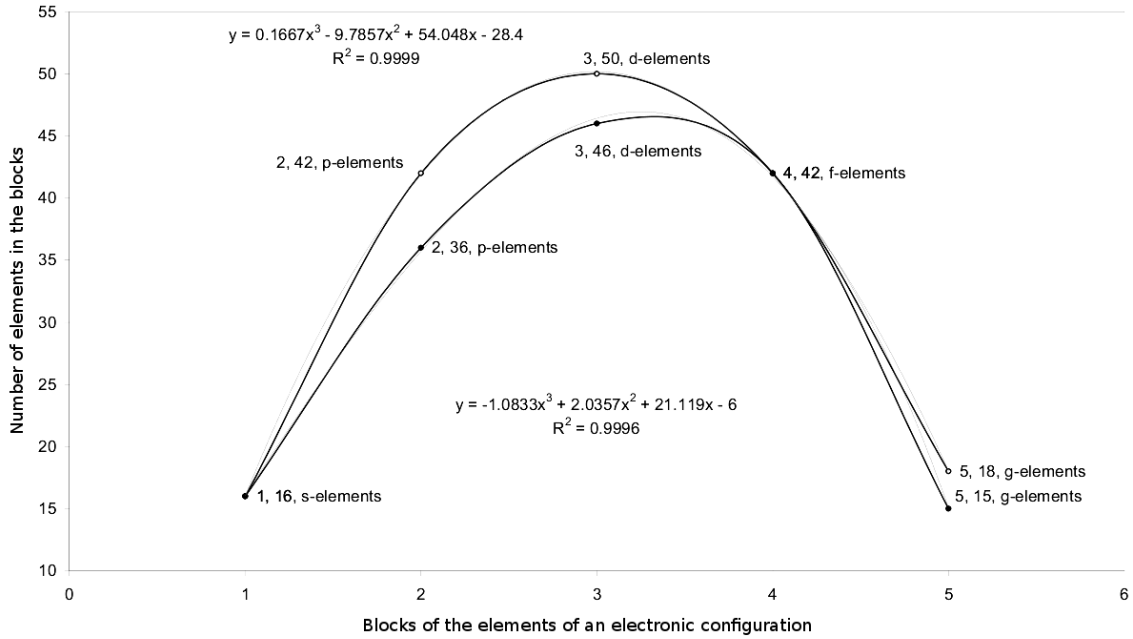

Fig. 2: Dependency, in the blocks, between the number of the elements and the electron configuration. The upper arc — the Table of 168 elements. The lower arc — the Table of 155 elements.

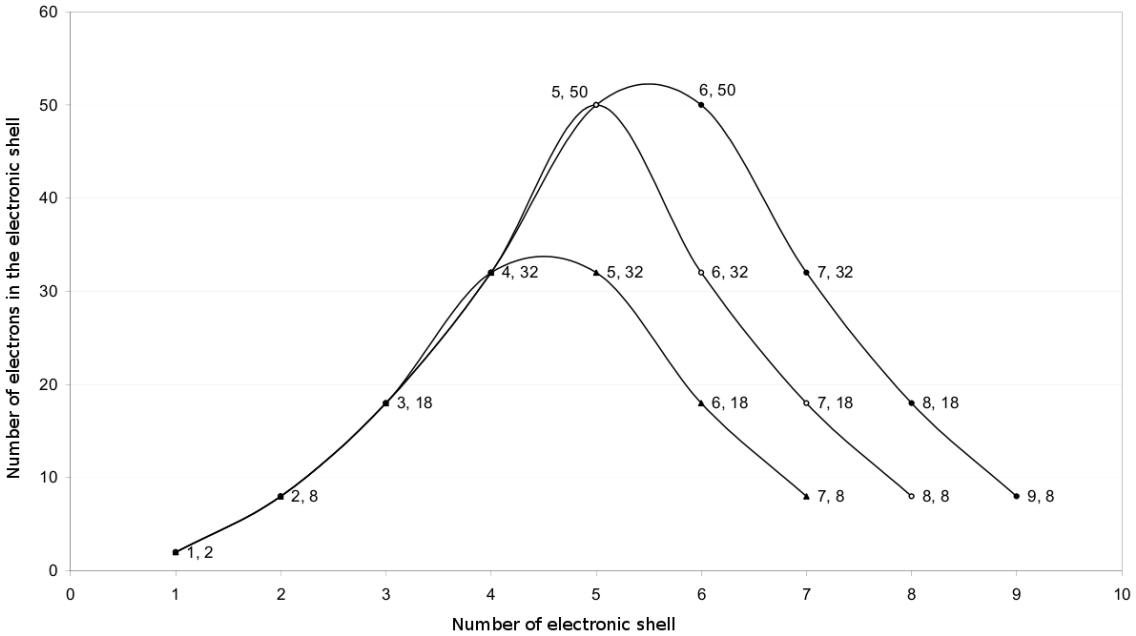

Fig. 3: Dependency of the number of electrons in the electron shells from the shell number, for three versions of the Periodic Table of Elements — T.118, T.168, T.218 (from up to down).

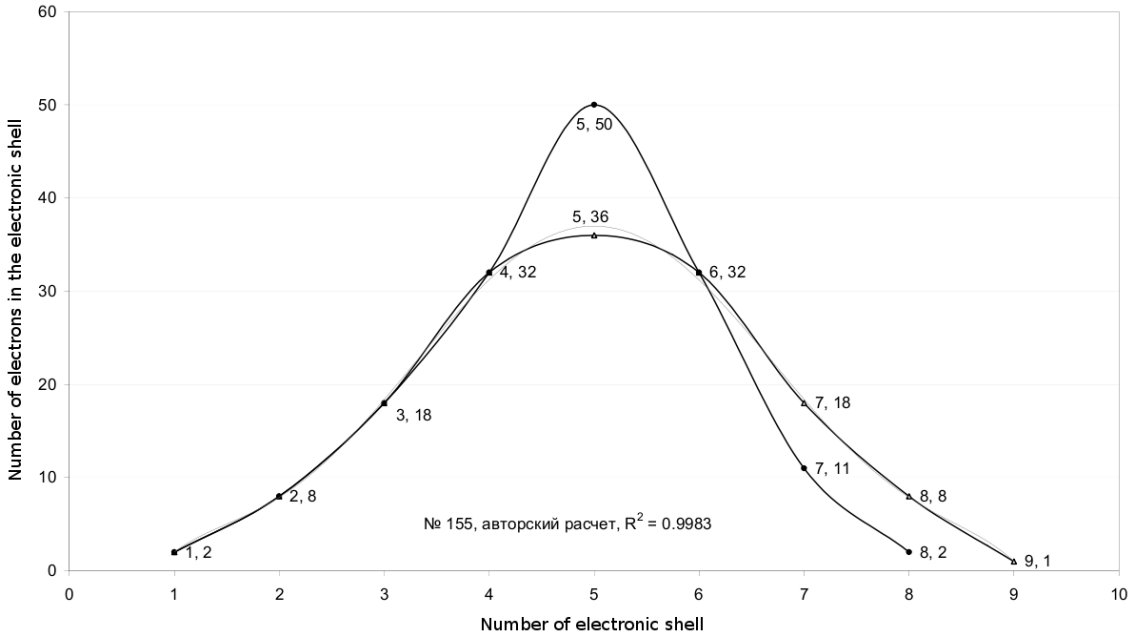

Fig. 4: Dependency of the number of electrons in the electron shells from the shell number, for element No.155 according to the tabular data (the upper arc) and the author's calculation (the lower arc).

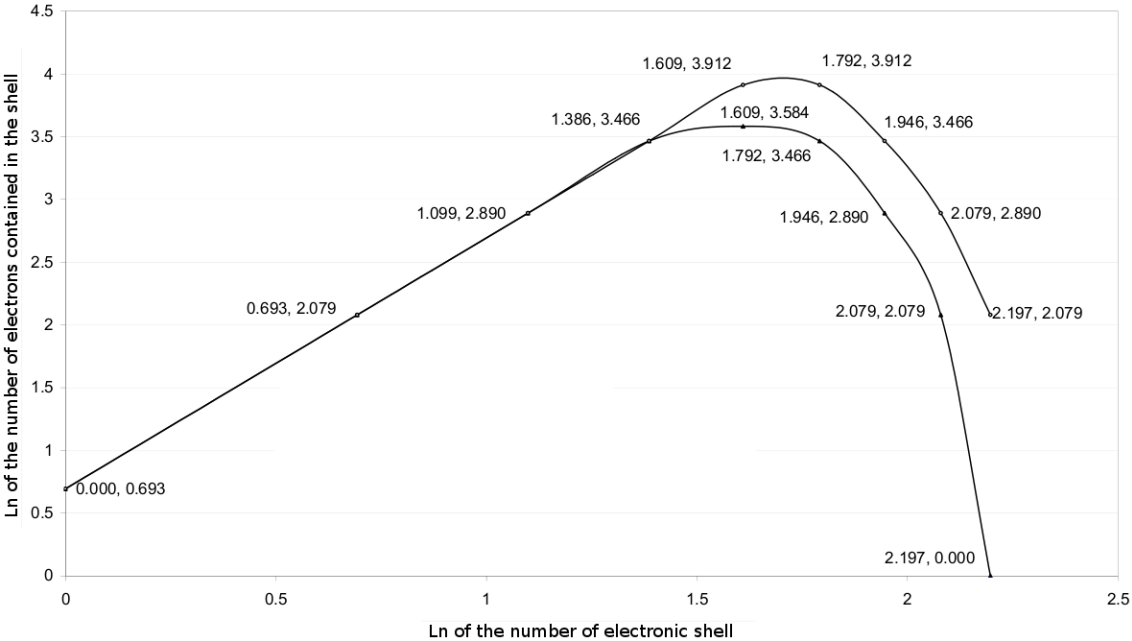

Fig. 5: Dependency of the number of electrons in the electron shells from the shell number (presented in the logarithm coordinates), for T.218 (the upper arc) and for T.155 according to the author's calculation (the lower arc).

Dynamical 3-Space: Cosmic Filaments, Sheets and Voids

Reginald T. Cahill
School of Chemical and Physical Sciences, Flinders University, Adelaide 5001, Australia
E-mail: Reg.Cahill@flinders.edu.au

Observations of weak gravitational lensing combined with statistical tomographic techniques have revealed that galaxies have formed along filaments, essentially one-dimensional lines or strings, which form sheets and voids. These have, in the main, been interpreted as "dark matter" effects. To the contrary here we report the discovery that the dynamical 3-space theory possesses such filamentary solutions. These solutions are purely space self-interaction effects, and are attractive to matter, and as well generate electromagnetic lensing. This theory of space has explained bore hole anomalies, supermassive black hole masses in spherical galaxies and globular clusters, flat rotation curves of spiral galaxies, and other gravitational anomalies. The theory has two constants, G and α, where the bore hole experiments show that $\alpha \approx 1/137$ is the fine structure constant.

1 Introduction

Observations of weak gravitational lensing and statistical tomographic techniques have revealed that galaxies have formed along filaments, essentially one-dimensional lines or strings [1], see Fig.1. These have, in the main, been interpreted as "dark matter" effects. Here we report the discovery that the dynamical 3-space theory possesses such filamentary solutions, and so does away with the "dark matter" interpretation. The dynamical 3-space theory is a uniquely determined generalisation of Newtonian gravity, when that is expressed in terms of a velocity field, instead of the original gravitational acceleration field [2, 3]. This velocity field has been repeatedly detected via numerous light speed anisotropy experiments, beginning with the 1887 Michelson-Morley gas-mode interferometer experiment [4, 5]. This is a theory of space, and has explained bore hole anomalies, supermassive black hole masses in spherical galaxies and globular clusters, flat rotation curves of spiral galaxies, and other gravitational anomalies. The theory has two constants, G and α, where the bore hole experiments show that $\alpha \approx 1/137$ is the fine structure constant. The filamentary solutions are purely a consequence of the space self-interaction dynamics, and are attractive to matter, and as well generate electromagnetic lensing. The same self-interaction dynamics has been shown to generate inflow singularities, *viz* black holes [6], with both the filaments and black holes generating long-range non-Newtonian gravitational forces. The dynamical 3-space also has Hubble expanding universe solutions that give a parameter-free account of the supernova redshift-magnitude data, without the need for "dark matter" or "dark energy" [7]. The black hole and filament solutions are primordial remnants of the big bang in the epoch when space was self-organising, and then provided a framework for the precocious clumping of matter, as these inflow singularities are long-range gravitational attractors. That α determines the strength of these phenomena implies that we are seeing evidence of a unification of space, gravity and quantum theory, as conjectured in Process Physics [2].

2 Dynamical 3-Space

The dynamics of space is easily determined by returning to Galileo's discoveries of the free-fall acceleration of test masses, and using a velocity field to construct a minimal and unique formulation that determines the acceleration of space itself [2, 8]. In the case of zero vorticity we find

$$\nabla\cdot\left(\frac{\partial \mathbf{v}}{\partial t} + (\mathbf{v}\cdot\nabla)\mathbf{v}\right) + \frac{\alpha}{8}\left((trD)^2 - tr(D^2)\right) + ... = -4\pi G\rho \quad (1)$$

$$\nabla\times\mathbf{v} = \mathbf{0}, \quad D_{ij} = \frac{1}{2}\left(\frac{\partial v_i}{\partial x_j} + \frac{\partial v_j}{\partial x_i}\right), \quad (2)$$

G is Newton's constant, which has been revealed as determining the dissipative flow of space into matter, and α is a dimensionless constant, that experiment reveals to be the fine structure constant. The space acceleration is determined by the Euler constituent acceleration

$$\mathbf{a} = \frac{\partial \mathbf{v}}{\partial t} + (\mathbf{v}\cdot\nabla)\mathbf{v} \quad (3)$$

The matter acceleration is found by determining the trajectory of a quantum matter wavepacket to be [9]

$$\mathbf{g} = \frac{\partial \mathbf{v}}{\partial t} + (\mathbf{v}\cdot\nabla)\mathbf{v} + (\nabla\times\mathbf{v})\times\mathbf{v}_R \quad (4)$$

$$-\frac{\mathbf{v}_R}{1-\dfrac{\mathbf{v}_R^2}{c^2}}\frac{1}{2}\frac{d}{dt}\left(\frac{\mathbf{v}_R^2}{c^2}\right) + ... \quad (5)$$

where $\mathbf{v}(\mathbf{r}, t)$ is the velocity of a structured element of space wrt to an observer's arbitrary Euclidean coordinate system, but which has no ontological meaning. The relativistic term in (5) follows from extremising the elapsed proper time wrt

a quantum matter wave-packet trajectory $\mathbf{r}_o(t)$, see [2]. This ensures that quantum waves propagating along neighbouring paths are in phase.

$$\tau = \int dt \sqrt{1 - \frac{\mathbf{v}_R^2(\mathbf{r}_0(t), t)}{c^2}} \qquad (6)$$

where $\mathbf{v}_R(\mathbf{r}_o(t), t) = \mathbf{v}_o(t) - \mathbf{v}(\mathbf{r}_o(t), t)$, is the velocity of the wave packet, at position $\mathbf{r}_0(t)$, wrt the local 3-space, and $\mathbf{g} = d\mathbf{r}_O/dt$. This shows that (i) the matter "gravitational" geodesic is a quantum wave refraction effect, with the trajectory determined by a Fermat maximum proper-time principle, and (ii) that quantum systems undergo a local time dilation effect caused by their absolute motion wrt space. The last term in (5) causes the precession of planetary orbits.

It is essential that we briefly review some of the many tests that have been applied to this dynamical 3-space.

2.1 Direct Observation of 3-Space

Numerous direct observations of 3-space involve the detection of light speed anisotropy. These began with the 1887 Michelson-Morley gas-mode interferometer experiment, that gives a solar system galactic speed in excess of 300 km/s, [4, 5]*. These experiments have revealed components of the flow, a dissipative inflow, caused by the sun and the earth, as well as the orbital motion of the earth. The largest effect is the galactic velocity of the solar system of 486 km/s in the direction RA = 4.3°, Dec = −75°, determined from spacecraft earth-flyby Doppler shift data [10], a direction first detected by Miller in his 1925/26 gas-mode Michelson interferometer experiment [11].

2.2 Newtonian Gravity Limit

In the limit of zero vorticity and neglecting relativistic effects (2) and (5) give

$$\nabla \cdot \mathbf{g} = -4\pi G\rho - 4\pi G\rho_{DM}, \quad \nabla \times \mathbf{g} = \mathbf{0} \qquad (7)$$

where

$$\rho_{DM} = \frac{\alpha}{32\pi G}\left((trD)^2 - tr(D^2)\right). \qquad (8)$$

This is Newtonian gravity, but with the extra dynamical term which has been used to define an effective "dark matter" density. This is not necessarily non-negative, so in some circumstances ant-gravity effects are possible, though not discussed herein.This ρ_{DM} is not a real matter density, of any form, but is the matter density needed within Newtonian gravity to explain dynamical effects caused by the α-term in (2). This term explains the flat rotation curves of spiral galaxies, large light bending and lensing effects from galaxies, and other effects. However, it is purely a space self-interaction effect.

*Amazingly it continues to be claimed that this experiment was null.

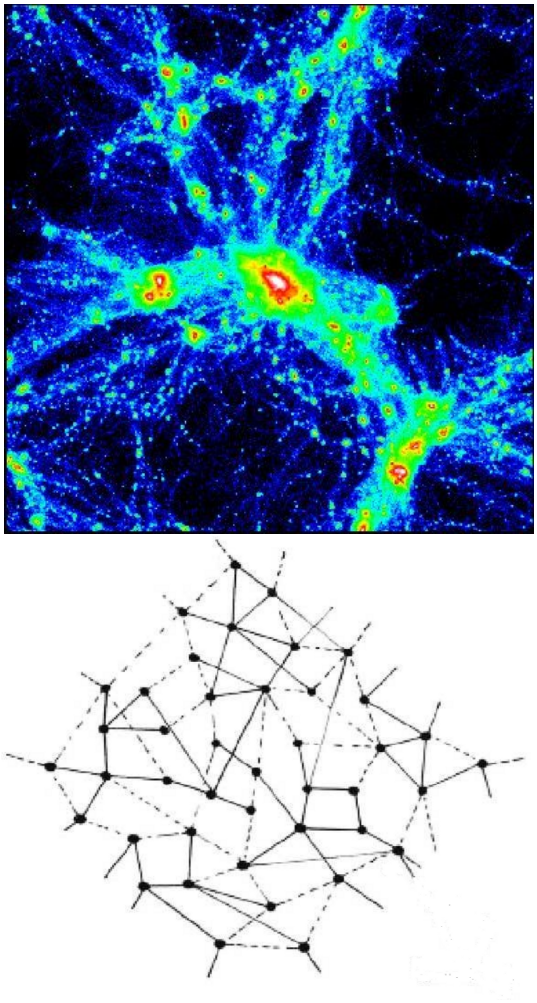

Fig. 1: Top: Cosmic filaments as revealed by gravitational lensing statistical tomography. From J.A. Tyson and G. Bernstein, Bell Laboratories, Physical Sciences Research, http://www.bell-labs.com/org/physicalsciences/projects/darkmatter/darkmatter.html. Bottom: Cosmic network of primordial filaments and primordial black holes, as solution from (2).

2.3 Curved Spacetime Formalism

Eqn.(6) for the elapsed proper time may be written

$$d\tau^2 = dt^2 - \frac{1}{c^2}(d\mathbf{r}(t) - \mathbf{v}(\mathbf{r}(t), t)dt)^2 = g_{\mu\nu}(x)dx^\mu dx^\nu, \qquad (9)$$

which introduces a curved spacetime metric $g_{\mu\nu}$. However this spacetime has no ontological significance — it is merely a mathematical artifact, and as such hides the underlying dynamical 3-space. Its only role is to describe the geodesic of the matter quantum wave-packet in gerneral coordinates. The metric is determined by solutions of (2). This induced metric is not determined by the Einstein-Hilbert equations, which originated as a generalisation of Newtonian gravity, but without the knowledge that a dynamical 3-space had indeed been

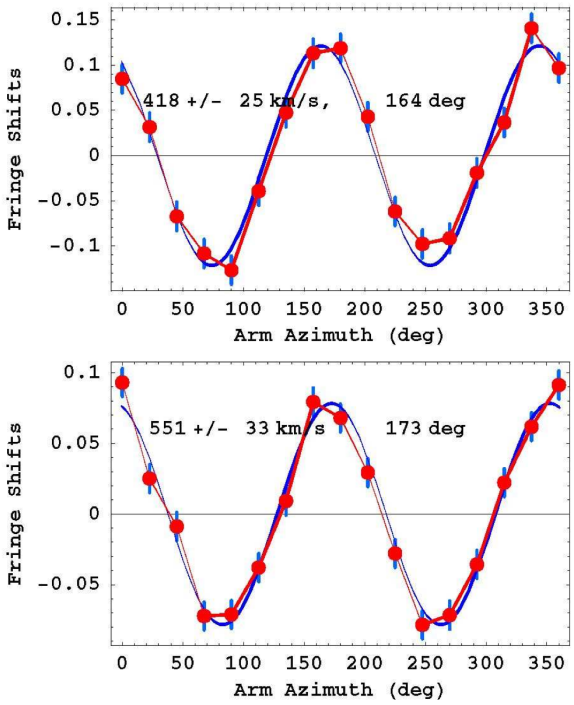

Fig. 2: (a) A typical Miller averaged-data from September 16, 1925, $4^h40'$ Local Sidereal Time (LST) — an average of data from 20 turns of the gas-mode Michelson interferometer. Plot and data after fitting and then subtracting both the temperature drift and Hicks effects from both, leaving the expected sinusoidal form. The error bars are determined as the rms error in this fitting procedure, and show how exceptionally small were the errors, and which agree with Miller's claim for the errors. (b) Best result from the Michelson-Morley 1887 data — an average of 6 turns, at 7^h LST on July 11, 1887. Again the rms error is remarkably small. In both cases the indicated speed is v_P — the 3-space speed projected onto the plane of the interferometer. The angle is the azimuth of the 3-space speed projection at the particular LST. The speed fluctuations from day to day significantly exceed these errors, and reveal the existence of 3-space flow turbulence — i.e. gravitational waves.

detected by Michelson and Morley in 1887 by detecting light speed anisotropy.

2.4 Gravitational Waves

Eqn.(2) predicts time dependent flows, and these have been repeatedly detected, beginning with the Michelson and Morley experiment in 1887. Apart from the sidereal earth-rotation induced time-dependence, the light-speed anisotropy data has always shown time-dependent fluctuations/turbulence, and at a scale of some 10% of the background galactic flow speed. This time dependent velocity field induces "ripples" in the spacetime metric in (9), which are known as "gravitational waves". They cannot be detected by a vacuum-mode Michelson interferometer.

2.5 Matter Induced Minimal Black Holes

For the special case of a spherically symmetric flow we set $\mathbf{v}(\mathbf{r}, t) = -\hat{\mathbf{r}}v(r, t)$. Then (2) becomes, with $v' = \partial v/\partial r$,

$$\frac{\partial v'}{\partial t} + vv'' + \frac{2}{r}vv' + (v')^2 + \frac{\alpha}{2r}\left(\frac{v^2}{2r} + vv'\right) = -4\pi G\rho \qquad (10)$$

For a matter density $\rho(r)$, with maximum radius R, (10) has an exact inhomogeneous static solution [12]

$$v(r)^2 = \begin{cases} \dfrac{2G}{(1-\frac{\alpha}{2})r}\displaystyle\int_0^r 4\pi s^2\rho(s)ds \\ +\dfrac{2G}{(1-\frac{\alpha}{2})r^{\frac{\alpha}{2}}}\displaystyle\int_r^R 4\pi s^{1+\frac{\alpha}{2}}\rho(s)ds, & 0<r\leq R \\ \dfrac{2\gamma}{r}, \qquad r>R \end{cases} \qquad (11)$$

where

$$\gamma = \frac{G}{(1-\frac{\alpha}{2})}\int_0^R 4\pi s^2\rho(s)ds = \frac{GM}{(1-\frac{\alpha}{2})} \qquad (12)$$

Here M is the total matter mass. As well the middle term in (11) also has a $1/r^{\alpha/2}$ inflow-singularity, but whose strength is mandated by the matter density, and is absent when $\rho(r) = 0$ everywhere. This is a minimal attractor or "black hole"*, and is present in all matter systems. For the region outside the sun, $r > R$, Keplerian orbits are known to well describe the motion of the planets within the solar system, apart from some small corrections, such as the Precession of the Perihelion of Mercury, which follow from relativistic term in (2). The sun, as well as the earth, has only an induced "minimal attractor", which affects the interior density, temperature and pressure profiles [12]. These minimal black holes contribute to the external $g = GM^\star/r^2$ gravitational acceleration, through an effective mass $M^\star = M/(1-\alpha/2)$. The 3-space dynamics contributes an effective mass [2]

$$M_{BH} = \frac{M}{1-\frac{\alpha}{2}} - M = \frac{\alpha}{2}\frac{M}{1-\frac{\alpha}{2}} \approx \frac{\alpha}{2}M. \qquad (13)$$

These induced black hole "effective" masses have been detected in numerous globular clusters and spherical galaxies and their predicted effective masses have been confirmed in some 19 such cases, as shown in Fig. 3, [6]. The non-Newtonian effects in (11) are also detectable in bore hole experiments.

2.6 Earth Bore Holes Determine α

The value of the parameter α in (2) was first determined from earth bore hole g-anomaly data, which shows that gravity decreases more slowly down a bore hole than predicted by Newtonian gravity, see Figs.4 and 5. From (5) and (11) we find

*The term "black hole" refers to the existence of an event horizon, where the in-flow speed reaches c, but otherwise has no connection to the putative "black holes" of GR.

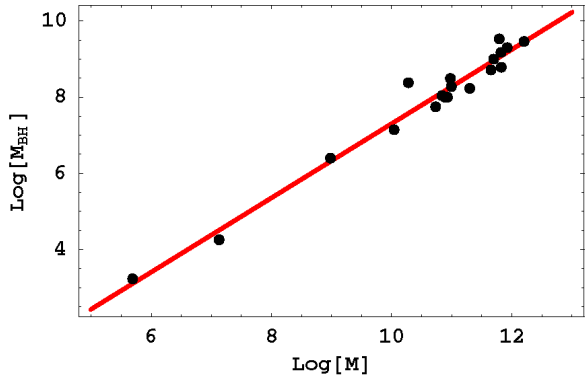

Fig. 3: The data shows $\mathrm{Log}_{10}[M_{BH}]$ for the minimal induced black hole masses M_{BH} for a variety of spherical matter systems, from Milky Way globular clusters to spherical galaxies, with masses M, plotted against $\mathrm{Log}_{10}[M]$, in solar masses M_0. The straight line is the prediction from (13) with $\alpha = 1/137$. See [6] for references to the data.

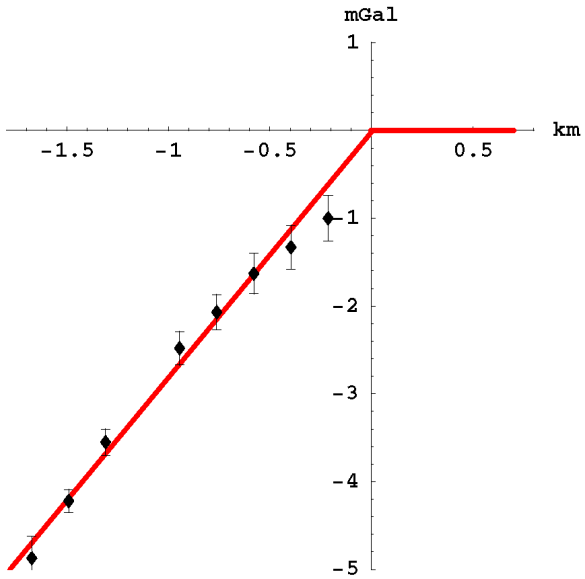

Fig. 4: The data shows the gravity residuals for the Greenland Ice Shelf [13] Airy measurements of the $g(r)$ profile, defined as $\Delta g(r) = g_{Newton} - g_{observed}$, and measured in mGal (1mGal = 10^{-3} cm/s^2) and plotted against depth in km. The borehole effect is that Newtonian gravity and the new theory differ only beneath the surface, provided that the measured above-surface gravity gradient is used in both theories. This then gives the horizontal line above the surface. Using (15) we obtain $\alpha^{-1} = 137.9 \pm 5$ from fitting the slope of the data, as shown. The non-linearity in the data arises from modelling corrections for the gravity effects of the irregular sub ice-shelf rock topography. The ice density is 920 kg/m^3. The near surface data shows that the density of the Greenland ice, compressed snow, does not reach its full density until some 250m beneath the surface — a known effect.

the gravitational acceleration at radius $r = R + d$ to be

$$g(d)=\begin{cases} -\dfrac{GM}{(1-\alpha/2)(R+d)^2}+\dfrac{2\pi G\rho(R)d}{(1-\alpha/2)}+\ldots \\ \qquad -\dfrac{4\pi R^2 G\rho(R)G}{(1-\alpha/2)(R+d)^2}, \quad d<0 \\ -\dfrac{GM}{(1-\alpha/2)(R+d)^2}, \quad d>0 \end{cases} \tag{14}$$

In practice the acceleration above the earth's surface must be measured in order to calibrate the anomaly, which defines the coefficient $\overline{GM} = GM/(1-\alpha/2)$ in (14). Then the anomaly is

$$\Delta g = g_{NG}(d) - g(d) = 2\pi\alpha G\rho(R)d + O(\alpha^2), \quad d<0 \tag{15}$$

to leading order in α, and where $g_{NG}(d)$ is the Newtonian gravity acceleration, given the value of $\overline{GM}$ from the above-surface calibration, for a near-surface density $\rho(R)$. The experimental data then reveals α to be the fine structure constant, to within experimental errors [6]. The experiments have densities that differ by more than a factor of 2, so the result is robust.

2.7 G Measurement Anomalies

There has been a long history of anomalies in the measurement of Newton's gravitational constant G, see Fig. 7. The explanation is that the gravitational acceleration external to a piece of matter is only given by application of Newton's inverse square law for the case of a spherically symmetric mass. For other shapes the α-dependent interaction in (2) results in forces that differ from Newtonian gravity at $O(\alpha)$. The anomalies shown in Fig. 7 result from analysing the one-parameter, G, Newtonian theory, when gravity requires a two parameter, G and α, analysis of the data. The scatter in the measured G values appear to be of $O(\alpha/4)$. This implies that laboratory measurements to determine G will also measure α [2].

2.8 Expanding Universe

The dynamical 3-space theory (2) has a time dependent expanding universe solution, in the absence of matter, of the Hubble form $v(r,t) = H(t)r$ with $H(t) = 1/(1+\alpha/2)t$, giving a scale factor $a(t) = (t/t_0)^{4/(4+\alpha)}$, predicting essentially a uniform expansion rate. This results in a parameter-free fit to the supernova redshift-magnitude data, as shown in fig.8, once the age $t_0 = 1/H_0$ of the universe at the time of observation is determined from nearby supernova. In sharp contrast the Friedmann model for the universe has a static solution — no expansion, unless there is matter/energy present. However to best fit the supernova data fictitious "dark matter" and "dark energy" must be introduced, resulting in the ΛCDM model. The amounts $\Omega_\Lambda = 0.73$ and $\Omega_{DM} = 0.23$ are eas-

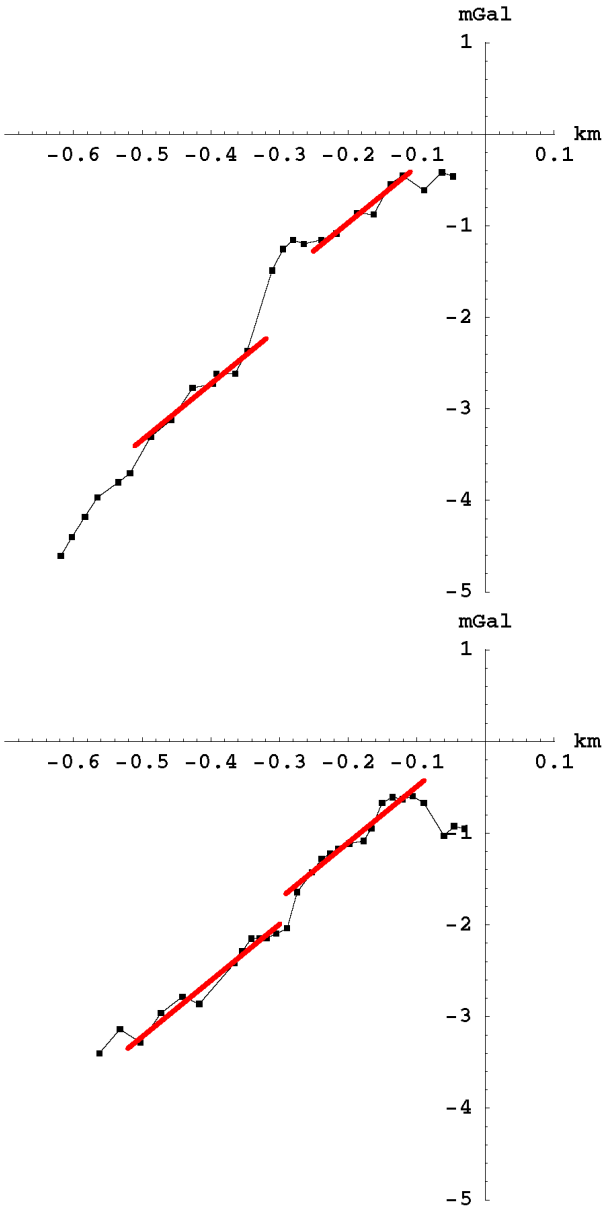

Fig. 5: Gravity residuals $\Delta g(r)$ from two of the Nevada bore hole experiments [14] that give a best fit of $\alpha^{-1} = 136.8 \pm 3$ on using (15). Some layering of the rock is evident. The rock density is 2000 kg/m^3 in the linear regions.

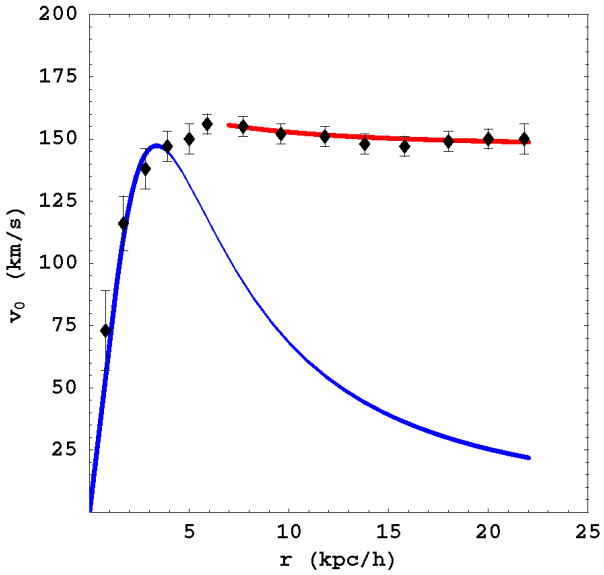

Fig. 6: Plots of the rotation speed data for the spiral galaxy NGC3198. Lower curve shows Newtonian gravity prediction, while upper curve shows asymptotic flat rotation speeds from (19).

ily determined by best fitting the ΛCDM model to the above uniformly expanding result, without reference to the observational supernova data. But then the ΛCDM has a spurious exponential expansion which becomes more pronounced in the future. This is merely a consequence of extending a poor curve fitting procedure beyond the data. The 3-space dynamics (2) results in a hotter universe in the radiation dominated epoch, with effects on Big Bang Nucleosynthesis [15], and also a later decoupling time of some 1.4×10^6 years.

3 Primordial Black Holes

In the absence of matter the dynamical 3-space equation (2) has black hole solutions of the form

$$v(r) = -\frac{\beta}{r^{\alpha/4}} \tag{16}$$

for arbitrary β, but only when $\alpha \neq 0$. This will produce a long range gravitational acceleration, essentially decreasing like $1/r$,

$$g(r) = -\frac{\alpha\beta^2}{4r^{1+\alpha/2}} \tag{17}$$

as observed in spiral galaxies. The inflow in (16) describes an inflow singularity or "black hole" with arbitrary strength. This is unrelated to the putative black holes of General Relativity. This corresponds to a primordial black hole. The dark matter density for these black holes is

$$\rho_{DM}(r) = \frac{\alpha\beta^2(2-\alpha)}{256\pi G r^{2+\alpha/2}} \tag{18}$$

This decreases like $1/r^2$ as indeed determined by the "dark matter" interpretation of the flat rotation curves of spiral galaxies. Here, however, it is a purely 3-space self-interaction effect.

In general a spherically symmetric matter distribution may have a static solution which is a linear combination of the inhomogeneous matter induced solution in (11) and the square of the homogeneous primordial black hole solution in (16), as (10) is linear in $v(r)^2$ and its spatial derivatives.

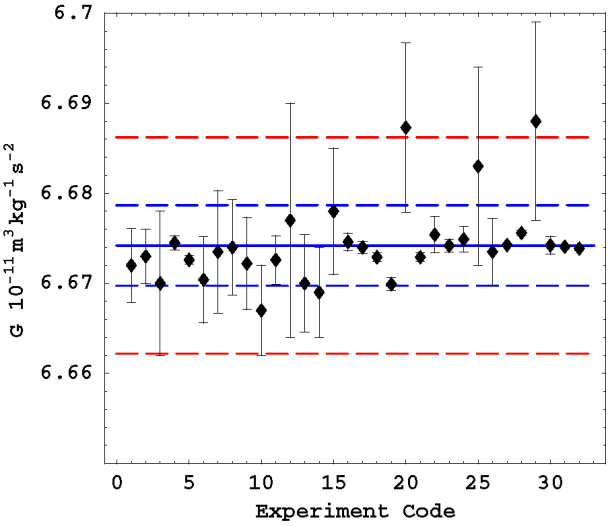

Fig. 7: Results of precision measurements of G published in the last sixty years in which the Newtonian theory was used to analyse the data. These results show the presence of a systematic effect, not in the Newtonian theory, of fractional size $\Delta G/G \approx \alpha/4$. The upper horizontal dashed line shows the value of G from ocean Airy measurements [17], while the solid line shows the current CODATA G value of $6.67428(\pm 0.00067) \times 10^{-11} m^3/kgs^2$, with much lager experimental data range, exceeding $\pm\alpha G/8$, shown by dashed lines as a guide. The lower horizontal line shows the actual value of G after removing the space self-interaction effects via $G \to (1 - \alpha/2)G$ from the ocean value of G. The CODATA G value, and its claimed uncertainty, is seen to be spurious.

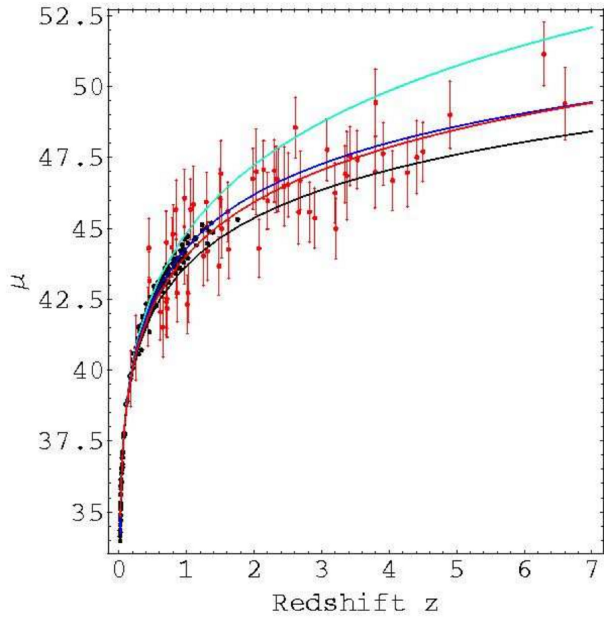

Fig. 8: Hubble diagram showing the supernovae data using several data sets, and the Gamma-Ray-Bursts data (with error bars). Upper curve (green) is ΛCDM "dark energy" only $\Omega_\Lambda = 1$, lower curve (black) is ΛCDM matter only $\Omega_M = 1$. Two middle curves show best-fit of ΛCDM "dark energy"-"dark-matter" (blue) and dynamical 3-space prediction (red), and are essentially indistinguishable. We see that the best-fit ΛCDM "dark energy"-"dark-matter" curve essentially converges on the uniformly-expanding parameter-free dynamical 3-space prediction. The supernova data shows that the universe is undergoing a uniform expansion, wherein a fit to the FRW-GR expansion was forced, requiring "dark energy", "dark matter" and a future "exponentially accelerating expansion".

However this is unlikely to be realised, as a primordial black hole would cause a precocious in-fall of matter, which is unlikely to remain spherically symmetric, forming instead spiral galaxies.

3.1 Spiral Galaxy Rotation Curves

Spiral galaxies are formed by matter in-falling on primordial black hole, leading to rotation of that matter, as the in-fall will never be perfectly symmetric. The black hole acceleration in (17) would support a circular matter orbit with orbital speed

$$v_o(r) = \frac{(\alpha\beta^2)^{1/2}}{2r^{\alpha/4}} \tag{19}$$

which is the observed asymptotic "flat" orbital speed in spiral galaxies, as illustrated in Fig. 6 for the spiral galaxy NGC3198. So the flat rotation curves are simply explained by (2).

4 Primordial Filaments

Eqn.(2) also has cosmic filament solutions. Writing (2) in cylindrical coordinates (r, z, ϕ), and assuming cylindrical symmetry with translation invariance along the z axis, we have for a radial flow $v(r, t)$

$$\frac{1}{r}\frac{\partial v}{\partial t} + \frac{\partial v'}{\partial t} + \frac{vv'}{r} + v'^2 + vv'' + \alpha\frac{vv'}{4r} = 0 \tag{20}$$

where here the radial distance r is the distance perpendicular to the z axis. This has static solutions with the form

$$v(r) = -\frac{\mu}{r^{\alpha/8}} \tag{21}$$

for arbitrary μ. The gravitational acceleration is long-range and attractive to matter, i.e. **g** is directed inwards towards the filament,

$$g(r) = -\frac{\alpha\mu^2}{8r^{1+\alpha/4}} \tag{22}$$

This is for a single infinite-length filament. The dark matter density (8) is

$$\rho_{DM}(r) = -\frac{\alpha\mu^2}{1024\pi G r^{2+\alpha/4}} \tag{23}$$

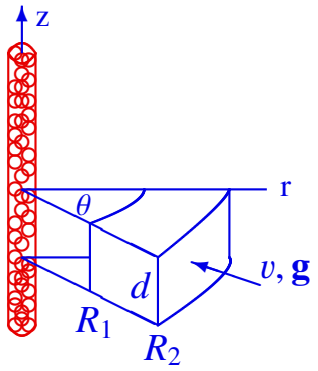

Fig. 9: Sector integration volume, with radii R_1 and R_2, about a filament. For the filament to exist the quantum foam substructure to 3-space must be invoked at short distances.

and negative. But then (7), with $\rho = 0$, would imply a repulsive matter acceleration by the filament, and not attractive as in (22). To resolve this we consider the sector integration volume in Fig.9. We obtain from (22) and using the divergence theorem (in which **dA** is directed outwards from the integration volume)

$$\int_{\mathcal{V}} \nabla\cdot\mathbf{g}dv = \int_{\mathcal{A}} \mathbf{g}\cdot\mathbf{dA} = \frac{\alpha\mu^2\theta d}{8}\left(\frac{1}{R_1^{\alpha/4}} - \frac{1}{R_2^{\alpha/4}}\right) \qquad (24)$$

which is positive because $R_1 < R_2$. This is consistent with (7) for the negative ρ_{DM}, but only if R_1 is finite. However if $R_1 = 0$, as for the case of the integration sector including the filament axis, there is no R_1 term in (24), and the integral is now negative. This implies that (21) cannot be the solution for some small r. The filament solution is then only possible if the dynamical 3-space equation (1) is applicable only to macroscopic distances, and at short distances higher order derivative terms become relevant, such as $\nabla^2(\nabla\cdot\mathbf{v})$. Such terms indicate the dynamics of the underlying quantum foam, with (1) being a derivative expansion, with higher order dervatives becoming more significant at shorter distances.

5 Filament Gravitational Lensing

We must generalise the Maxwell equations so that the electric and magnetic fields are excitations within the dynamical 3-space, and not of the embedding space. The minimal form in the absence of charges and currents is

$$\begin{aligned} \nabla\times\mathbf{E} &= -\mu_0\left(\frac{\partial\mathbf{H}}{\partial t} + \mathbf{v}.\nabla\mathbf{H}\right), \quad \nabla.\mathbf{E} = \mathbf{0}, \\ \nabla\times\mathbf{H} &= \epsilon_0\left(\frac{\partial\mathbf{E}}{\partial t} + \mathbf{v}.\nabla\mathbf{E}\right), \quad \nabla.\mathbf{H} = \mathbf{0} \end{aligned} \qquad (25)$$

which was first suggested by Hertz in 1890 [16], but with $\mathbf{v}$ then being only a constant vector field. As easily determined the speed of EM radiation is now $c = 1/\sqrt{\mu_0\epsilon_0}$ with respect to the 3-space. The time-dependent and inhomogeneous velocity field causes the refraction of EM radiation. This can be computed by using the Fermat least-time approximation. This ensures that EM waves along neighbouring paths are in phase. Then the EM ray paths $\mathbf{r}(t)$ are determined by minimising the elapsed travel time:

$$T = \int_{s_i}^{s_f} \frac{ds|\frac{d\mathbf{r}}{ds}|}{|c\hat{\mathbf{v}}_R(s) + \mathbf{v}(\mathbf{r}(\mathbf{s}),\mathbf{t}(\mathbf{s})|}, \qquad (26)$$

$$\mathbf{v}_R = \frac{d\mathbf{r}}{dt} - \mathbf{v}(\mathbf{r}(\mathbf{t}),\mathbf{t}) \qquad (27)$$

by varying both $\mathbf{r}(s)$ and $t(s)$, finally giving $\mathbf{r}(t)$. Here s is a path parameter, and $c\hat{\mathbf{v}}_R$ is the velocity of the EM radiation wrt the local 3-space, namely c. The denominator in (26) is the speed of the EM radiation wrt the observer's Euclidean spatial coordinates. Eqn.(26) may be used to calculate the gravitational lensing by black holes, filaments and by ordinary matter, using the appropriate 3-space velocity field. Because of the long-range nature of the inflow for black holes and filaments, as in (16) and (21), they produce strong lensing, compared to that for ordinary matter*, and also compared with the putative black holes of GR, for which the in-flow speed decreases like $1/\sqrt{r}$, corresponding to the acceleration field decreasing like $1/r^2$. The EM lensing caused by filaments and black holes is the basis of the stochastic tomographic technique for detecting these primordial 3-space structures.

6 Filament and Black Hole Networks

The dynamical 3-space equation produces analytic solutions for the cases of a single primordial black hole, and a single, infinite length, primordial filament. This is because of the high symmetry of theses cases. However analytic solutions corresponding to a network of finite length filaments joining at black holes, as shown in Fig.1, are not known. For this case numerical solutions will be needed. It is conjectured that the network is a signature of primordial imperfections or defects from the epoch when the 3-space was forming, in the earliest moments of the big bang. It is conjectured that the network of filaments and black holes form a cosmic network of sheets and voids. This would amount to a dynamical breakdown of the translation invariance of space. Other topological defects are what we know as quantum matter [2].

7 Conclusions

The recent discovery that a dynamical 3-space exists has resulted in a comprehensive investigation of the new physics, and which has been checked against numerous experimental and observational data. This data ranges from laboratory Cavendish-type G experiments to the expansion of the universe which, the data clearly shows, is occurring at a uniform rate, except for the earliest epochs. Most significantly

*Eqn:(26) produces the known sun light bending [3].

the dynamics of space involves two parameters: G, Newton's gravitational constant, which determines the rate of dissipative flow of space into matter, and α, which determines the space self-interaction dynamics. That this is the same constant that determines the strength of electromagnetic interactions shows that a deep unification of physics is emerging. It is the α term in the space dynamics that determines almost all of the new phenomena. Most importantly the epicycles of spacetime physics, *viz* dark matter and dark energy, are dispensed with.

Submitted on February 16, 2011 / Accepted on February 21, 2011

References

1. Fabian A. C. (ed.), Clusters and Superclustors of Galaxies, *NATO ASI Series C*, Vol. 366, Kluwer, 1992.
2. Cahill R. T. Process Physics: From Information Theory to Quantum Space and Matter, Nova Science Pub., New York, 2005.
3. Cahill R. T. Dynamical 3-Space: A Review, in: Ether Space-time and Cosmology: New Insights into a Key Physical Medium, Duffy M. and Lévy J. (eds.), *Apeiron*, 2009, v. 16, 135–200.
4. Cahill R. T., Kitto K. Michelson-Morley Experiments Revisited, *Apeiron*, 2003, v. 10, no. 2, 104–117.
5. Cahill R. T. The Michelson and Morley 1887 Experiment and the Discovery of Absolute Motion, *Progress in Physics*, 2005, v. 3, 25–29.
6. Cahill R. T. 3-Space Inflow Theory of Gravity: Boreholes, Blackholes and the Fine Structure Constant, *Progress in Physics*, 2006, v. 2, 9–16.
7. Cahill R. T. Unravelling the Dark Matter — Dark Energy Paradigm, *Apeiron*, 2009, v. 16, no. 3, 323–375.
8. Cahill R. T. Dynamical 3-Space: Emergent Gravity, Should the Laws of Gravitation be Reconsidered?, Múnera H. A. (ed.), Montreal: Apeiron 2011.
9. Cahill R. T. Dynamical Fractal 3-Space and the Generalised Schrödinger Equation: Equivalence Principle and Vorticity Effects, *Progress in Physics*, 2006, v. 1, 27–34.
10. Cahill R. T. Combining NASA/JPL One-Way Optical-Fiber Light-Speed Data with Spacecraft Earth-Flyby Doppler-Shift Data to Characterise 3-Space Flow, *Progress in Physics*, 2009, v. 4, 50–64.
11. Miller D. C. The Ether-Drift Experiment and the Determination of the Absolute Motion of the Earth, *Reviews of Modern Physics*, 1933, v. 5, 203–242.
12. May R. D., Cahill R. T. Dynamical 3-Space Gravity Theory: Effects on Polytropic Solar Models, *Progress in Physics*, 2011, v. 1, 49–54.
13. Ander M. E., Zumberge M. A., Lautzenhiser T., Parker R. L., Aiken C. L. V., Gorman M. R., Nieto M. M., Cooper A. P. R., Ferguson J. F., Fisher E., McMechan G. A., Sasagawa G., Stevenson J. M., Backus G., Chave A. D., Greer J., Hammer P., Hansen B. L., Hildebrand J. A., Kelty J. R., Sidles C., Wirt J. Test of Newton's Inverse-Square Law in the Greenland Ice Cap, *Physical Review Letters*, 1989, v. 62, 985–988.
14. Thomas J., Vogel P. Testing the Inverse-Square Law of Gravity in Boreholes at the Nevada Test Site, *Physical Review Letters*, 1990, v. 65, 1173–1176.
15. Cahill R. T. Dynamical 3-Space Predicts Hotter early Universe: Resolves CMB-BBN ^{7}Li and ^{4}He Abundance Anomalies, *Progress in Physics*, 2010, v. 1, 67–71.
16. Hertz H. On the Fundamental Equations of Electro-Magnetics for Bodies in Motion, *Wiedemann's Annalen*, 1962, v. 41, 369. Electric Waves, Collection of Scientific Papers, Dover Pub., New York, 1890.
17. Zumberge M. A., Hildebrand J. A., Stevenson J. M., Parker R. L., Chave A. D., Ander M. E., Spiess F. N. Submarine Measurement of the Newtonian Gravitational Constant, *Physical Review Letters*, 1991, v. 67, 3051–3054.

Black Holes in the Framework of the Metric Tensor Exterior to the Sun and Planets

Chifu E. Ndikilar
Department of Physics, Gombe State University, P.M.B 127, Gombe, Gombe State, Nigeria
E-mail: ebenechifu@yahoo.com

The conditions for the Sun and oblate spheroidal planets in the solar system to reduce to black holes is investigated. The metric tensor exterior to oblate spheroidal masses indicates that for the Sun to reduce to a black hole, its mass must condense by a factor of 2.32250×10^5. Using Schwarzschild's metric, this factor is obtained as 2.3649×10^5. Similar results are obtained for oblate spheroidal planets in the solar system.

1 Introduction

It is well known that whenever an object becomes sufficiently compact, general relativity predicts the formation of a black hole: a region of space from which nothing, not even light can escape. The collapse of any mass to the Schwarzschild radius appears to an outside observer to take an infinite time and the events at distances beyond this radius are unobservable from outside, thus the name black hole. From an astronomical point of view, the most important property of compact objects such as black holes is that they provide a superbly efficient mechanism for converting gravitational energy into radiation [1].

The world line element in Schwarzschild's field is well known to be given by [1]

$$c^2d\tau^2 = c^2\left[1-\frac{2GM}{c^2r}\right]dt^2-\left[1-\frac{2GM}{c^2r}\right]^{-1}dr^2 - r^2d\theta^2 - r^2\sin^2\theta d\phi^2. \quad (1)$$

This metric has a singularity, (denoted by r_s) called the Schwarzschild singularity (or radius) at

$$r_s = \frac{2GM}{c^2}. \quad (2)$$

For most physical bodies in the universe, the Schwarzschild radius is much smaller than the radius of their surfaces. Hence for most bodies, there does not exist a Schwarzschild singularity. It is however, speculated that there exist some bodies in the universe with the Schwarzschild radius in the exterior region. Such bodies are called black holes [1].

In this article, the factor by which the radius of the Sun and oblate spheroidal planets is reduced to form a black hole is computed using the oblate spheroidal space-time metric. The results are compared to those obtained using Schwarzschild's metric.

2 Oblate Spheroidal Space-Time Metric

It has been established [2] that the covariant metric tensor in the region exterior to a static homogeneous oblate spheroid in oblate spheroidal coordinates is given as

$$g_{00} = \left(1+\frac{2}{c^2}f(\eta,\xi)\right) \quad (3)$$

$$g_{11} = -\frac{a^2}{1+\xi^2-\eta^2}\left[\eta^2\left(1+\frac{2}{c^2}f(\eta,\xi)\right)^{-1}+\frac{\xi^2(1+\xi^2)}{(1-\eta^2)}\right] \quad (4)$$

$$g_{12}\equiv g_{21} = -\frac{a^2\eta\xi}{1+\xi^2-\eta^2}\left[1-\left(1+\frac{2}{c^2}f(\eta,\xi)\right)^{-1}\right] \quad (5)$$

$$g_{22} = -\frac{a^2}{1+\xi^2-\eta^2}\left[\xi^2\left(1+\frac{2}{c^2}f(\eta,\xi)\right)^{-1}+\frac{\eta^2(1-\eta^2)}{(1+\xi^2)}\right] \quad (6)$$

$$g_{33} = -a^2(1+\xi^2)(1-\eta^2) \quad (7)$$

$$g_{\mu\nu} = 0;\ \text{otherwise}. \quad (8)$$

Thus, the world line element in this field can be written as

$$c^2d\tau^2 = c^2g_{00}dt^2 - g_{11}d\eta^2 - 2g_{12}d\eta d\xi - g_{22}d\xi^2 - g_{33}d\phi^2. \quad (9)$$

Multiplying equation (9) all through by $\left(\frac{1}{dt}\right)^2$ yields

$$c^2\left(\frac{d\tau}{dt}\right)^2 = c^2g_{00} - g_{11}\left(\frac{d\eta}{dt}\right)^2 - 2g_{12}\frac{d\eta}{dt}\frac{d\xi}{dt} - g_{22}\left(\frac{d\xi}{dt}\right)^2 - g_{33}\left(\frac{d\phi}{dt}\right)^2. \quad (10)$$

It can be concluded that the space velocity(v_s) is given as

$$v_s = g_{11}\left(\frac{d\eta}{dt}\right)^2 + 2g_{12}\frac{d\eta}{dt}\frac{d\xi}{dt} + g_{22}\left(\frac{d\xi}{dt}\right)^2 + g_{33}\left(\frac{d\phi}{dt}\right)^2, \quad (11)$$

and the velocity of local time

$$v_\tau = c\frac{d\tau}{dt}. \quad (12)$$

The gravitational velocity can equally be defined with the aid of equation (3) as

$$v_G = \sqrt{-2f(\eta,\xi)}. \tag{13}$$

This implies that

$$c^2 = v_\tau^2 + v_G^2 + v_s^2 \tag{14}$$

or

$$c = \left|\vec{v}_\tau^2 + \vec{v}_G^2 + \vec{v}_s^2\right|. \tag{15}$$

3 Black holes in oblate spheroidal space time of Sun and planets

In the absence of gravity and acceleration, $f(\eta,\xi) = 0$ and thus $v_G = 0$. Hence, v_s can be written explicitly as

$$\begin{aligned} v_s^2 = &\left[\frac{a^2\eta^2}{1+\xi^2-\eta^2} + \frac{\xi^2\left(1+\xi^2\right)}{1-\eta^2}\right]\left(\frac{d\eta}{dt}\right)^2 \\ &+\frac{a^2}{1+\xi^2-\eta^2}\left[\xi^2 + \frac{\eta^2(1-\eta^2)}{1+\xi^2}\right]\left(\frac{d\xi}{dt}\right)^2 \\ &+a^2\left(1+\xi^2\right)\left(1-\eta^2\right)\left(\frac{d\phi}{dt}\right)^2. \end{aligned} \tag{16}$$

Thus in the absence of gravity, equation(14) reduces to

$$\frac{d\tau}{dt} = \sqrt{1-\frac{v_s^2}{c^2}}. \tag{17}$$

It can basically be seen that equation(15) establishes a maximum value of c and hence the gravitational velocity v_G can never exceed c. An approximate expression for $f(\eta,\xi)$ along the equator of an oblate spheroid [3] is

$$f(\eta,\xi) \approx \frac{B_0}{3\xi^2}\left(1+3\xi^2\right)i + \frac{B_2}{30\xi^3}\left(7+15\xi^2\right)i \tag{18}$$

where B_0 and B_2 are constants. Equation(18) can be written equally as

$$f(\eta,\xi) \approx -\left(\frac{C}{\xi} + \frac{D}{\xi^3}\right) \tag{19}$$

where C and D are equally constants. These constants can easily be computed for the oblate spheroidal astrophysical bodies in the solar system and results are presented in Table 1.

Setting the gravitational velocity v_G to be equal to the maximum value c, in equation (13), an approximate expression for the parameter ξ for a black hole in oblate spheroidal space time can be obtained as

$$\xi_{blackhole} \approx \frac{2C}{c^2}. \tag{20}$$

Table 1: Basic constants for oblate spheroidal bodies in the solar system

Body	C [$\times 10^{-9}$ Nmkg^{-1}]	D [$\times 10^{-9}$ Nmkg^{-1}]
Sun	−46796.04	−15598.70
Earth	−0.743851	−0.247962
Mars	−0.1132	−0.03780
Jupiter	−3.77107	−1.25803
Saturn	−0.879543	−0.29356
Uranus	−0.842748	−0.28102
Neptune	−1.065429	−0.35516

Table 2: Reduction ratio for oblate spheroidal masses in the solar system to reduce to black holes

Body	$\xi_{surface}$	$\xi_{blackhole}$	reduction ratio: $\frac{\xi_{surface}}{\xi_{blackhole}}$
Sun	241.52	1.1×10^{-3}	2.32250×10^5
Earth	12.01	1.6×10^{-8}	7.50625×10^8
Mars	09.17	2.0×10^{-9}	4.58500×10^9
Jupiter	02.64	8.3×10^{-8}	3.18070×10^7
Saturn	01.97	1.9×10^{-8}	1.03684×10^8
Uranus	03.99	1.8×10^{-8}	2.21667×10^8
Neptune	04.30	2.3×10^{-8}	1.86950×10^8

Hence the parameter $\xi_{blackhole}$ for various bodies in the solar system is computed using equation (20) and the reduction ratio for oblate spheroidal masses in the solar system to reduce to black holes is obtained (Table 2).

The reduction ratio can equally be calculated using Schwarzschild's expression. The equatorial radius (r) for the bodies is divided by the Schwarzschild's radius (r_{schw}) to obtain the reduction ratio. The results are shown in Table 3.

4 Conclusion

This short article presents the notion of black holes in the metric tensor exterior to oblate spheroidal masses. Equation (20) is an approximate expression for the parameter ξ of an oblate spheroid to collapse to a black hole.Reductions ratios computed using the oblate spheroidal metric for Sun and planets in the Solar system authenticates the soundness of metric. The closeness of the reduction ratio for oblate spheroidal masses in the solar system computed using the metric tensor in oblate spheroidal space time to that in Schwarzschild's metric is remarkable.Basically, since the Sun and planets under consideration are oblate spheroidal in nature, the values obtained using the metric tensor contain slight corrections to values obtained using Schwarzschild's metric.

Submitted on March 21, 2011 / Accepted on March 24, 2011

Table 3: Schwarzschild's reduction ratio

Body	r [$\times 10^3$ m]	r_{schw} [m]	reduction ratio: $\frac{r}{r_{schw}}$
Sun	$700,000$	2.96×10^3	2.36490×10^5
Earth	6378	8.80×10^{-3}	7.24773×10^8
Mars	3396	9.9×10^{-4}	3.43030×10^9
Jupiter	$71,490$	2.8	2.55320×10^7
Saturn	$60,270$	8.5×10^{-1}	7.09059×10^7
Uranus	$25,560$	1.3×10^{-1}	1.96615×10^8
Neptune	$24,760$	1.5×10^{-1}	1.65067×10^8

References

1. Weinberg S. Gravitation and cosmology. J. Wiley, New York, 1972, pp. 175–188.
2. Chifu E. N., Usman A., Meludu O. C. Orbits in Homogeneous Oblate Spheroidal Gravitational Space Time, *Progress in Physics*, 2009, v. 3, 49–53.
3. Chifu E. N., Usman A., Meludu O. C. Gravitational Spectral Shift Exterior to the Sun, Earth and the Other Oblate Spheroidal Planets, *Progress in Physics*, 2010, v. 4, 56–60.

Isotopes and the Electron Configuration of the Blocks in the Periodic Table of Elements, upto the Last Element No.155

Albert Khazan

E-mail: albkhazan@gmail.com

This is a theoretical study, which first manifests which connexion exists between isotopes and the electron blocks, and how the electron blocks are located in the version of the Periodic Table of Elements which ends with element No.155.

1 Introduction

It is known that elements of the Periodic Table of Elements have fractional numerical values of atomic masses. This is because the elements consists of, as regularly, a mix of inborn (native) isotopes. For this reason we conclude that the average weighted atomic mass of all stable isotopes of any element (taking their distribution in the Earth crust) is that atomic mass which is used in all calculations. Because it is equal to the sum of the electric charge of an atomic nucleus and the number of neutrons in it, the isotopes are determined by the condition $A = Z + N$, where A is the atomic mass, Z is the charge, N is the number of neutrons of the nucleus. With all these, it is necessary to keep in mind that, having the same number of protons in a nucleus, the nucleus may contain different number of neutrons which do not change the chemical properties of the atoms: all isotopes of the same element bear the same electric charge of its nucleus, but change only with the number of neutrons in it.

2 Calculation according to the table of isotopes

According to the data provided by *Nuclear Periodic Table* [1], all spectacularity of the data was split into blocks, wherein the number of isotopes was determined, namely: 431 (s), 1277 (p), 1612 (d), 1147 (f). As is seen in Fig. 1, the obtained results form a smooth arc with $R^2 = 1$. Because all the isotopes are grouped into clocks of the electron configuration alike elements of the Periodic Table, we are lawful to conclude that the *same law* lies in the ground of the geometric configurations. It is necessary to note that, with reaching the top of the arc, the number of the isotopes very lowers, that was as well observed in the case of elements of the Periodic Table [2].

3 Version of the Periodic Table of Elements, which limits by element No.155

It is known that the "blocks" of the Periodic Table of Elements are sets of adjacent groups [3, 4]. The names of the blocks originate in the number of the spectroscopic lines of the atomic orbitales in each of them: **s**harp, **p**rincipal, **d**iffuse, **f**undamental. During the last decades, one suggested to extend the Periodic Table upto 218 elements, with appearance a **g**-block in it [5]. If, in the version of the Periodic Table consisting of only 118 elements, the blocks draw a smooth arc with $R^2 = 1$ (see Fig. 2), the appearance of additional elements in the Table requires new construction of the blocks, which should be set up in another configuration.

Earleir [5], we suggested a version of the Periodic Table which contained Period 8 with 37 elements (two lines with 18 and 1 elements in Group 1). In this form, the Periodic Table satisfies the common structure of the location of the elements. However, once lanthanides and actinides have been extended into a common scheme, the heaviest element No.155 (which ends the Table in this its version) became shifted for 4 positions to right. Therefore, a question rose: how to locate these 37 elements in the new version of the Table so that they would completely satisfy all the rules of the electron configuration of the blocks?

First, we added 2 elements to block **s** upto the begining of Period 8. Then we added 6, 10, and 14 elements (respectively) to blocks **p**, **d**, **f**. Concerning the rest 4 elements, we created a new block **g**. All these changes are shown in Fig. 2 (the upper arc). As is seen, the arc has the same form as the lower arc, and shows that fact that the number of elements of the last block reaches the actual limit.

On the basis of that has been said above, a long-period form of the Periodic Table of Elements was constructed by the Author (see Fig. 3). It differs from the hypothetical forms of the Periodic Table by the real data consisting our Table. Element No.155 is the last (heaviest) in our version of the Table, thus this element "closes" the Table. Element No.155 also opens and closes Period 9, being located in Group 1 of this Period.

This scheme of calculation is applicable to all Tables of Elements containing more than 118 elements. The necessity of our study, presented herein, and the suggested version of the Table which limits by element No.155, is due to that fact the law of hyperbolas we used previously in the Periodic Table [5] provided not only the possibility to calculate the upper limit of the Table (element No.155 and its parameters such as atomic mass 411.66), but also allowed to determine its location in the extended version of the Table of Elements.

If earlier the theoretical physical chemists discussed the possibility to add a number of elements over 118 to the Table of Elements (they suggested to do it as new blocks they referred to as superactinide series, eka-superactinide, Ubb-series, Usb-series), we now obviously see that this step is non-

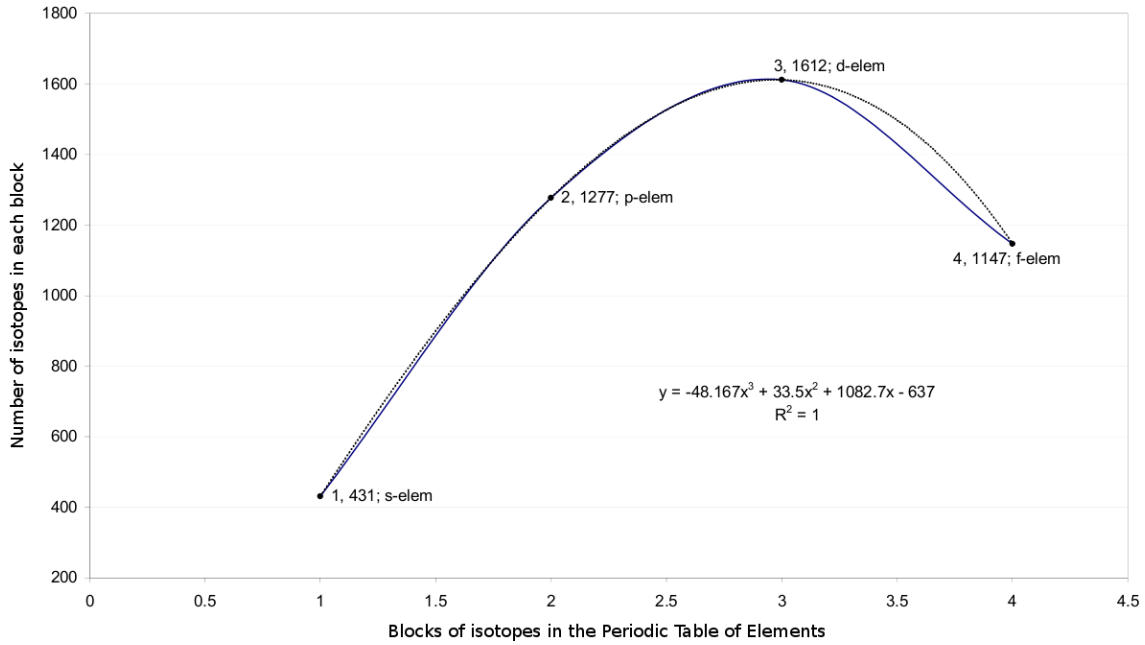

Fig. 1: Dependency of the number of the isotopes in the blocks from their names according to the elements of the electron configuration.

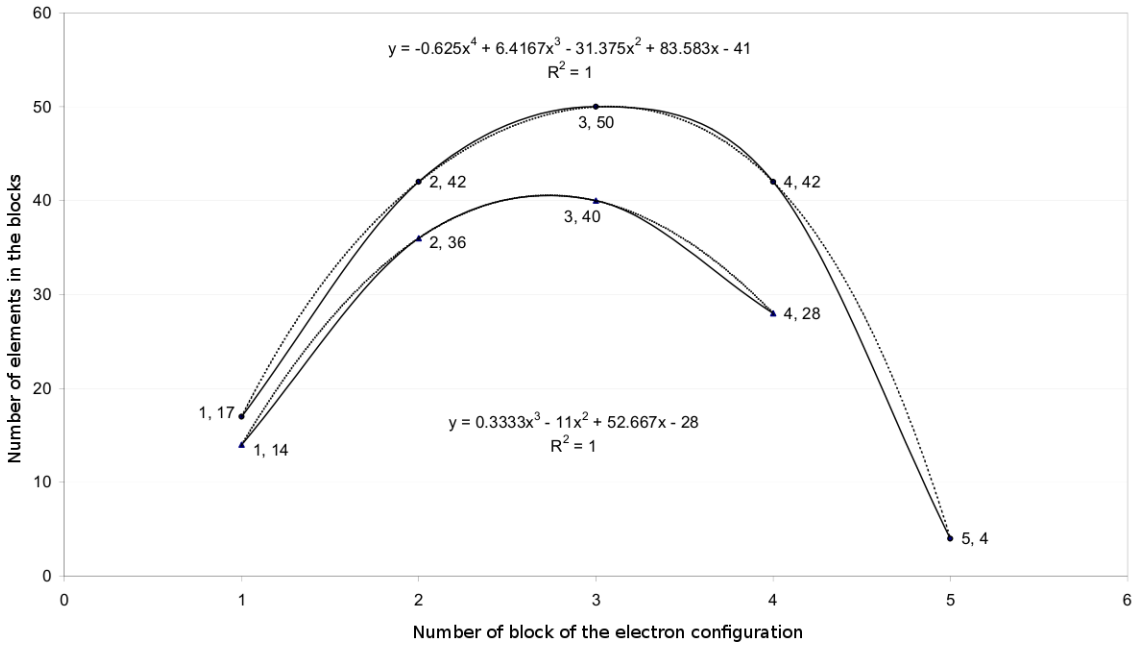

Fig. 2: Results of calculation of the electron configuration of the elements. The lower arc has been calculated for the version of the Periodic Table containing 118 elements. The upper arc has been calculated for the version of the Periodic Table containing 155 elements (suggested by the Author [5]).

1	2																																								
3	4																																						5	6	7	8	9	10
11	12																																					13	14	15	16	17	18
19	20																																					31	32	33	34	35	36
37	38																																					49	50	52	52	53	54
55	56						57	58	59	60	61	62	63	64	65	66	67	68	69	70	71	72	73	74	75	76	77	78	79	80	81	82	83	84	85	86						
87	88						89	90	91	92	93	94	95	96	97	98	99	100	101	102	103	104	105	106	107	108	109	110	111	112	113	114	115	116	117	118						
119	120	121	122	123	124	125	126	127	128	129	130	131	132	133	134	135	136	137	138	139	140	141	142	143	144	145	146	147	148	149	150	151	152	153	154						
155																																										

s-block	g-block	f-block	d-block	p-block

Fig. 3: Periodic Table of Elements, which is limited by element No.155 (suggested by the Author).

sense. Despite the bulky mathematical apparatus of Quantum Mechanics was applied to calculation of stability of the elements, it never led to a result about a limit of the Periodic Table of Elements. This was never claimed in the basis of the quantum mechanical calculations. This is because that the conditions of micro-scales, where the laws of Quantum Mechanics work, do not provide the necessary data for the calculation. Only common consideration of the conditions of micro-world and macro-world, as the author did in the recent study [5], allowed to develop the fundamental law of hyperbolas in the Periodic Table of Elements, which starts from the positions of macro-scale then continues upto the electron configuration of the elements (wherein it works properly as well, as we seen in this paper) that led to that final version of the Periodic Table of Elements, which has been presented in this paper.

Submitted on February 29, 2011 / Accepted on April 04, 2011

References

1. Nuclear Periodic Table from the Radiochemistry Society, http://www.radiochemistry.org/periodictable/NuclearPeriodicTable.html
2. Khazan A. Electron configuration and element No.155 of the Periodic Table of Elements. *Progress in Physics*, 2011, v.2, 39–43.
3. Janet C. La Classification Hélicoïdale des Éléments Chimiques. Beauvais: Imprimerie Départementale de l'Oise, 1928.
4. Casson L. Notice biographique sur la vie et de l'oeuvre de Charles Janet. *Bull. Soc. Acad. de l'Oise*, Beauvais, 2008, 232.
5. Khazan A. Upper Limit in Mendeleev's Periodic Table — Element No.155. Svenska fysikarkivet, Stockholm, 2010.

On the Cold Big Bang Cosmology

Armando V.D.B. Assis

Departmento de Física, Universidade Federal de Santa Catarina — UFSC, Trindade 88040-900, Florianópolis, SC, Brazil.
E-mail: armando.assis@pgfsc.ufsc.br

We solve the general relativity (GR) field equations under the cosmological scope via one extra postulate. The plausibility of the postulate resides within the Heisenberg indeterminacy principle, being heuristically analysed throughout the appendix. Under this approach, a negative energy density may provide the positive energy content of the universe via fluctuation, since the question of conservation of energy in cosmology is weakened, supported by the known lack of scope of the Noether's theorem in cosmology. The initial condition of the primordial universe turns out to have a natural cutoff such that the temperature of the cosmological substratum converges to the absolute zero, instead of the established divergence at the very beginning. The adopted postulate provides an explanation for the cosmological dark energy open question. The solution agrees with cosmological observations, including a 2.7K CMBT prediction.

1 Revisiting the Theoretical Assumptions

The study of the dynamics of the entire universe is known as Cosmology [1–3]. The inherent simplicity in the mathematical treatment of the Cosmology, although the entire universe must be under analysis, should be recognized as being due to Copernicus. Indeed, since the primordial idea permeating the principle upon which the simplicity arises is just an extension of the copernican revolution*: the cosmological principle. This extension, the cosmological principle, just asseverates we are not in any sense at a privileged position in our universe, implying that the average large enough scale† *spatial* properties of the physical universe are the same from point to point at a given cosmological instant. Putting these in a mathematical jargon, one says that the large enough scale spatial geometry at a given cosmological instant t is exactly the same in spite of the position of the observer at some point belonging to this t-sliced three-dimensional universe or, equivalently, that the spatial part of the line element of the entire universe is the same for all observers. Hence, the simplicity referred above arises from the very two principal aspects logically encrusted in the manner one states the cosmological principle:

- The lack of a privileged physical description of the universe at a t-sliced large enough scale $\Rightarrow$ large enough scale $\Rightarrow$ one neglects all kind of known physical interactions that are unimportant on the large enough scales $\Rightarrow$ remains gravity;
- The lack of a privileged physical description of the universe at a t-sliced large enough scale $\Rightarrow$ large enough scale $\Rightarrow$ one neglects local irregularities of a global t-sliced substratum representing the t-sliced universe $\forall$ cosmological instants $t \Rightarrow$ substratum modelled as a fluid without t-sliced spatially localized irregularities $\Rightarrow$ homogeneous and isotropic t-sliced‡ fluid.

One shall verify the t-local characteristic of the the cosmological principle, i.e., that non-privileged description does not necessarily hold on the global time evolution of that t-sliced spacelike hypersurfaces. In other words, two of such t-sliced hypersurfaces at different instants would not preserve the same aspect, as experimentally asseverated by the expansion of the universe. Hence, some further assumption must be made regarding the time evolution of the points belonging to the t-sliced spacelike hypersurfaces:

- The particles of the cosmological fluid are encrusted in spacetime on a congruence of timelike geodesics from a point in the past, i.e., the substratum is modelled as a perfect fluid.

Hence, the following theoretical ingredients are available regarding the above way in which one mathematically construct a cosmological model:

Gravity modeled by Einstein's General Relativity field equations (in natural units):

$$G_{\mu\nu} - \Lambda g_{\mu\nu} = 8\pi T_{\mu\nu}. \tag{1}$$

Homogeneity is mathematically translated by means of a geometry (metric) that is the same from point to point, spatially speaking. Isotropy is mathematically translated by means of a lack of privileged directions, also spatially speaking. These two characteristics easily allow one to consider spaces equipped with constant curvature K. From a differential geometry theorem, Schur's, a n-dimensional space $\mathbb{R}^n$, $n \geq 3$, in which a η-neighbourhood has isotropy $\forall$ points

*Copernicus told us that the Earth is not the center of our planetary system, namely the solar system, pushing down the historical button leading to the collapse of the established *anthropocentric status quo*.

†One must understand large enough scale as being that of cluster of galaxies.

‡One shall rigorously attempt to the fact: the isotropy and homogeneity are t-sliced referred, i.e., these two properties logically emerging from the cosmological principle hold upon the entire fluid at t, holding spatially at t, i.e., homogeneity and isotropy are spatial properties of the fluid. Regarding the time, one observer can be at an own proper τ-geodesic...

belonging to it, has constant curvature K throughout η. Since we are considering, spatially, global isotropy, then K is constant everywhere. Hence, one defines the Riemann tensor:

$$R_{abcd} = K\,(g_{ac}g_{bd} - g_{ad}g_{bc})\,, \tag{2}$$

spatially speaking.

As indicated before, homogeneity and isotropy are spatial properties of the geometry. Time evolution, e.g.: expansion, can be conformally agreed with these two spatial properties logically emerging from the cosmological principle in terms of Gaussian normal coordinates. Mathematically, the spacetime cosmological metric has the form:

$$ds^2 = dt^2 - [a(t)]^2\, d\sigma^2. \tag{3}$$

Since spatial coordinates for a spatially fixed observer do not change, $ds^2 = dt^2 \Rightarrow g_{tt} = 1$.

Regarding the spatial part of the line element, the Schwarzschild metric is spherically symmetric, a guide to our purposes. From the Scharzschild metric (signature $+ - - -$):

$$ds^2 = e^{2\nu(r)}dt^2 - e^{2\lambda(r)}dr^2 - r^2 d\theta^2 - r^2\sin^2\theta\, d\phi^2, \tag{4}$$

one easily writes down the spatial part of the spacetime cosmological metric:

$$d\sigma^2 = e^{2f(r)}dr^2 + r^2 d\theta^2 + r^2\sin^2\theta\, d\phi^2. \tag{5}$$

One straightforwardly goes through the tedious calculation of the Christoffel symbols and the components of the Ricci tensor, finding:

$$e^{2f(r)} = \frac{1}{1 - Kr^2}. \tag{6}$$

Absorbing constants* by the scale factor in eqn. (3), one normalizes the curvature constant K, namely $k \in \{-1;\, 0;\, +1\}$. Hence, the cosmological spacetime metric turns out to be in the canonical form:

$$ds^2 = dt^2 - [a(t)]^2\left(\frac{dr^2}{1 - kr^2} + r^2 d\theta^2 + r^2\sin^2\theta\, d\phi^2\right). \tag{7}$$

Now, regarding the fluid substratum, one sets in co-moving coordinates ($dt/d\tau = 1$, $u^\mu = (1;\, 0;\, 0;\, 0)$):

$$T^\mu{}_\nu = 0,\ \mu \neq \nu;\ \ T^0{}_0 = \rho;\ \ T^\mu{}_\mu = -p\,,\ \ \text{for } \mu \in \{1;\, 2;\, 3\} \tag{8}$$

since the particles in the fluid are clusters of galaxies falling together with small averaged relative velocities compared with the cosmological dynamics, where the substratum turns out to be averaged described by an average substratum density ρ and by an average substratum pressure p.

The Einstein tensor in eqn. (1), $G_{\mu\nu}$, is related to the Ricci tensor $R_{\mu\nu} = R^\gamma{}_{\mu\gamma\nu}$ (the metric contraction of the curvature tensor (Riemann tensor)), to the Ricci scalar $R = R^\mu{}_\mu$ (the metric contraction of the Ricci tensor) and to the metric $g_{\mu\nu}$ itself:

$$G_{\mu\nu} = R_{\mu\nu} - \frac{1}{2}\,R\,g_{\mu\nu}\,. \tag{9}$$

The curvature tensor $R^\alpha{}_{\beta\gamma\delta}$ is obtained via a metric connection, the Christoffel $\Gamma^\alpha{}_{\beta\delta}$ symbols in our case of non-torsional manifold:

$$R^\alpha{}_{\beta\gamma\delta} = \partial_\gamma\Gamma^\alpha{}_{\beta\delta} - \partial_\delta\Gamma^\alpha{}_{\beta\gamma} + \Gamma^\epsilon{}_{\beta\delta}\Gamma^\alpha{}_{\epsilon\gamma} - \Gamma^\epsilon{}_{\beta\gamma}\Gamma^\alpha{}_{\epsilon\delta}\,, \tag{10}$$

where the metric connection is obtained, in the present case, from the Robertson-Walker cosmological spacetime geometry given by eqn. (7) (from which one straightforwardly obtains the metric coefficients of the diagonal metric tensor in the desired covariant or contravariant representations) via:

$$\Gamma^\alpha{}_{\beta\gamma} = g^{\alpha\delta}\Gamma_{\delta\beta\gamma}\,, \tag{11}$$

being the metric connection (Christoffel symbols) of the first kind $\Gamma_{\delta\beta\gamma}$ given by:

$$\Gamma_{\delta\beta\gamma} = \frac{1}{2}\left(\frac{\partial g_{\beta\gamma}}{\partial x^\delta} + \frac{\partial g_{\gamma\delta}}{\partial x^\beta} - \frac{\partial g_{\delta\beta}}{\partial x^\gamma}\right). \tag{12}$$

These set of assumptions under such mathematical apparatus lead one to the tedious, but straightforward, derivation, via eqn. (1), of the ordinary differential cosmological equations emerging from the relation between the Einstein's tensor, $G_{\mu\nu}$, the Robertson-Walker spacetime cosmological metric of the present case, $g_{\mu\nu}$ via eqn. (7), and the stress-energy tensor, $T_{\mu\nu}$ via metric contraction of the eqn. (8) (signature $+ \ - \ - \ -$):

$$\frac{\dot{R}^2 + kc^2}{R^2} = \frac{8\pi G}{3c^2}\,(\rho + \tilde{\rho})\,; \tag{13}$$

$$\frac{2R\ddot{R} + \dot{R}^2 + kc^2}{R^2} = -\frac{8\pi G}{c^2}\,(p + \tilde{p})\,, \tag{14}$$

where we are incorporating the cosmological constant Λ through the energy density and the pressure of the vacuum: $\tilde{\rho}$ and $\tilde{p}$, respectively. One also must infer we are no more working with natural units. The scale factor becomes $R(t)$, and one must interpret it as the magnification length scale of the cosmological dynamics, since $R(t)$ turns out to be length. This measures how an unitary length of the pervading cosmological substratum at t_0 becomes stretched as the universe goes through a time evolution from t_0 to t. One should not literally interpret it as an increase of the distance between two points, e.g., in a case of expansion, a stretched stationary wavelength connecting two cosmological points at a t_0-sliced spacelike substratum would remain stationarily connecting the very same two points after the stretched evolution to the respective t-sliced spacelike substratum, but less energetically.

*Defining $r' = \sqrt{|K|}\,r$, one straightforwardly goes through...

2 A Cold Beginning?

Applying the following conservation criteria:

$$\nabla_\mu T^\mu_{\ t} = \partial_\mu T^\mu_{\ t} + \Gamma^\mu_{\mu\nu} T^\nu_{\ t} - \Gamma^\nu_{\mu t} T^\mu_{\ \nu} = 0, \tag{15}$$

one finds via the diagonal stress-energy tensor (see eqn. (8)), the metric connection (see eqs. (11) and (12)) and the spacetime cosmological geometry of the present case (eqn. (7)):

$$\frac{\partial}{\partial t}(\rho + \tilde{\rho}) + 3\frac{\dot{R}}{R}(\rho + \tilde{\rho} + p + \tilde{p}) = 0. \tag{16}$$

eqn. (16) is the first law of thermodynamics applied to our substratum (including vacuum), since, despite of geometry, a spatial slice of the substratum has volume $\alpha(k)\,[R(t)]^3$, density $(\rho(t) + \tilde{\rho})^*$ and energy $(\rho(t) + \tilde{\rho})\,\alpha(k)\,[R(t)]^3$, implying that $dE + pdV = 0$ turns out to be eqn. (16). $\alpha(k)$ is the constant that depends on geometry (open, $k = -1$; flat, $k = 0$; closed, $k = 1$) to give the correct volume expression of the mentioned spatial slice of the t-sliced cosmological substratum.

Now, we go further, considering the early universe as being dominated by radiation. In the ultrarelativistic limit, the equation of state is given by:

$$\rho - 3p = 0. \tag{17}$$

Putting this equation of state in eqn. (16) and integrating, one obtains the substratum pressure as a function of the magnification scale R:

$$4\ln\|R\| + \ln\|p\| = C' \;\Rightarrow\; \|p\| = \frac{e^{C'}}{R^4} \;\Rightarrow\; p = \pm\frac{C^+}{R^4}, \tag{18}$$

where $C^+ \geq 0$ is a constant of integration. In virtue of eqn. (18), eqn. (14) is rewritten in a total differential form:

$$2R\dot{R}d\dot{R} + \left(\dot{R}^2 + kc^2 \pm \frac{8\pi G}{c^2}\frac{C^+}{R^2} + \frac{8\pi G}{c^2}\tilde{p}R^2\right)dR = 0. \tag{19}$$

Indeed, eqn. (19) is a total differential of a constant $\lambda(R, \dot{R}) = constant$:

$$d\lambda(R,\dot{R}) = \frac{\partial\lambda(R,\dot{R})}{\partial\dot{R}}d\dot{R} + \frac{\partial\lambda(R,\dot{R})}{\partial R}dR = 0, \tag{20}$$

since:

$$\frac{\partial\lambda(R,\dot{R})}{\partial\dot{R}} = 2R\dot{R} \;\Rightarrow\; \frac{\partial^2\lambda(R,\dot{R})}{\partial R\,\partial\dot{R}} = 2\dot{R}; \tag{21}$$

$$\frac{\partial\lambda(R,\dot{R})}{\partial R} = \dot{R}^2 + kc^2 \pm \frac{8\pi G}{c^2}\frac{C^+}{R^2} + \frac{8\pi G}{c^2}\tilde{p}R^2 \;\Rightarrow \tag{22}$$

$$\frac{\partial^2\lambda(R,\dot{R})}{\partial\dot{R}\,\partial R} = 2\dot{R} \;\therefore\; \frac{\partial^2\lambda(R,\dot{R})}{\partial R\,\partial\dot{R}} = \frac{\partial^2\lambda(R,\dot{R})}{\partial\dot{R}\,\partial R} = 2\dot{R}. \tag{23}$$

Integrating, one has:

$$\int\partial\lambda(R,\dot{R}) = \int 2R\dot{R}\,\partial\dot{R} = 2R\int\dot{R}\,d\dot{R} + h(R) \;\therefore \tag{24}$$

$$\lambda(R,\dot{R}) = R\dot{R}^2 + h(R), \tag{25}$$

where $h(R)$ is a function of R. From eqs. (22) and (25):

$$\frac{\partial}{\partial R}\lambda(R,\dot{R}) = \dot{R}^2 + kc^2 \pm \frac{8\pi G}{c^2}\frac{C^+}{R^2} + \frac{8\pi G}{c^2}\tilde{p}R^2 \Rightarrow$$

$$h(R) = \int\left(kc^2 \pm \frac{8\pi G}{c^2}\frac{C^+}{R^2} + \frac{8\pi G}{c^2}\tilde{p}R^2\right)dR \;\therefore \tag{26}$$

$$h(R) = kc^2R \mp \frac{8\pi G}{c^2}\frac{C^+}{R} + \frac{8\pi G}{3c^2}\tilde{p}R^3. \tag{27}$$

Putting this result from eqn. (27) in eqn. (25):

$$\lambda(R,\dot{R}) = R\dot{R}^2 + kc^2R \mp \frac{8\pi G}{c^2}\frac{C^+}{R} + \frac{8\pi G}{3c^2}\tilde{p}R^3 = constant \tag{28}$$

is the general solution of the total differential equation eqn. (19). Dividing both sides of eqn. (28) by $R^3 \neq 0$:

$$\frac{\lambda(R,\dot{R})}{R^3} = \frac{\dot{R}^2 + kc^2}{R^2} \mp \frac{8\pi G}{c^2}\frac{C^+}{R^4} + \frac{8\pi G}{3c^2}\tilde{p}, \tag{29}$$

using the eqn. (13), one obtains:

$$\frac{\lambda(R,\dot{R})}{R^3} = \frac{8\pi G}{c^2}\left(\frac{\rho}{3} \mp \frac{C^+}{R^4}\right) + \frac{8\pi G}{3c^2}(\tilde{\rho} + \tilde{p}) \;\therefore \tag{30}$$

$$\lambda(R,\dot{R}) = constant = 0, \tag{31}$$

in virtue of eqns. (17), (18) and $\tilde{\rho} + \tilde{p} = 0$ for the background vacuum. Of course, the same result is obtained from eqn. (13), since this equation is a constant of movement of eqn. (14), being eqn. (16) the connection between the two. Neglecting the vacuum contribution in relation to the ultrarelativistic substratum, one turns back to the eqn. (28), set the initial condition $R = R_0$, $\dot{R} = 0$, at $t = 0$, obtaining for the substratum pressure:

$$p(R) = k\frac{c^4R_0^2}{8\pi GR^4}, \tag{32}$$

and for the magnification scale velocity:

$$\dot{R}^2 = -kc^2\left(1 - \frac{R_0^2}{R^2}\right). \tag{33}$$

Now, robustness† requires an open universe with $k = -1$. Hence, the locally flat substratum energy is given by‡:

$$E^+ = -4\pi R^3 p(R) \Rightarrow R_0 = -\frac{2GE_0^+}{kc^4}, \tag{34}$$

*One shall remember the cosmological principle: on average, for large enough scales, at t-sliced substratum, the universe has the same aspect in spite of the spatial localization of the observer in the t-slice $\Rightarrow \rho = \rho(t)$. Also, since Λ is constant, $\tilde{\rho}$ and $\tilde{p}$ are constants such that $\tilde{\rho} + \tilde{p} = 0$.

†For, $\dot{R}^2 \in \mathbb{R}$ in eqn. (33) with $R \geq R_0$.

‡The Hawking-Ellis dominant energy condition giving the positive energy, albeit the expansion dynamics obtained via eqn. (32).

in virtue of eqn. (32) and the initial condition $E^+ = E_0^+$, $R = R_0$ at $t = 0$. Returning to eqn. (33), one obtains the magnification scale velocity:

$$\dot{R} = c\sqrt{1 - \frac{4G^2\left(E_0^+\right)^2}{c^8R^2}}, \tag{35}$$

giving $\dot{R} \to c$ as $R \to \infty$. Rewriting eqn. (35), one obtains the dynamical Schwarzchild horizon:

$$R = \frac{2G}{c^4}\frac{E_0^+}{\sqrt{1 - \dot{R}^2/c^2}}. \tag{36}$$

We will not use the eqn. (34) (now you should read the appendix to follow the following argument) to obtain the energy from the energy density and volume for $t \neq 0$, since we do not handle very well the question of the conservation of energy in cosmology caused by an inherent lack of application of the Noether's theorem. In virtue of the adopted initial conditions, an initial uncertainty R_0 related to the initial spatial position of an arbitrary origin will be translated to a huge uncertainty R at the actual epoch. Indeed, one never knows the truth about the original position of the origin, hence the uncertainty grows as the universe enlarge. The primordial energy from which the actual energy of the universe came from was taken as E_0^+ at the beginning. This amount of energy is to be transformed over the universe evolution, giving the present amount of the universe, i.e., the energy of an actual epoch t-sliced hypersurface of simultaneity. But this energy at each instant t of the cosmological evolution turns out to be the transformed primordial indeterminacy E_0^+, since E_0^+ is to be obtained via the Heisenberg indeterminacy principle. In other words, we argue that the energetic content of the universe at any epoch is given by the inherent indeterminacy caused by the primordial indeterminacy. At any epoch, one may consider a copy of all points pertaining to the same hypersurface of simultaneity but at rest, i.e., an instantaneous non-expanding copy of the expanding instantaneous hypersurface of simultaneity. Related to an actual R indeterminacy of an origin in virtue of its primordial R_0 indeterminacy, one has the possibility of an alternative shifted origin at R. This shifted origin expands with $\dot{R}$ in relation to that non-expanding instantaneous copy of the universe at t. Since the primordial origin was considered to encapsulate the primordial energy E_0^+, this energy at the shifted likely alternative origin should be $E_0^+/\sqrt{1 - \dot{R}^2/c^2}$, since, at R, a point expands with $\dot{R}$ in relation to its non-expanding copy. We postulate:

- The actual energy content of the universe is a consequence of the increasing indeterminacy of the primordial era. Any origin of a co-moving reference frame within the cosmological substratum has an inherent indeterminacy. Hence, the indeterminacy of the energy content of the universe may create the impression that the universe has not enough energy, raising illusions as dark energy and dark matter speculations. In other words, since the original source of energy emerges as an indeterminacy, we postulate this indeterminacy continues being the energy content of the observational universe: $\delta E(t) = E^+(t) = E_0^+/\sqrt{1 - \dot{R}^2/c^2}$.

This result is compatible with the Einstein field equations. The compatibility is discussed within the appendix. In virtue of this interpretation, eqn. (36) has the aspect of the Schwarzchild radius, hence the above designation. The t-instantaneous locally flat spreading out rate of dynamical energy at t-sliced substratum is given by the summation over the ν-photonic frequencies:

$$\dot{R}\frac{d}{dR}\left(\frac{E_0^+}{\sqrt{1 - \dot{R}^2/c^2}}\right) =$$

$$= \frac{8\pi^2R^2h}{c^2}\int_0^\infty \frac{\nu^3}{\exp\left(h\nu/k_BT\right) - 1}d\nu = \frac{8\pi^6k_B^4R^2}{15c^2h^3}T^4, \tag{37}$$

where k_B is the Boltzmann constant, h the Planck constant and T the supposed rapid thermodynamically equilibrated t-sliced locally flat instantaneous cosmological substratum temperature. Now, setting, in virtue of the Heisenberg principle:

$$\frac{E_0^+R_0}{c} \approx h \overset{(34)}{\Rightarrow} \left(E_0^+\right)^2 = \frac{hc^5}{2G}, \tag{38}$$

one obtains, in virtue of eqn. (37):

$$T^4 = \frac{15c^7h^3}{16\pi^6Gk_B^4}\frac{1}{R^2}\sqrt{1 - \frac{2Gh}{c^3R^2}}. \tag{39}$$

Hence, the temperature of the cosmological substratum vanishes* at $t = 0$, rapidly reaching the maximum $\approx 10^{32}K$, and assintotically decreasing to zero again as $t \to \infty$.

Indeed. $R_0 = R(t = 0) = \sqrt{2Gh/c^3}$, in virtue of eqs. (34) and (38), giving $T^4(R_0) = T^4(t = 0) = 0$. Also, the maximum temperature is $T \approx 10^{32}K$, from eqn. (39), occuring when $R = R_{max} = \sqrt{3/2}R_0 = \sqrt{3Gh/c^3}$, as one obtains by $dT^4/dR = 0$ with $d^2T^4/dR^2 < 0$. Below†, one infers these properties of eqn. (39).

*We argue there is no violation of the third law of thermodynamics, since one must go from the future to the past when trying to reach the absolute zero, violating the second law of thermodynamics. At $t = 0$, one is not reaching the absolute zero since there is no past before the beginning of the time. To reach the absolute zero, in an attempt to violate the Nernst principle, one must go from the past to the future.

†The eqn. (39) is simply rewritten to plot the graph, i.e.: $T_{max}^4 = \left(5\sqrt{3}\,c^{10}h^2\right)/\left(48\pi^6G^2k_B^4\right)$ and, as obtained before, $R_0 = \sqrt{2Gh/c^3}$.

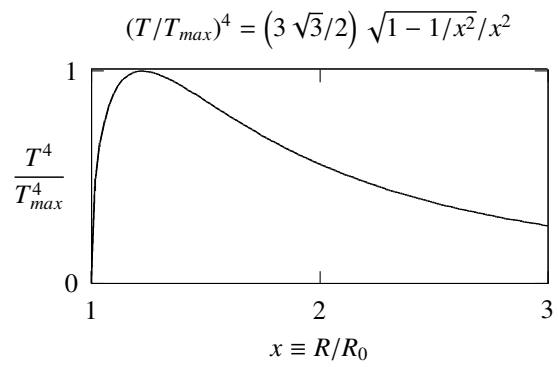

Now, one puts the result of eqn. (38) in eqn. (35) and integrates:

$$\int_{(2Gh/c^3)^{1/2}}^{R} \frac{R}{\sqrt{R^2 - 2Gh/c^3}} dR = c\int_0^t d\tau, \qquad (40)$$

obtaining:

$$t = \frac{1}{c}\sqrt{R^2 - 2Gh/c^3} \Rightarrow t(R_{max}) = \sqrt{\frac{Gh}{c^5}} \approx 10^{-43}\,\mathrm{s}, \qquad (41)$$

for the elapsed time from $t = 0$ to the instant in which the substratum temperature reaches the maximum value $T \approx 10^{32}$ K. The initial acceleration, namely the explosion/ignition acceleration at $t = 0$ of the substratum is obtained from eqn. (35):

$$\ddot{R} = \dot{R}\frac{d\dot{R}}{dR} = \frac{4G^2\left(E_0^+\right)^2}{c^6R^3} \overset{(38)}{=} \frac{2Gh}{cR^3} \therefore \qquad (42)$$

$$\ddot{R}\left(R = R_0 = \sqrt{2Gh/c^3}\right) = \sqrt{\frac{c^7}{2Gh}} \approx 10^{51}\,\mathrm{m/s^2}. \qquad (43)$$

An interesting calculation is the extension of the eqn. (39) formula to predict the actual temperature of the universe. Since $2Ghc^{-3}R^{-2} \ll 1$ for actual stage of the universe, eqn. (39) is approximately given by:

$$T^4 \approx \frac{15c^7h^3}{16\pi^6Gk_B^4}\frac{1}{R^2} \Rightarrow R^2 \approx \frac{15c^7h^3}{16\pi^6Gk_B^4}\frac{1}{T^4}. \qquad (44)$$

Also, for actual age of the universe, eqn. (41) is approximately given by:

$$t \approx \frac{R}{c} \overset{(44)}{=} \sqrt{\frac{15c^5h^3}{16\pi^6Gk_B^4}}\frac{1}{T^2} \quad \therefore \qquad (45)$$

$$T^2_{\mathrm{Now}} = \sqrt{\frac{15c^5h^3}{16\pi^6Gk_B^4}}\, t^{-1}_{\mathrm{Now}} = 5.32\times10^{20}t^{-1}_{\mathrm{Now}}\left(\mathrm{K^2s}\right). \qquad (46)$$

Before going further on, one must remember we are not in a radiation dominated era. Hence, the left-hand side and the right-hand side of eqn. (37) must be adapted for this situation. The left-hand accomplishes the totality of spreading out energy in virtue of cosmological dynamics. It equals the right-hand side in an ultrarelativistic scenario. But, as the universe evolves, the right-hand side becomes a fraction of the totality of spreading out energy. Rigorously, as the locally flatness of the t-sliced substratum increases, one multiplies both sides of eqn. (37) by $(4/c)\times\left(1/4\pi R^2\right)$ and obtains the t-sliced instantaneously spreading out enclosed energy density. Hence the right-hand side of eqn. (37) turns out to be multiplied by the ratio between the total cosmological density* ρ_c and the radiation density ρ_r. Hence, eqn. (46) is rewritten:

$$\sqrt{\frac{\rho_c}{\rho_r}}\, T^2_{\mathrm{Now}} = 5.32\times10^{20}t^{-1}_{\mathrm{Now}}\left(\mathrm{K^2s}\right). \qquad (47)$$

The actual photonic density is $\rho_r = 4.7\times10^{-31}\,\mathrm{kg/m^3}$ and the actual total cosmological density is $\rho_c = 1.3\times10^{-26}\,\mathrm{kg/m^3}$. For the reciprocal age of universe, t^{-1}_{Now} in eqn. (47), one adopts the Hubble's constant, for open universe, $H = t^{-1}_{\mathrm{Now}} = 2.3\times10^{-18}\,\mathrm{s^{-1}}$. Hence, by eqn. (47), one estimates the actual temperature of the universe:

$$T^2_{\mathrm{Now}} = \sqrt{\frac{4.7\times10^{-31}}{1.3\times10^{-26}}}\times5.32\times10^{20}\times2.3\times10^{-18}\ \mathrm{K^2} \therefore \qquad (48)$$

$$T_{\mathrm{Now}} = 2.7\,\mathrm{K}, \qquad (49)$$

very close to the CMB temperature.

3 Appendix

From eqns. (17) and (32):

$$\rho = 3p = -\frac{3c^4R_0^2}{8\pi G}\frac{1}{R^4} \Rightarrow E_\rho = -\frac{c^4R_0^2}{2G}\frac{1}{R}, \qquad (50)$$

since $k = -1$; E_ρ is the energy (negative) obtained from volume and ρ. From eqn. (34), $R_0^2 = 4G^2(E_0^+)^2/c^8$. Hence, eqn. (50) is rewritten:

$$E_\rho = -\frac{2G}{c^4}\left(E_0^+\right)^2\frac{1}{R}. \qquad (51)$$

With the eqn. (36), we reach:

$$E_\rho = -E_0^+\sqrt{1-\dot{R}^2/c^2}. \qquad (52)$$

This negative energy arises from the adopted negative pressure solution. But, its fluctuation is positive:

$$\delta E_\rho = \frac{E_0^+}{\sqrt{1-\dot{R}^2/c^2}}\frac{\dot{R}\,\delta\dot{R}}{c^2}, \qquad (53)$$

since both, $\dot{R}$ and $\delta\dot{R}$, are positive within our model (see eqn. (40)). Let δt be the time interval within this fluctuation process. Multiplying both sides of the eqn. (53) by δt, we obtain:

$$\delta E_\rho\,\delta t = \frac{E_0^+}{\sqrt{1-\dot{R}^2/c^2}}\left(\dot{R}\delta\dot{R}/c^2\right)\delta t. \qquad (54)$$

*Actually, the critical one, since observations asseverate it.

The above relation must obey the Heisenberg indeterminacy principle, and one may equivalently interpret it under the following format:

$$\delta E_\rho \, \delta t = \frac{E_0^+}{\sqrt{1 - \dot{R}^2/c^2}} \, (\delta t)^* \approx h, \tag{55}$$

An energy indeterminacy having the magnitude of the actual cosmological energy content carries an indeterminacy $\delta\dot{R} \approx c$ about the magnification scale velocity $\dot{R}$ with $\dot{R} \approx c$. For such an actual scenario in which $\dot{R} \approx c$ (see eqn. (35) with $R \to \infty$), we have:

$$\delta t \approx (\delta t)^* \Rightarrow \delta E_\rho \Big|_{R_0}^{\infty} = E^+ = \frac{E_0^+}{\sqrt{1 - \dot{R}^2/c^2}}, \tag{56}$$

if* $\dot{R} \to c$. Now, let's investigate the primordial time domain $t \approx 0$. To see this, we rewrite $\dot{R}\delta\dot{R}$ within the eqn. (54). Firstly, from eqn. (35):

$$\dot{R} = c\sqrt{1 - R_0^2/R^2} \Rightarrow \dot{R}\,\delta\dot{R} = \frac{c^2 R_0^2}{R^3}\,\delta R, \tag{57}$$

where $R_0 = \sqrt{2Gh/c^3}$ as obtained before. Within the primordial time domain $t \approx 0$, we have $R \approx R_0$ and $\delta R \approx R_0$, as discussed before. Hence, the eqn. (57) reads:

$$\dot{R}\,\delta\dot{R} \approx c^2. \tag{58}$$

if $t \approx 0$. Back to the eqn. (54) we obtain again:

$$\delta t \approx (\delta t)^* \Rightarrow \delta E_\rho \Big|_{\approx R_0} = E^+ = \frac{E_0^+}{\sqrt{1 - \dot{R}^2/c^2}}, \tag{59}$$

if $t \approx 0$. This justify the use of $E^+ = E_0^+/\sqrt{1 - \dot{R}^2/c^2}$ within our postulate, emerging from the positive fluctuation of the negative energy E_ρ obtained from volume and the negative energy density ρ stated via the fluid state equation, eqn. (17), and entering within the field equations.

Acknowledgements

A.V.D.B.A is grateful to Y.H.V.H and CNPq for financial support.

Submitted on April 10, 2011 / Accepted on April 13, 2011

References

1. Bondi H. Cosmology. Dover Publications, Inc., New York, 2010.
2. Bondi H. Negative mass in General Relativity. *Review of Modern Physics*, 1957, v. 29 (3), 423–428.
3. Carrol S. Spacetime and Geometry. An Introduction to General Relativity. Addison Wesley, San Francisco, 2004.

*Eqn. (56) holds from $t > 10^{-43}$ seconds, as one easily verify from eqn. (35).

LETTERS TO PROGRESS IN PHYSICS

LETTERS TO PROGRESS IN PHYSICS

Arthur Marshall Stoneham

(1940–2011)

Vahan Minasyan and Valentin Samoilov
Scientific Center of Applied Research, JINR, Joliot-Curie 6, Dubna, 141980, Russia
E-mails: mvahan@scar.jinr.ru; scar@off-serv.jinr.ru

The memory of the prominent British physicist, Prof. Arthur Marshall Stoneham (1940–2011), will live in our hearts and souls.

Arthur Marshall Stoneham (1940–2011)

Marshall Stoneham was born in 1940 in Barrow-in-Furness, Cumbria. He was educated at Barrow Grammar School for Boys before reading physics at Bristol University. In 1964 he completed his doctorate at Bristol under Prof. Maurice Pryce. After completing his thesis, Marshall started working for the Atomic Energy Authority in the Theoretical Physics Division at Harwell. At that time, Harwell faced challenges posed by the nuclear programme, involving the construction of reactors and the safe disposal of radioactive waste. Marshall's main work was the Theory of Defects in Solids. His book on the subject left its mark on a generation, aided by Marshall's habit of referring people to the precise place in the book where their answer was. It has never been out of print since it was first published. Marshall's group at Harwell became a leading light for both the nuclear industry and beyond. He became a division head, AEA chief scientist and retained his interest in nuclear power (both fission and fusion) to the end.

At University College London (where he moved in 1995 as Massey Professor of Physics) he and his colleague John Finney built up the London Centre of Nanotechnology. He was an Honorary Fellow of Wolfson College, Oxford University, from 1985, was elected a Fellow of the Royal Society in 1989 and in 2010 had started his term as President of the Institute of Physics. His colleagues will remember him for his support (even when that support took the form of asking a killer question at the end of your presentation after apparently having slept through it), for the way he promoted their work — even if it was by remarking, "Oh they could sort that out in a few days". It never took less than three months. Above all, in a life that was filled to overflowing he found time for people; to listen, to encourage, to advise. Marshall was a prolific writer. In addition to several books, he was author or co-author of over 500 publications.

Marshall had a great love of music and played the French horn, inspired by a recording of Dennis Brain playing the Mozart horn concertos which his father bought for him (and regretted!) at the age of 18. His love of wind music led him to form his own music group in 1971, the Dorchester Wind Players. Throughout the '80s and '90s he dedicated himself to the massive task of compiling a directory of every piece of wind music in the world ever written for two or more instruments, into a *Wind Ensemble Sourcebook*. Marshall's professional life took him all over the world and he used these travel opportunities to rummage in obscure music libraries and even monasteries in his quest. The project took years, but eventually he and his co-authors published *Wind Ensemble Sourcebook* in 1997. It runs to 450 pages, containing records of 12,000 works by 2,200 composers, and it has two companion volumes. The whole enterprise was truly a world first and will probably never be equalled.

In 1962 Marshall married Doreen, another physicist, and also from Barrow-in-Furness. They have two physicist daughters and he would often joke that he had "done his bit" for women in science. Marshall was a director in his and his wife's specialist laboratory, Oxford Authentication, which authenticates pottery and porcelain antiquities using thermoluminescence dating.

Marshall died on 18 February from complications arising from pancreatic cancer.

Commencing in 2002 Prof. Stoneham helped us by scientific way. He had given scientific directions which then

became the basis of our research studies. Due to his scientific support, we published many important papers in the science connected with understanding structures of light and solid. We never forget Arthur Marshall Stoneham who was a very noble man. His memory will live always in our souls.

We are very grateful to Doreen Stoneham who helped us by information connected with the early private life of Prof. Stoneham.

We also thank the Editor of Chief of Progress in Physics, Dr. Dmitri Rabounski, who assisted us with this letter, and always helped us by scientific way.

Submitted on April 04, 2011 / Accepted on April 09, 2011

Progress in Physics is an American scientific journal on advanced studies in physics, registered with the Library of Congress (DC, USA): ISSN 1555-5534 (print version) and ISSN 1555-5615 (online version). The journal is peer reviewed and listed in the abstracting and indexing coverage of: Mathematical Reviews of the AMS (USA), DOAJ of Lund University (Sweden), Zentralblatt MATH (Germany), Scientific Commons of the University of St.Gallen (Switzerland), Open-J-Gate (India), Referential Journal of VINITI (Russia), etc. Progress in Physics is an open-access journal published and distributed in accordance with the Budapest Open Initiative: this means that the electronic copies of both full-size version of the journal and the individual papers published therein will always be acessed for reading, download, and copying for any user free of charge. The journal is issued quarterly (four volumes per year).

Electronic version of this journal: http://www.ptep-online.com

Postal address:
Department of Mathematics and Science,
University of New Mexico, 200 College Road, Gallup, NM 87301, USA

Printed in the United States of America